

Nusret KAYA.

IZMIR KATIP CELEBI UNIVERSITY

2018

**IZMIR KATIP CELEBI UNIVERSITY
GRADUATE SCHOOL OF NATURAL AND APPLIED SCIENCES**

**MANUFACTURING AND CHARACTERIZATION OF THERMAL
CONDUCTIVE POLYMERIC COMPOSITE MATERIALS**

PhD THESIS

Nusret KAYA

Department of Material Science and Engineering

SEPTEMBER 2018

**IZMIR KATIP CELEBI UNIVERSITY
GRADUATE SCHOOL OF NATURAL AND APPLIED SCIENCES**

**MANUFACTURING AND CHARACTERIZATION OF THERMAL
CONDUCTIVE POLYMERIC COMPOSITE MATERIALS**

PhD THESIS

**Nusret KAYA
D130111011**

Material Science and Engineering

Thesis Advisor: Prof.Dr. Şerafettin DEMİÇ

SEPTEMBER 2018

İZMİR KATİP ÇELEBİ ÜNİVERSİTESİ
FEN BİLİMLERİ ENSTİTÜSÜ

TERMAL İLETKEN POLİMERİK KOMPOZİT MALZEMELERİN
ÜRETİLMESİ VE KARAKTERİZASYONU

DOKTORA TEZİ

Nusret KAYA
D130111011

Malzeme Bilimi ve Mühendisliği Anabilim Dalı

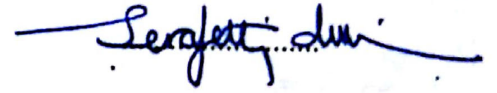
Tez Danışmanı: Prof. Dr. Şerafettin DEMİÇ

EYLÜL 2018

Nusret KAYA, a **PhD** student of **IKCU Graduate School of Natural and Applied Sciences**, successfully defended the thesis entitled “**MANUFACTURING AND CHARACTERIZATION OF THERMAL CONDUCTIVE POLYMERIC COMPOSITE MATERIALS**”, which he prepared after fulfilling the requirements specified in the associated legislations, before the jury whose signatures are below.

Thesis Advisor :

Prof. Dr. Şerafettin DEMİÇ
İzmir Katip Çelebi University

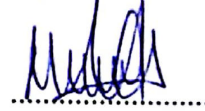


Jury Members :

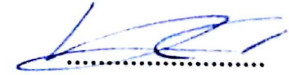
Doç. Dr. Mücahit SÜTÇÜ
İzmir Katip Çelebi University



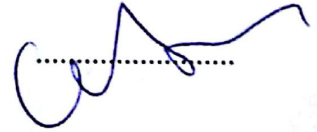
Doç. Dr. Mustafa CAN
İzmir Katip Çelebi University



Doç. Dr. Ayhan ORAL
Çanakkale Onsekiz Mart University



Dr. Öğr. Üy. Mustafa EROL
Dokuz Eylül University



Date of Submission : 14.08.2018

Date of Defense : 06.09.2018

To my family,

FOREWORD

This thesis has been written to fulfill the graduation requirements of the Material Science and Engineering Program at Izmir Katip Celebi University Graduate School of Natural and Applied Sciences. I was engaged in researching and writing this dissertation from October 2016 to July 2018.

My research questions were formulated together with my adviser, Şerafettin DEMİÇ, PhD, Prof. The research was difficult, but conducting extensive investigations have allowed me to answer the questions that we identified. Therefore, first and foremost, I would like to thank to Mr. DEMİÇ for his excellent guidance and support during this process.

I would like to thank to Mustafa CAN, PhD, Assoc. Prof. and Kutlay SEVER, PhD, Assoc. Prof. for their wonderful cooperation. It was always helpful to bat ideas about my research with them.

I also benefitted from debating issues with my friends and family. I would like to thank to my friend Yaşar Tarkman. If, I ever lost interest, they kept me motivated and helped a lot for the analyses. My parents deserve a particular note of thanks. My wife's wise counsel and kind words have, as always, served me well.

I also wish to thank all of the respondents of Central Research Laboratory of Izmir Katip Celebi, without their cooperation, I would not have been able to conduct the analysis.

This thesis was supported by Izmir Katip Celebi University, Coordination Office of Scientific Research Projects with the following research project number (2017-TDR-FB-0027).

September 2018

Nusret KAYA

TABLE OF CONTENTS

	<u>Page</u>
TABLE OF CONTENTS	xi
ABBREVIATIONS	xiii
LIST OF TABLES	xvii
LIST OF FIGURES	xix
1. INTRODUCTION	1
2. EXPERIMENTS	18
2.1 Materials.....	18
2.1.1 Polypropylene (PP)	18
2.1.2 Aluminum 2017 alloy and silicon carbide (SiC) metal-ceramic composites.....	18
2.1.3 Alumina (Al ₂ O ₃).....	20
2.1.4 Silicon carbide (SiC)	20
2.1.5 Coped carbon fiber (CF)	20
2.1.6 Aluminum nitride (AlN)	21
2.1.7 Hexagonal boron nitride (HBN)	21
2.1.8 Graphene (G).....	22
2.1.9 Super thermal conductive graphite (Gr).....	23
2.1.10 Surface modification agents	23
2.2 Composite Manufacturing.....	26
2.3 Composites Analysis	31
2.3.1 Mechanical analysis	31
2.3.1.1 Tensile tests	31
2.3.1.2 Flexural tests	31
2.3.2 Scanning electron microscopy (SEM) analysis.....	31
2.3.3 Simultaneous differential thermal (SDT) analysis	31
2.3.4 Differential scanning calorimetry (DSC) analysis	32
2.3.5 Dynamic mechanical analysis (DMA)	32
2.3.6 Thermal conductivity analysis	32
2.3.7 Surface electrical resistivity analysis	33
3. RESULTS AND DISCUSSION	34
3.1 Mechanical Analysis (Tensile and Flexural Properties)	34
3.2 SEM Analysis	46
3.3 SDT Analysis	55
3.4 DSC Analysis	75
3.5 DMA Analysis	87
3.6 Thermal Conductivity Analysis	108
3.7 Electrical Resistivity	116
4. CONCLUSION	123
5. APPENDIX	128

6. REFERENCES	130
7. CURRICULUM VITAE (CV)	142

ABBREVIATIONS

PP	: Polypropylene
LED	: Light Emitting Diodes
CF	: Carbon fiber
CB	: Carbon Black
G	: Graphene
CNTs	: Carbon nanotubes
Al₂O₃	: Alumina
AlN	: Aluminum nitride
SiC	: Silicon carbide
BN	: Boron nitride
MMCs	: Metal-matrix composites
PMCs	: Polymer-matrix composites
AlSiC	: Aluminum-Silicon Carbide composite
AlSi	: Aluminum-Silicon composite
Cu-diamond	: Copper diamond composite
Al-diamond	: Aluminum diamond composite
Cu-W	: Tungsten-copper (W–Cu) composites
CuMo	: Molybdenum Copper composite
IC	: Integrated circuit
HTC	: High thermal conductivity
TIMs	: Thermal interface materials
PE	: Polyethylene
PVC	: Poly (vinyl chloride)
HDPE	: High-density polyethylene
LLDPE	: Linear low-density polyethylene
PI	: Polyamide
AlN	: Aluminum nitride
HBN	: Hexagonal boron nitride
CBN	: Cubic boron nitride
SiO₂	: Silicondioxide
ZnO	: Zinc oxide
Si₃N₄	: Silicon nitride
CTE	: Coefficient of thermal expansion
PDMS	: Poly (dimethylsiloxane)
TGA	: Thermogravimetric analysis
PS	: Polystyrene
PVDF	: Polyvinylidene difluoride
CPC	: Conductive polymer composites
PTFE	: Poly(tetrafluoroethylene)
PMMA	: Poly (methyl methacrylate)
PET	: Poly(ethylene terephthalate)

SEM	: Scanning electron microscopy
PSD	: Particle size distribution
Gr	: Graphite
SDT	: Simultaneous differential thermal analysis
DSC	: Differential scanning calorimetry analysis
DMA	: Dynamic mechanical analysis
M0	: Unmodified
M1	: Ethyltrimethoxysilane
M2	: 3-(Trimethoxysilyl) propyl methacrylate
M3	: (3-Glycidyloxypropyl) trimethoxysilane
M4	: (3-Aminopropyl) tetraethoxysilane
M5	: Vinyltrimethoxysilane
DTA	: Differential thermal analysis
DTG	: Differential thermal gravimetric analysis
MPa	: Mega Pascal
W/m.K	: Watt per meter Kelvin
Kg/m³	: kilogram per cubic meter
T_g	: Glassy transition Temperature
T_m	: Melting Temperature
J/g.K	: Joule per gram Kelvin
ppm/K	: Parts per million per Kelvin
T_D	: Decomposition Temperature
D₁₀	: Cumulative particle size of 10 percent of particles volume
D₅₀	: Cumulative particle size of 50 percent of particles volume
D₉₀	: Cumulative particle size of 90 percent of particles volume
10AlSiC-PP	: 10% (w/w) AlSiC particles loaded PP matrix composite
20AlSiC-PP	: 20% (w/w) AlSiC particles loaded PP matrix composite
30AlSiC-PP	: 30% (w/w) AlSiC particles loaded PP matrix composite
40AlSiC-PP	: 40% (w/w) AlSiC particles loaded PP matrix composite
50AlSiC-PP	: 50% (w/w) AlSiC particles loaded PP matrix composite
60AlSiC-PP	: 60% (w/w) AlSiC particles loaded PP matrix composite
SiC0CF-PP	: 50% (w/w) silicon carbide particles PP matrix composite
SiC1CF-PP	: 49% (w/w) silicon carbide particles and 1% (w/w) carbon fiber loaded PP matrix
SiC3CF-PP	: 47% (w/w) silicon carbide particles and 3% (w/w) carbon fiber loaded PP matrix
SiC5CF-PP	: 45% (w/w) silicon carbide particles and 5% (w/w) carbon fiber loaded PP matrix
SiC7CF-PP	: 43% (w/w) silicon carbide particles and 7% (w/w)

	carbon fiber loaded PP matrix
mV	: Millivolt
E'	: Storage modulus
E''	: Loss modulus
Tanδ	: Tan delta
AO-PP	:40% (w/w) alumina loaded PP matrix composite
AOG1-PP	:39.6% (w/w) alumina and 0.4% (w/w) graphene loaded PP matrix composite
AOG3-PP	: 38.8% (w/w) alumina and 1.2% (w/w) graphene loaded PP matrix composite
AOG5-PP	: 38.0% (w/w) alumina and 2% (w/w) graphene loaded PP matrix composite
AOG7-PP	: 37.2% (w/w) alumina and 2.8% (w/w) graphene loaded PP matrix composite
M0-PP	50% (w/w) unmodified alumina loaded PP composite
M1-PP	: 50% (w/w) ethyltrimethoxysilane modified alumina loaded PP composite
M2-PP	: 50% (w/w) 3-(Trimethoxysilyl) propyl methacrylate modified alumina loaded PP composite
M3-PP	: 50% (w/w) (3-Glycidyloxypropyl) modified alumina loaded PP composite trimethoxysilane
M4-PP	: 50% (w/w) (3-Aminopropyl) tetraethoxysilane modified alumina loaded PP composite
M5-PP	: 50% (w/w) Vinyltrimethoxysilane modified alumina loaded PP composite
5AIN-PP	5% (w/w) Aluminum nitride loaded PP matrix composite
10AIN-PP	10% (w/w) Aluminum nitride loaded PP matrix composite
15AIN-PP	15% (w/w) Aluminum nitride loaded PP matrix composite
20AIN-PP	20% (w/w) Aluminum nitride loaded PP matrix composite
25AIN-PP	25% (w/w) Aluminum nitride loaded PP matrix composite
25AIN5Gr-PP	25% (w/w) Aluminum nitride and 5% (w/w) graphite loaded PP matrix composite
20AIN10Gr-PP	20% (w/w) Aluminum nitride and 10% (w/w) graphite loaded PP matrix composite
15AIN15Gr-PP	15% (w/w) Aluminum nitride and 15% (w/w) graphite loaded PP matrix composite
10AIN20Gr-PP	10% (w/w) Aluminum nitride and 20% (w/w) graphite loaded PP matrix composite
5HBN-PP	5% (w/w) Hexagonal boron nitride loaded PP matrix composite
10HBN-PP	10% (w/w) Hexagonal boron nitride loaded PP matrix composite

15HBN-PP	15% (w/w) Hexagonal boron nitride loaded PP matrix composite
10HBN5Gr-PP	10% (w/w) Hexagonal boron nitride and 5% (w/w) graphite loaded PP matrix composite
10HBN10Gr-PP	10% (w/w) Hexagonal boron nitride and 10% (w/w) graphite loaded PP matrix composite
10HBN15Gr-PP	10% (w/w) Hexagonal boron nitride and 15% (w/w) graphite loaded PP matrix composite
10HBN20Gr-PP	10% (w/w) Hexagonal boron nitride and 20% (w/w) graphite loaded PP matrix composite
10HBN20Gr1MaPP-PP	10% (w/w) Hexagonal boron nitride , 20% (w/w) graphite and 1%(w/w) maleic anhydride grafted polypropylene loaded PP matrix composite
10HBN20Gr2MaPP-PP	10% (w/w) Hexagonal boron nitride , 20% (w/w) graphite and 2%(w/w) maleic anhydride grafted polypropylene loaded PP matrix composite
10HBN20Gr3MaPP-PP	10% (w/w) Hexagonal boron nitride , 20% (w/w) graphite and 3%(w/w) maleic anhydride grafted polypropylene loaded PP matrix composite
MaPP	Maleic anhydride grafted polypropylene

LIST OF TABLES

Page

Table 1.1: Thermal, mechanic and electrical properties of some kinds of thermal conductive filler's [73].	8
Table 1.2: Commodity polymers, some physical and thermal properties are given from Netzsch instrument thermal analysis of polymers chard.	16
Table 2.1: Chemical and physical properties of PP MH418.	18
Table 2.2: Alumina particles silane modification agents list.	25
Table 2.3: Zeta potential of silane modified alumina particles	25
Table 2.4: Composites weight (%) recipes and prices.	28
Table 3.1: Thermal degradation; onset temperature, degradation temperature (T_d), offset temperature, melting temperature (T_m), and residue.	55
Table 3.2: DSC analysis results of all composites	76
Table 3.3: Glassy transition temperature (T_g) of neat PP and composites obtained from storage modulus (E'), loss modulus (E''), and $\text{Tan}\delta$ values.	87

LIST OF FIGURES

Page

Figure 1.1: Modified heat sink scheme with electrically insulating composite.....	4
Figure 1.2: Electronic packaging examples; (a) IC applications, (b) Microchips, (c) Liquid epoxy encapsulation.	5
Figure 1.3: The surface roughness between the heats well and the device is measured by TIM.	6
Figure 2.1: AlSiC metal-ceramic composite particles scanning electron microscopy (SEM) image was taken by ZEISS trademark VP30 model scanning electron microscope. A was a 500X magnification of particles and B was a 30.000X magnification of particles.....	19
Figure 2.2: AlSiC metal-ceramic composite particles values were obtained for D_{50} , 37μ	19
Figure 2.3: PSD of alumina particles D_{50} value was 14μ	20
Figure 2.4: AlN ceramic particles scanning electron microscopy (SEM) image was taken by ZEISS trademark VP30 model scanning electron microscope. A was 5000X magnification of particles and B was EDAX spectroscopy (elemental composition analysis) of AlN particles.	21
Figure 2.5: HBN ceramic particles scanning electron microscopy (SEM) image was taken by ZEISS trademark VP30 model scanning electron microscope. A was 1000X magnification of particles and B was EDAX spectroscopy (elemental composition analysis) of HBN particles.	22
Figure 2.6: Graphene nano-plaques particles SEM image was taken by product technical data sheets. A was a 13.000X magnification of particles and B was the Raman spectrum of graphene nano-plaques particles.....	22
Figure 2.7: Super thermal conductive graphite particles scanning electron microscopy (SEM) image and orientation of carbon atoms into graphite were given from Momentive marketing bulletin.	23
Figure 2.8: Silane modification reaction mechanism of -OH bonds included substrate surface [116].	24
Figure 2.9: Sample preparation Equipment.	27
Figure 3.1: Tensile strength and tensile elastic modulus of neat PP, 10AlSiC-PP, 20AlSiC-PP, 30AlSiC-PP, 40AlSiC-PP, 50AlSiC-PP, and 60AlSiC-PP	34
Figure 3.2: Flexural strength and flexural elastic modulus of neat PP, 10AlSiC-PP, 20AlSiC-PP, 30AlSiC-PP, 40AlSiC-PP, 50AlSiC-PP, and 60AlSiC-PP	35
Figure 3.3: Tensile strength and tensile elastic modulus of neat PP, AO-PP, AOG1-PP, AOG3-PP, AOG5-PP, and AOG7-PP	36
Figure 3.4: Flexural strength and flexural elastic modulus of neat PP, AO-PP, AOG1-PP, AOG3-PP, AOG5-PP, and AOG7-PP	37
Figure 3.5: Tensile strength and tensile elastic modulus of neat PP, M0-PP, M1-PP, M2-PP, M3-PP, M4-PP, and M5-PP.....	38
Figure 3.6: Flexural strength and flexural elastic modulus of neat PP, M0-PP, M1-PP, M2-PP, M3-PP, M4-PP, and M5-PP	39

Figure 3.7: Tensile strength and tensile elastic modulus of neat PP, SiC0CF-PP, SiC1CF-PP, SiC3CF-PP, SiC5CF-PP, and SiC7CF-PP	40
Figure 3.8: Flexural strength and flexural elastic modulus of neat PP, SiC0CF-PP, SiC1CF-PP, SiC3CF-PP, SiC5CF-PP, and SiC7CF-PP	41
Figure 3.9: Tensile strength and tensile elastic modulus of neat PP, 5AlN-PP, 10AlN-PP, 15AlN-PP, 20AlN-PP, 25AlN-PP, 25AlN5Gr-PP, 20AlN10Gr-PP, 15AlN15Gr-PP, and 10AlN20Gr-PP	42
Figure 3.10: Flexural strength and flexural elastic modulus of neat PP, 5AlN-PP, 10AlN-PP, 15AlN-PP, 20AlN-PP, 25AlN-PP, 25AlN5Gr-PP, 20AlN10Gr-PP, 15AlN15Gr-PP, and 10AlN20Gr-PP	43
Figure 3.11: Tensile strength and tensile elastic modulus of neat PP, 5HBN-PP, 10HBN-PP, 15HBN-PP, 10HBN5Gr-PP, 10HBN10Gr-PP, 10HBN15Gr-PP, 10HBN20Gr-PP, 10HBN20Gr1MaPP-PP, 10HBN20Gr2MaPP-PP, and 10HBN20Gr3MaPP-PP.....	44
Figure 3.12: Flexural strength and flexural elastic modulus of neat PP, 5HBN-PP, 10HBN-PP, 15HBN-PP, 10HBN5Gr-PP, 10HBN10Gr-PP, 10HBN15Gr-PP, 10HBN20Gr-PP, 10HBN20Gr1MaPP-PP, 10HBN20Gr2MaPP-PP, and 10HBN20Gr3MaPP-PP.....	45
Figure 3.13: 1000X SEM images A)10AlSiC-PP, B)20AlSiC-PP, C)30AlSiC-PP, D)40AlSiC-PP, E)50AlSiC-PP, and F)60AlSiC-PP	47
Figure 3.14: 1000X SEM images of, A)AO-PP, B)AOG1-PP, C)AOG3-PP, D)AOG5-PP and E)AOG7-PP	48
Figure 3.15: 1000X SEM images of, A)M0-PP, B)M1-PP, C)M2-PP, D)M3-PP, E)M4-PP and F)M5-PP	49
Figure 3.16: 1000X SEM images of, A) SiC0CF-PP, B) SiC1CF-PP, C) SiC3CF-PP, D) SiC5CF-PP and E) SiC7CF-PP.....	51
Figure 3.17: 1000X SEM images of, A) 5AlN-PP, B) 10AlN-PP, C) 15AlN-PP, D) 20AlN-PP, E) 25AlN-PP, F) 25AlN5Gr-PP, G) 20AlN10Gr-PP, H) 15AlN15Gr-PP, and L) 10AlN20Gr-PP.....	53
Figure 3.18: 1000X SEM images of, A)5HBN-PP, B)10HBN-PP, C)15HBN-PP, D)10HBN5Gr-PP, E)10HBN10Gr-PP, F)10HBN15Gr-PP, G)10HBN20Gr-PP, H)10HBN20Gr1MaPP-PP, K)10HBN20Gr2MaPP-PP, and L)10HBN20Gr3MaPP-PP.....	55
Figure 3.19: TGA thermogram of neat PP, 10AlSiC-PP,20AlSiC-PP, 30AlSiC-PP, 40AlSiC-PP, 50AlSiC-PP, and 60AlSiC-PP.....	58
Figure 3.20: DTG thermogram of neat PP, 10AlSiC-PP, 20AlSiC-PP, 30AlSiC-PP, 40AlSiC-PP, 50AlSiC-PP, and 60AlSiC-PP.....	59
Figure 3.21: DTA thermogram of neat PP, 10AlSiC-PP,20AlSiC-PP, 30AlSiC-PP, 40AlSiC-PP, 50AlSiC-PP, and 60AlSiC-PP.....	60
Figure 3.22: TGA thermogram of neat PP, AO-PP, AOG1-PP, AOG3-PP, AOG5-PP and AOG7-PP.....	61
Figure 3.23: DTG thermogram of neat PP, AO-PP, AOG1-PP, AOG3-PP, AOG5-PP and AOG7-PP.....	62
Figure 3.24: DTA thermogram of neat PP, AO-PP, AOG1-PP, AOG3-PP, AOG5-PP and AOG7-PP.....	63
Figure 3.25: TGA thermogram of neat PP, M0-PP, M1-PP, M2-PP, M3-PP, M4-PP and M5-PP.....	64
Figure 3.26: DTG thermogram of neat PP, M0-PP, M1-PP, M2-PP, M3-PP, M4-PP and M5-PP.....	65

Figure 3.27: DTA thermogram of neat PP, M0-PP, M1-PP, M2-PP, M3-PP, M4-PP and M5-PP.....	66
Figure 3.28: TGA thermogram of neat PP, SiC0CF-PP, SiC1CF-PP, SiC3CF-PP, SiC5CF-PP and SiC7CF-PP.....	67
Figure 3.29: DTG thermogram of neat PP, SiC0CF-PP, SiC1CF-PP, SiC3CF-PP, SiC5CF-PP and SiC7CF-PP.....	68
Figure 3.30: DTA thermogram of neat PP, SiC0CF-PP, SiC1CF-PP, SiC3CF-PP, SiC5CF-PP and SiC7CF-PP.....	69
Figure 3.31: TGA thermogram of neat PP, 5AlN-PP, 10AlN-PP, 15AlN-PP, 20AlN-PP, 25AlN-PP, 25AlN5Gr-PP, 20AlN10Gr-PP, 15AlN15Gr-PP, and 10AlN20Gr-PP.....	70
Figure 3.32: DTG thermogram of neat PP, 5AlN-PP, 10AlN-PP, 15AlN-PP, 20AlN-PP, 25AlN-PP, 25AlN5Gr-PP, 20AlN10Gr-PP, 15AlN15Gr-PP, and 10AlN20Gr-PP.....	71
Figure 3.33: DTA thermogram of neat PP, 5AlN-PP, 10AlN-PP, 15AlN-PP, 20AlN-PP, 25AlN-PP, 25AlN5Gr-PP, 20AlN10Gr-PP, 15AlN15Gr-PP, and 10AlN20Gr-PP.....	72
Figure 3.34: TGA thermogram of neat PP, 5HBN-PP, 10HBN-PP, 15HBN-PP, 10HBN5Gr-PP, 10HBN10Gr-PP, 10HBN15Gr-PP, 10HBN20Gr-PP, 10HBN20Gr1MaPP-PP, 10HBN20Gr2MaPP-PP, and 10HBN20Gr3MaPP-PP.....	73
Figure 3.35: DTG thermogram of neat PP, 5HBN-PP, 10HBN-PP, 15HBN-PP, 10HBN5Gr-PP, 10HBN10Gr-PP, 10HBN15Gr-PP, 10HBN20Gr-PP, 10HBN20Gr1MaPP-PP, 10HBN20Gr2MaPP-PP, and 10HBN20Gr3MaPP-PP.....	74
Figure 3.36: DTA thermogram of neat PP, 5HBN-PP, 10HBN-PP, 15HBN-PP, 10HBN5Gr-PP, 10HBN10Gr-PP, 10HBN15Gr-PP, 10HBN20Gr-PP, 10HBN20Gr1MaPP-PP, 10HBN20Gr2MaPP-PP, and 10HBN20Gr3MaPP-PP.....	75
Figure 3.37: DSC thermogram of neat PP, 10AlSiC-PP, 20AlSiC-PP, 30AlSiC-PP, 40AlSiC-PP, 50AlSiC-PP, and 60AlSiC-PP.....	80
Figure 3.38: DSC thermogram of neat PP, AO-PP, AOG1-PP, AOG3-PP, AOG5-PP, and AOG7-PP.....	81
Figure 3.39: DSC thermogram of neat PP, M0-PP, M1-PP, M2-PP, M3-PP, M4-PP and M5-PP.....	82
Figure 3.40: DSC thermogram of neat PP, SiC0CF-PP, SiC1CF-PP, SiC3CF-PP, SiC5CF-PP, and SiC7CF-PP.....	83
Figure 3.41: DSC thermogram of neat PP, 5AlN-PP, 10AlN-PP, 15AlN-PP, 20AlN-PP, 25AlN-PP, 25AlN5Gr-PP, 20AlN10Gr-PP, 15AlN15Gr-PP, and 10AlN20Gr-PP.....	84
Figure 3.42: DSC thermogram of neat PP, 5HBN-PP, 10HBN-PP, 15HBN-PP, 10HBN5Gr-PP, 10HBN10Gr-PP, 10HBN15Gr-PP, 10HBN20Gr-PP, 10HBN20Gr1MaPP-PP, 10HBN20Gr2MaPP-PP, and 10HBN20Gr3MaPP-PP.....	86
Figure 3.43: Storage Modulus of neat PP, 10AlSiC-PP, 20AlSiC-PP, 30AlSiC-PP, 40AlSiC-PP, 50AlSiC-PP, and 60AlSiC-PP.....	90
Figure 3.44: Loss Modulus of neat PP, 10AlSiC-PP, 20AlSiC-PP, 30AlSiC-PP, 40AlSiC-PP, 50AlSiC-PP, and 60AlSiC-PP.....	91

Figure 3.45: Tan δ of neat PP, 10AlSiC-PP, 20AlSiC-PP, 30AlSiC-PP, 40AlSiC-PP, 50AlSiC-PP, and 60AlSiC-PP.....	92
Figure 3.46: Storage Modulus of neat PP, AO-PP, AOG1-PP, AOG3-PP, AOG5-PP and AOG7-PP.....	93
Figure 3.47: Loss Modulus of neat PP, AO-PP, AOG1-PP, AOG3-PP, AOG5-PP and AOG7-PP.....	94
Figure 3.48: Tan δ of neat PP, AO-PP, AOG1-PP, AOG3-PP, AOG5-PP and AOG7-PP	95
Figure 3.49: Storage Modulus of neat PP, M0-PP, M1-PP, M2-PP, M3-PP, M4-PP and M5-PP.....	96
Figure 3.50: Loss Modulus of neat PP, M0-PP, M1-PP, M2-PP, M3-PP, M4-PP and M5-PP.....	97
Figure 3.51: Tan δ of neat PP, M0-PP, M1-PP, M2-PP, M3-PP, M4-PP and M5-PP	98
Figure 3.52: Storage Modulus of neat PP, SiC0CF-PP, SiC1CF-PP, SiC3CF-PP, SiC5CF-PP and SiC7CF-PP.....	99
Figure 3.53: Loss Modulus of neat PP, SiC0CF-PP, SiC1CF-PP, SiC3CF-PP, SiC5CF-PP and SiC7CF-PP	100
Figure 3.54: Tan δ of neat PP, SiC0CF-PP, SiC1CF-PP, SiC3CF-PP, SiC5CF-PP and SiC7CF-PP	101
Figure 3.55: Storage Modulus of neat PP, 5AlN-PP, 10AlN-PP, 15AlN-PP, 20AlN-PP, 25AlN-PP, 25AlN5Gr-PP, 20AlN10Gr-PP, 15AlN15Gr-PP, and 10AlN20Gr-PP	102
Figure 3.56: Loss Modulus of neat PP, 5AlN-PP, 10AlN-PP, 15AlN-PP, 20AlN-PP, 25AlN-PP, 25AlN5Gr-PP, 20AlN10Gr-PP, 15AlN15Gr-PP, and 10AlN20Gr-PP	103
Figure 3.57: Tan δ of neat PP, 5AlN-PP, 10AlN-PP, 15AlN-PP, 20AlN-PP, 25AlN-PP, 25AlN5Gr-PP, 20AlN10Gr-PP, 15AlN15Gr-PP, and 10AlN20Gr-PP	104
Figure 3.58: Storage Modulus of neat PP, 5HBN-PP, 10HBN-PP, 15HBN-PP, 10HBN5Gr-PP, 10HBN10Gr-PP, 10HBN15Gr-PP, 10HBN20Gr-PP, 10HBN20Gr1MaPP-PP, 10HBN20Gr2MaPP-PP, and 10HBN20Gr3MaPP-PP	105
Figure 3.59: Loss Modulus of neat PP, 5HBN-PP, 10HBN-PP, 15HBN-PP, 10HBN5Gr-PP, 10HBN10Gr-PP, 10HBN15Gr-PP, 10HBN20Gr-PP, 10HBN20Gr1MaPP-PP, 10HBN20Gr2MaPP-PP, and 10HBN20Gr3MaPP-PP	106
Figure 3.60: Tan δ of neat PP, 5HBN-PP, 10HBN-PP, 15HBN-PP, 10HBN5Gr-PP, 10HBN10Gr-PP, 10HBN15Gr-PP, 10HBN20Gr-PP, 10HBN20Gr1MaPP-PP, 10HBN20Gr2MaPP-PP, and 10HBN20Gr3MaPP-PP.....	107
Figure 3.61: Thermal conductivity and thermal effusivity values of neat PP, 10AlSiC-PP, 20AlSiC-PP, 30AlSiC-PP, 40AlSiC-PP, 50AlSiC-PP and 60AlSiC-PP	109
Figure 3.62: Thermal conductivity and thermal effusivity values of neat PP, AO-PP, AOG1-PP, AOG3-PP, AOG5-PP, and AOG7-PP	110
Figure 3.63: Theoretical representation of alumina-G plaques orientation in to PP matrix and effects on the thermal conductivity measurement.....	111
Figure 3.64: Thermal conductivity and thermal effusivity values of neat PP, M0-PP, M1-PP, M2-PP, M3-PP, M4-PP, and M5-PP	112

Figure 3.65: Thermal conductivity and thermal effusivity values of neat PP, SiC0CF-PP, SiC1CF-PP, SiC3CF-PP, SiC5CF-PP, and SiC7CF-PP.....	113
Figure 3.66: Thermal conductivity and thermal effusivity values of neat PP, 5AlN-PP, 10AlN-PP, 15AlN-PP, 20AlN-PP, 25AlN-PP, 25AlN5Gr-PP, 20AlN10Gr-PP, 15AlN15Gr-PP, and 10AlN20Gr-PP.....	114
Figure 3.67: Thermal conductivity and thermal effusivity values of neat PP, 5HBN-PP, 10HBN-PP, 15HBN-PP, 10HBN5Gr-PP, 10HBN10Gr-PP, 10HBN15Gr-PP, 10HBN20Gr-PP, 10HBN20Gr1MaPP-PP, 10HBN20Gr2MaPP-PP, and 10HBN20Gr3MaPP-PP	115
Figure 3.68: Surface electrical resistivity values of neat PP, 10AlSiC-PP, 20AlSiC-PP, 30AlSiC-PP, 40AlSiC-PP, and 50AlSiC-PP	116
Figure 3.69: Surface electrical resistivity values of neat PP, SiC0CF-PP, SiC1CF-PP, SiC3CF-PP, SiC5CF-PP, and SiC7CF-PP	117
Figure 3.70: Surface electrical resistivity values of neat PP, M0-PP, M1-PP, M2-PP, M3-PP, M4-PP and M5-PP	118
Figure 3.71: Surface electrical resistivity values of neat PP, AO-PP, AOG1-PP, AOG3-PP, AOG5-PP, and AOG7-PP.....	119
Figure 3.72: Surface electrical resistivity values of neat PP, 5AlN-PP, 10AlN-PP, 15AlN-PP, 20AlN-PP, 25AlN-PP, 25AlN5Gr-PP, 20AlN10Gr-PP, 15AlN15Gr-PP, and 10AlN20Gr-PP.....	120
Figure 3.73: Surface electrical resistivity values of neat PP, 5HBN-PP, 10HBN-PP, 15HBN-PP, 10HBN5Gr-PP, 10HBN10Gr-PP, 10HBN15Gr-PP, 10HBN20Gr-PP, 10HBN20Gr1MaPP-PP, 10HBN20Gr2MaPP-PP, and 10HBN20Gr3MaPP-PP	121

ABSTRACT

MANUFACTURING AND CHARACTERIZATION OF THERMAL CONDUCTIVE POLYMERIC COMPOSITE MATERIALS

Electronic industry is growing dramatically in the last quarter of the century. Recent advances in electronics industry enable the miniaturization of micro transistors and the integration of more transistors into the electronic devices, resulting in a higher performance device. However, this condition increases the heat flow in the electronic devices. The performance of electronic devices depend on the working temperature, for this reason, it is important to remove the heat produced in the device as fast and efficiently as possible in order to hold the system temperature of the electronic device at the required temperature. Polymers, with low thermal and electrical conductivity and lightweight, can be used to address the problem. However, the thermal conductivity of polymers can be increased by loading high thermal conductive materials like ceramic, carbon and metal-based or mixtures of each others. In this thesis, for production of high thermal conductive and electrically insulator composites, aluminum-silicon carbide, alumina/graphene (G), silicon carbide (SiC)/carbon fiber (CF), hexagonal boron nitride (HBN)/graphite (Gr), aluminum nitride (AlN)/graphite hybrid filler prototype mixtures, and five different silane modified alumina particles were manufactured by the high speed thermokinetic mixer with polypropylene (PP) matrix at different ratios. All composites thermal properties investigated by differential scanning calorimetry, simultaneous differential thermal analyzer and through plane thermal conductivity measurement systems. Mechanical properties of composites were analyzed with universal mechanical test machine. Viscoelastic behaviors of composites tested with dynamical mechanical thermal analysis system. Texture of composites and fillers orientation into the PP matrix was investigated with scanning electron microscopy. Electrical resistivity of composites was measured with surface electrical resistivity measurement system. As a result, PP matrix through plane thermal conductivity increased with the all-composites. It was observed that the mechanical properties of the composite were improved by the addition of surface modification materials and carbon-based materials to the PP matrix.

Keywords: Composite, Thermal conductivity, Polypropylene, Electronic packing, Electrical resistivity.

ÖZET

TERMAL İLETKEN POLİMERİK KOMPOZİT MALZEMELERİN ÜRETİLMESİ VE KARAKTERİZASYONU

Elektronik endüstrisi yüzyılın son çeyreğinde önemli ölçüde artış göstermiştir. Elektronik endüstrisindeki son gelişmeler, mikro transistörlerin minyatürleştirilmesini ve daha fazla transistörün elektronik cihazlara entegrasyonu ile daha yüksek bir performans sağlamaktadır. Bununla birlikte, bu durum, elektronik cihazlarda ısı akışını arttırmaktadır. Elektronik cihazların performansı çalışma sıcaklığına bağlıdır, bu nedenle, elektronik cihazın sistem sıcaklığını gerekli ısıda tutabilmek için, cihazda üretilen ısının mümkün olduğunca hızlı ve verimli bir şekilde uzaklaştırılması önemlidir. Termal ve elektriksel iletkenliği düşük olan ve hafif olan polimerler problemi çözmek için kullanılabilir. Bununla birlikte, polimerlerin düşük termal iletkenliği, seramik, karbon ve metal bazlı veya birbirlerinin karışımları gibi yüksek termal iletken malzemeler yükleyerek artırılabilir. Bu tezde, yüksek ısıl iletken ve elektriksel yalıtkan kompozitlerin üretimi için alüminyum-silisyum karbür, alümina / grafen (G), silisyum karbür (SiC) / karbon fiber (CF), hekzagonal bor nitrür (HBN) / grafit (Gr) alüminyum nitrür (AlN) / grafit hibrit dolgu prototip karışımları ve beş farklı silan modifiye alümina partikülü farklı oranlarda polipropilen matriks ile yüksek hızlı termokinetik karıştırıcıda üretilmiştir. Diferansiyel taramalı kalorimetre, eşzamanlı diferansiyel termal analizör ve düzlemsel termal iletkenlik ölçüm sistemi ile incelenen tüm kompozitlerin termal özellikleri araştırıldı. Kompozitlerin mekanik özellikleri, evrensel mekanik test makinesi ile analiz edildi. Kompozitlerin viskoelastik davranışları, dinamik mekanik termal analiz sistemi ile test edildi. Taramalı elektron mikroskopu tekniği ile kompozit ve dolgu malzemelerinin PP matriksindeki yönelimi incelendi. Yüzey elektrik direnç ölçüm sistemi ile kompozitlerin elektriksel direnci ölçüldü. Sonuç olarak, düzlemsel ısı iletkenliği ile PP matrisi, tüm kompozit tariflerle arttırıldı. PP matrisine ilave yüzey modifikasyon maddeleri ve karbon bazlı malzeme ilavesiyle kompozitin mekanik özelliklerinin geliştiği görüldü.

Anahtar kelimeler: Kompozit, Termal iletkenlik, Polipropilen, Elektronik paketleme, Elektriksel direnç.

1. INTRODUCTION

In the past, home furniture and industrial products were made of wood, metal, glass, latter, and rubber. Since the 1900s, the use of these materials has become widespread due to the fact that they have experienced innovative developments in the polymer sector, they are easier to shape, easy to manufacture, lightweight, high chemical resistance, excellent insulation and low cost [1; 2; 3]. However, many of the polymers have low thermal conductivity and are thermally insulated [4; 5; 6]. Today, in modern technology, aerospace, automobile, sports equipment, underwater applications, transportation applications, the electricity industry and so on (thermally conductive, electrically conductive, anti-corrosive, high impact resistance, antimicrobial, etc.) for use in places [7; 8; 9; 10; 11]. Composites formed by the combination of metals, ceramics, and polymers have begun to meet the needs of many industries. For this reason, the areas of composite materials are developing considerably in order to meet the needs of producers and customers.

Electronic industry is growing dramatically in the last quarter of a century. Recent advances in electronics industry enable the miniaturization of micro transistors and the integration of more transistors into the electronic devices, resulting in a higher performance device [12; 13]. However, this condition not only increases the heat flow in the electronic device but also rises of the power consumption. The reliability and performance of electronic devices depend on the working temperature of the junction point, which shows exponentially small variations (10-20 °C), which causes the lifespan of the electronic device to reduces by two times [13; 14]. For this reason, it is important to remove the heat produced in the device as fast and efficiently as possible in order to hold the system temperature of the electronic device at the required temperature [15; 16; 17].

The ability of the material heat management is directly related to the dependability, performance and miniaturization potencies of the electronic devices. Excess heat radiation by high power densities increases the working temperature of the device, decreases its performance and brings to hardware failure [18; 19]. Heat management

is remarkable as a study issue. The relationship of thermal conductivity to heat waste is essential for this kind of application and heat transfer of material is the major mechanism for the cooling electronic devices [20; 21]. High electrical resistance is important to prevent leakage current which can generate a dysfunctional circuit [22; 23]. Because the heat generated by electronic devices and circuits must be destroyed to increase reliability and prevent malfunctions. Heat management is applied to cooling systems, packaging, and chipboard. Choice of material for the heat management applications; balance function, performance, manufacturing, safety, and cost have to evaluate all together [24; 25; 26; 27].

High thermal conductive and high electrical resistivity materials are needed for electronic packing. Other necessities for electronic packaging materials cover, but are not limited to, low weight, thermal misfire, small size, ease of production, and low cost [28]. Thermal misalignment between two different materials or between the material and the surroundings is necessary to defense bond failure, delamination, and bending. The last recommendation is that any possible 3D material, such as polymeric composite materials, can be shaped using the material injection molding method [29; 30]. The material to be used in this purpose must have high thermal conductivity and low electrical conductivity (high electrical resistance). With the high thermal conductivity and lightness of aluminum is the first choice for thermal management material. Recently, high thermal conductivity polymers and polymer-based composites have gained importance as an alternative to aluminum. Polymers and composites have the advantages of lightness compared to aluminum, easy fabrication, and design flexibility without a second process, energy consumption and low cost [31; 32; 33; 34; 35; 36; 37; 38; 39]. Some of these polymers and composites can exchange metals and ceramics in heat transfer devices and systems due to cost and energy savings. Some fillers and reinforcements such as carbon fiber (CF), carbon black (CB), graphene (G), carbon nanotubes (CNTs), ceramic powders and metal particles have been used to increase thermal conductivity, corrosion, strength, stiffness, abrasion resistance and other properties in polymer matrix based composites [40; 41; 42; 43]. In addition, polymer composites may exhibit properties such as insulation depending on properties or electrical conductivity such as diameter, distribution, the ratio of the polymer reinforcement material loaded to the polymer matrix.

Electronic components as like as light emitting diodes (LEDs) in the automotive industry have contributed to the need for heat management. In addition, heat sinks are used high voltage semiconductors and optoelectronic devices for heat management [44].

Aluminum is the first choice for thermal management material when Aluminum has high thermal conductivity and weightless properties. Recently, high thermal conductivity polymer composites have gained popularity as an alternative to aluminum. Polymer composites have the advantages of low weight compared to aluminum, design flexibility, easy manufacturing without another process and cheap [45]. Aluminum has a thermal conductivity of 200 W/m.K and the thermal conductivity of polymer composites is limited to 2 - 40 W/m.K. [46]. However some conditions, average thermal conductivity could be enough for some methods. Alumina (Al_2O_3), Aluminum nitride (AlN), Silicon carbide (SiC), and boron nitride (BN) show high thermal conductivity and low electrical conductivity into the polymer matrix.

Generally, thermal radiation in protective devices is prevented by the use of embedded heat sinks [47]. The shrinkage of the component parts increases the tensile stresses very much and needs more efficient heat removal from the device. If a suitable solution cannot be found, the inside temperature of the device will rise to the safe level. But, embedded heat sinks are very expensive, limited in fine packaging and sensitive to the thermal fracture. Also embedded heat sink thermal desorption is usually obtained by the use of epoxy molding components with silica [48]. The inclusion of silicon in the epoxies is intended to improve the thermal properties of the intended composite as well as to reduce the thermal expansion coefficient [49]. Silica has a low thermal conductivity of 1.5 W/m.K, which has a very little effect on thermal management. The evolutions in technology have once again resulted in higher power density and increased heat excesses due to the formation of epoxy-silica composites for electronic component parts.

In the search for an alternative, many solutions have been considered above the existing values. Materials comprising metal-matrix composites (MMCs) and polymer-matrix composites (PMCs), which are important for electronic packaging and which have been previously mentioned, are available. Rather than completely replacing existing heat wells, their development is a shorter, more achievable aim.

As can be seen in Figure 1.1, it can be joined with a standard aluminum heat sink to cut down the total conductivity of the insulating material. Recently, thermal insulation pads made of mica are used for electrical insulation in the mounting of electronic parts to heat sinks. Although these materials are electrically insulated, they have a low thermal conductivity of about 0.40 W/m.K and 0.70 W/m.K. By using materials with higher thermal conductivity instead of mica, the heat removed through the heat sink may be upgraded in a serious manner.

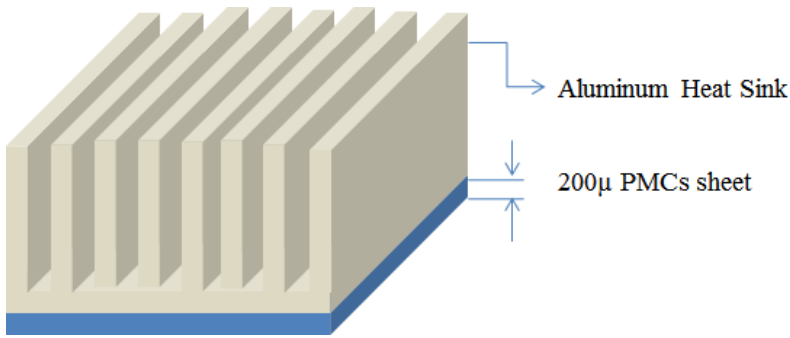


Figure 1.1: Modified heat sink scheme with electrically insulating composite.

Electronic packaging functionality may be searched by four basic fundamentals: signal distribution, heat removing, package protection and power waste [28]. This wide range of uses needs that any material used for electronic packaging has higher-up chemical, mechanical, thermal and environmental properties.

Multifunctional materials have an elevated potential for this application since they have improved to performance in terms of the missions mentioned. This approach suggests a single substance that offers many functions within the synergy that developed the total capacity of the specific parts. Decreasing the size, weight, cost, and complexity can be when yield and versatility are achieved. Electronic packaging requires structural materials, mechanical and chemical barrier, and multifunctional materials to supply thermal management. There are many different factors that cause electronic degradation such as moisture, pollutants, mobile ions, radiation (like alpha particles, gamma photons, and x-rays), and hazardous conditions including corrosion and oxidation [50; 51; 52]. Electronic packaging should be isolated from all adverse environmental effects and provide long-term reliability. Multifunctional materials have important properties, so optimization of the desired properties should be investigated to obtain the ideal property.

As a result of always increasing power concentration, producers of semiconductor electronic materials look for new multifunctional materials to change or develop existing standards. Many alternatives including metal-matrix composites (MMCs) [53] and polymer-matrix composites (PMCs) have been suggested to design existent heat sink materials [54]. These particle-reinforced isotropic composites, which have high mechanical properties, low linear dilatation ratio, and high thermal conductivity properties, have many essential properties related to electronic packaging [55]. Al-SiC [56], Al-Si [57], Cu-diamond [58], Al-diamond [59], Cu-W [60] and Cu-Mo [61], some of the MMCs have been evaluated. Although MMCs have many suitable properties, they limit the use of low electrical resistivity of composites as electronic packaging material.

Polymers are a standard component of many electronic packaging materials (Figure 1.2). These materials may be used as interphase dielectrics, protective coatings, mold adhesives, package blanks and passivation layers on an integrated circuit (IC). Recently, there is an increasing interest in the development of PMCs for electronic packaging uses.

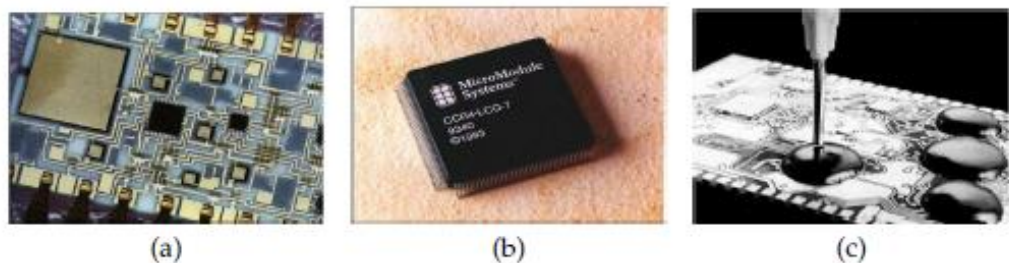


Figure 1.2: Electronic packaging examples; (a) IC applications, (b) Microchips, (c) Liquid epoxy encapsulation.

Temperature elevation during operation of the electronic device is generally dissipated by thermal conduction. Among the various ways used for heat dissipation, devices have heat sinks or heat radiators with high thermal conductivity (HTC) and low thermal expansion coefficient. However, where there is good thermal contact with the device and limits the use of high thermal conductivity to dissipate heat because of heat wells used for superficial thermal resistance arising from the surface roughness of both the heat sink. The surface roughness is usually observed in wavy

surface shapes where up to 98% of the interfaces are separated by air gaps. Improper surface contact reduces the heat dissipation capacity and confines air gaps between the surfaces due to the low thermal conductivity of the air ($k_{\text{air}} = 0.026\text{Wm}^{-1}\text{K}^{-1}$). A method for decreasing the thermal contact resistance between two surfaces and for providing an efficient heat path as shown in Figure 1.3 is generally the use of the thermal interface materials (TIMs).

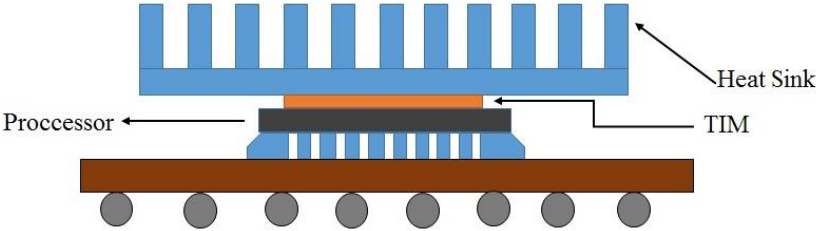


Figure 1.3: The surface roughness between the heats well and the device is measured by TIM.

TIMs are separated as thermal greases, thermal pads, phase change materials, and solders [62; 63; 64; 65; 66]. In all of the TIM classifications mentioned, thermal pads are heavily used for cooling electronic devices such as low power chipsets and mobile processors [33; 67]. Thermal pads are generally made of ceramic, metal or carbon reinforced viscoelastic polymers with a thickness of 100-2000 μm . Advantages of rubbery thermal pads are that they are easy to use and can compress up to 25% of their own thickness, which allows the material to absorb tolerance deviations in mounting [68].

Recently, increased attention has been shown due to thermal pads, ease of use and high compressibility [69]. TIMs are made from high thermal conductivity and dielectric fillers such as aluminum nitride (AlN), boron nitride (BN), silicon carbide (SiC) and aluminum oxide (Al_2O_3) [70; 71]. An ideal TIM should not only have high thermal conductivity but also low thermal expansion [72]. In addition, the material has to be easily deformable with small pressure in all of the asymmetric surfaces of the areas matched.

Thermal conductivity and electrically insulating PMCs are important in electronic packaging because the composites can prevent thermal fatigue and provide excellent heat dissipation. Fillers such as diamond, BN, AlN, SiC, and Al_2O_3 are used as

thermally conductive but dielectric polymer materials. Other polymers, such as polyethylene (PE), poly (vinyl chloride) (PVC), high-density polyethylene (HDPE), linear low-density polyethylene (LLDPE), polypropylene (PP) and polyamide (PI) use in a polymer matrix.

Table 1.1: Thermal, mechanic and electrical properties of some kinds of thermal conductive filler's [73].

	CBN [74]	HBN [75]	Al₂O₃ [76]	SiO₂ [75]	AlN [77]	ZnO [78]	SiC [79]	Graphene [80]	Carbon Fiber [81]	Graphite [80]
Thermal Properties										
Thermal Conductivity (W/m.K)	130	600	30	1.4	260	54	60	500-600	1.5 (in plane)	2-800
Heat Capacity(J/g.K, at 25°C)	14.8	19.7	0.798	0.689	0.734	0.523	1.18	2.1(in plane)	1.13	0.721
Theoretical Density (Kg/m³)	3450	2100	3980	2200	3260	5640	3210	2250	1700	2260
Electrical Properties										
Dielectric Constant (F/m)	1.8	6.2	9.7	3.8	8.8	9.8	9.7	3.3	3.2	10-15
Volume Resistivity (ohm⁻¹)	10 ¹⁴	10 ¹⁴	10 ¹⁴	10 ¹⁴	10 ¹⁴	10 ⁷	10 ¹²	31	10 ⁴	3
Mechanical Properties										
Thermal Exption Coefficiant (ppm/K)	1.2	-2.7	6.7	0.5	4.4	0.7	7.9	-8.0	0.3	-1.5
Elastic Modulus (GPa)	400	36.5	340	72	400	12	410	130.5	228	34
Knoop Hardness (Kg/mm²)	45	-	1200	500	1200	387	2400	600	275	300

There are few ceramics, carbon-based, and metallic fillers that increase the electrical and thermal conductivity of thermosets and thermoplastics. On the other side, there is some ceramic filler such as Al_2O_3 , AlN , hexagonal boron nitride (HBN), cubic boron nitride (CBN), silicon (SiO_2) and zinc oxide ZnO , which enhance the electrical conductivity of polymers, which enhance thermal conduction but are desirable in somebody applications. Except for HBN, all these alternative fillers are abrasive and can damage the processing equipment during manufacturing. On the contrary, HBN is a soft, slippery material and can be compounded with polymers, minimal effect on the processing equipment. Table 1.1 gives the properties of filler materials properties which were obtained from various sources.

Boron nitride is another important advantage of other carbon-based reinforcements in white color. It looks cleaner in the production environment and provides a wider range of colors for plastics. The color limit in graphite and carbon black plastics is limited because the plastic composites made of these materials are between black or dark gray.

A lot of studies have been done in this area. Zhou et al. have focused on the thermal conductivity of polyethylene (PE) / silicon nitride (Si_3N_4) and/or silicon carbide whiskers (SiC_w). Use of Si_3N_4 / SiC_w in combination with 9: 1 weight ratio improves thermal stability and reduces thermal expansion coefficient [82]. In the other study; The effect of the content and particle size of BN supplements on the thermal conductivity and mechanical properties of silicone rubber [83]. The results show that at the constant reinforcement loading level, bigger BN particles have higher thermal conductivity than small ones. The use of a mixture of small and big BN particles in silicon rubber results in better thermal conductivity. This behavior is associated with high packing density and ease of formation of conductive paths.

Sim et al. were studied the thermal properties of silicon filled with thermally conductive but electrically insulating Al_2O_3 or ZnO filler's as a thermal pad [33]. The effect of thermal conductivity and coefficient of thermal expansion (CTE) on micron-sized Al_2O_3 or ZnO supplements made with poly (dimethylsiloxane) (PDMS) was investigated. As a result, it has been observed that the thermal conductivity of the thermal pads increases with the increasing of Al_2O_3 and ZnO , and the CTE decreases. Thermogravimetric analysis (TGA) has shown that it improves the

thermal stability of PDMS by the addition of Al_2O_3 or ZnO reinforcing materials [33]. Moreover, the ZnO -reinforced PDMS exhibits higher thermal performance than Al_2O_3 due to its better thermal conductivity.

Kemaloğlu et al. mechanical and morphological properties of the effects of the level of loading of BN particles in micro or nano-size [83]. BN was used in 3-micron size and 2 nano size in different sizes and shapes. Generally, the BN particles added to the PDMS matrix increase the modulus, hardness and thermal conductivity while decreasing the tensile strength, breaking strain, CTE values. Nano size reinforcements have a greater effect on the tensile properties of composites at any loading level than micron size BNs. The aspect ratio of the reinforcement is very effective in achieving high thermal conductivity in composite systems. It has been observed that the dielectric constants of the composites change between dielectric constants of PDMS and BN [83].

Yu et al. the thermal conductivities of polystyrene (PS) / AlN composites were investigated by AlN reinforcement particles surrounding the PS matrix particles with a specific distribution of reinforcement within the composite [84]. The effect of the size and temperature of the PS particles on the content was investigated. As a result, it has been observed that the thermal conductivity of the 20% by volume AlN reinforced PS composite has 5 times higher thermal conductivity than the pure PS. Large particles for the PS matrix increased the thermal conductivity of the composite. In order to determine the thermal conductivity of the composite, they investigated the relationship between composites and AlN reinforcements in two models [84].

Xu et al. polyvinylidene fluoride (PVDF) or AlN and/or SiC buried in an epoxy matrix [71]. The PVDF composites showed high thermal conductivity, with 60% of the volume being reinforced in different shapes, with the same size ($7\ \mu\text{m}$), whiskers volume ratio: particles, 1: 25.7. In short, compared to the use of whiskers or particles alone, AlN whiskers and AlN particles have been found to increase thermal conductivity and lower thermal expansion coefficient when combined properly. Compared to neat PVDF, AlN reinforced composites increase tensile strength while reducing module and ductility. AlN is dissolved in water-immersed PVDF composites[71].

Hong et al. polygonal AlN and planar BN combination reinforced epoxy composites were investigated to increase the thermal conductivity of the composites [85]. The dual distribution of AlN / BN composites indicated that they have a strong influence on the thermal conducting paths by increasing the packing efficiency and the interfacial resistance of the particles. The highest thermal conductivity of AlN: BN = 1: 1 volume reached 8.0W/m.K.

Cho et al. This study reveals that BN besides AlN is also a high thermal conductivity and excellent electrical insulator. However, AlN reacted easily with moisture in the air to form aluminum oxide (Al_2O_3) and stated that it caused deterioration in thermal conductivity. BN is more chemically stable than AlN. The in-plane thermal conductivity of HBN is 60 W/mK and the out-of-plane thermal conductivity 3 W/m.K is 20 times [86].

Zhou et al. investigated the effect of size and content of reinforcements on BN reinforced high-density polyethylene (HDPE) thermal properties [87]. Thermal conductivity, thermal diffusivity, and heat capacities are increased by the amount of BN. In the case of BN reinforced composites in the same context, thermal conductivity and thermal diffusion are determined to be dependent on the size of BN. The combination of BN particles in different sizes showed higher thermal conductivity than the combination of BN particles in one dimension.

Li et al. investigated the effect of hybrid BN ceramics combined with binary particle sizes on the thermal conductivity of novalac resin composites. Large BN particle reinforced novalac resin composites showed higher thermal conductivity than small BN particles. The BN content significantly increased the thermal conductivity. Combination reinforcement of 0.5 μm and 15 μm BN particles at 2: 1 weight ratio showed the highest thermal conductivity of this work. The Maxwell-Euchen model can be used to determine the thermal conductivity of composites whose weight is less than 70% by weight [88].

Ishida et al. polybenzoxazine / 88 wt% BN composites were tested on 32.5W/mK [89]. The binary particle size combination is effective in improving the packing density of the BN in the resultant composite by increasing the thermal net. As the content of BN increases, the water absorption decreases.

Zhou et al. describe the relation between the thermal conductivity of HDPE / BN composites and the diffusion state of BN particles in composites. The content and size of the BN have an important effect in improving the thermal conductivity of the composites by affecting the dispersibility of the BN in the composite. The BN particles and the alumina short fiber hybrid reinforcement system exhibited higher thermal conductivity than the composites containing uniform reinforcement [90].

Zhou et al. the thermal conductivity of BN-doped silicon composites at different sizes in the same context has higher thermal conductivity than single-particle-sized BN-reinforced composites [91]. For this reason, it is stated that the BN particles are the effect on the thermal conductivity and other properties of the composites. In addition, the combination of BN particles of different sizes, and the combination of differently shaped reinforcements, significantly increased the thermal conductivity of the composites compared to the uniform reinforced composites.

Xie et al. AlN with high thermal conductivity, low dielectric constant and low cost as ceramic reinforcements [92]. As a polymer, polyimide (PI) packing material with low dielectric constant and loss, low thermal expansion, high strength and thermal stability properties, circuit boards and a wide area as a dielectric are used.

In previous studies, Chen et al. [93; 94; 95] studied the preparation and properties of the polyimide-AlN nanocomposite. As the polyimide matrix AlN reinforcement was added, the thermal conductivity increased significantly and the coefficient of thermal expansion decreased significantly. However, the dielectric and electrical properties of the composites have not been investigated. Xie et al. observed that the thermal properties of the polyimide-AlN composite in the polyimide matrix improved significantly without loss of dielectric properties [92]. The results showed that the thermal stability and thermal conductivity of the composite increased with increasing AlN amount, the dielectric constant decreased slightly and the electrical properties changed at a low level. It has also been observed that the dielectric and thermal conductivity properties are also influenced by the binder content. In addition, the thermal conductivity and dielectric properties of the investigated composites follow classical composite theories.

Polymers characteristically have low electrical conductivity and are often used where isolators are required [96]. Polymers, for example, are used in flexible coatings of

electrical wires and cables [97]. They can also be used in printed circuit boards, transformers, end-fittings, and capacitors [98; 99; 100].

One of the most commonly used methods for developing thermal conductivity for polymer composites is to form a continuous conduction network between the particles along the matrix material. By forming a thermally conductive stable path between the particles, the composite can improve the heat dissipation feature. Significant improvements in thermal conductivity can be seen when the leakage threshold is reached. This threshold corresponds to the point where the reinforcement particles contact the other [31].

In polymeric composites, it is known that thermal conductivity is improved by applying 3 different techniques:

- The first is the use of thermally conductive reinforcing materials by forming continuous nets into the matrix [101; 102; 103; 104; 105; 106].
- The other method is to reduce the number of thermal resistance connections between adjacent reinforcement particles using large size particles [107; 108].
- Finally, the choice of reinforcing materials, which are less superficial, can reduce the thermal contact resistance between interacting reinforcing materials [36; 109]. In addition, it is proposed to use low molecular weight polymers to improve the wetting and reinforcement-matrix adhesion [110; 111].

All these suggestions provide a good adhesion between the polymer and the reinforcement otherwise, the air gaps reduce the efficiency of the k-value. Thus, the compatibility between the polymer and the reinforcing material is also suggested to reduce the formation of voids [112].

In the context of polymeric composites, the amount of reinforcement component significantly improves the electrical conductivity. This event is called leakage threshold. At this point, the reinforcing particles interact with each other by forming a connected 3-dimensional conductive network throughout the composite. The internal connection of the particles provides an uninterrupted path through the material to the electrons. In situations where conductive polymer composites (CPC) are the target material, the reinforcement component must exceed this threshold. In

the context of this application, if the polymer matrix of the electrically conductive reinforcements is added, the amount must be below the leakage threshold to provide high electrical resistance [113].

Thermal management has gained great importance with the developing electronic industry and microprocessor technologies. The removal of heat from a system that is turned on in a transistor or semiconductor chip application is a factor that directly affects the system's operating efficiency. Thermal management is crucial in such applications where the energy is converted to heat, to prevent the basic materials that make up the devices from being damaged.

Many studies in the literature have suggested that ceramic fillers of very different types may be suitable for electronic packaging applications because their electrical conductivity is poor but their thermal conductivity is good. It is in the models and studies about the distributions and orientations of the thermally conductive particles in the polymer matrix.

Lots of polymers and their derivatives have been used for thermal conductive materials application areas. Polymer prices and reinforcement materials limitations were changed cost efficient and easy manufacturing polymers.

Commodity polymers are found in our daily life usage from low-value items such as plastic bags to high-value items which don't require precise and high mechanical properties. Those polymers exhibit relatively low mechanical properties and cost. The range of products includes plates, cups, carrying trays, medical Trays, containers, seeding trays, printed material and other disposable items. Commodity polymers are polymers that are used in high volume and a wide range of applications such as photographic and magnetic tape, clothing, beverage, trash containers, a film for packaging, and a variety of household products where mechanical properties and service environments are not critical. The commodity polymer structure is specified by the conformation and the configuration. The chain configuration and orientation are formed during polymerization [114; 115]. Thermoplastic polymers consist of long, uncross-linked chain molecules. During processing, these chain molecules are easily oriented, which leads to the anisotropy of the mechanical and other properties.

Examples of commodity polymers are Polyethylene (PE), Polypropylene (PP), Polystyrene (PS), Poly(vinyl chloride) (PVC), Polytetrafluoroethylene (PTFE),

Poly(methyl methacrylate) (PMMA), Poly(ethylene terephthalate) (PET), and more. Thermal conductivity and the other specific properties of some commodity polymer are given in Table 1.2.

Table 1.2: Commodity polymers, some physical and thermal properties are given from Netzsch instrument thermal analysis of polymers chard.

Polymer	Young Module (MPa)	Thermal Conductivity (W/m.K)	Density (Kg/m³)	Glassy transition Temp. T_g (°C)	Melting Temp. T_m (°C)	Specific heat capacity at 25°C (J/g.K)	CLTE (ppm/K)	Decomposition Temp. T_D (°C)
Poly ethylene (PE)	500-1000	0,33-0,45	850-900	-78	105-115	1,8-2,5	190-250	475-490
High density polyethylene (HDPE)	600-1400	0,33-0,53	940-960	<-100	125-135	1,8-2,7	200-250	487-498
Low density polyethylene (LDPE)	200-400	0,3-0,34	910-930	-30 to -10	100-110	1,8-3,4	400	487-498
Linear low density polyethylene (LLDPE)	250-700	NA	910-940	-125 to -70	122-127	NA	200	475-485
Polypropylene (PP)	1300-1800	0,17-0,25	900-910	-20 to +20	165-175	1,8	130-180	447
Polyvinylchloride (PVC)	2700-3000	0,126-0,293	1380-1550	80-90	NA	0,84-1,17	60-80	290-460
Poly(methyl methacrylate) (PMMA)	3100-3300	0,16-0,25	1150-1190	Syn. 115 atac. 105 isotac. 45	NA	1,45-1,47	90-110	360-390
Polyethylene-co-vinylacetate (EVA)	7-120	0,35	920-950	-40+20	30-110	2,3	160-200	480
Polyethylene terephthalate (PET)	2100-3100	0,24	1330-1450	70-85	245-260	1,04-1,17	80-100	425-440
Polystyrene (PS)	3100-3300	0,14-0,18	1050	80-105	NA	1,3	50-70	443
Polytetrafluoroethylene (PTFE)	400-750	0,23-0,25	2130-2230	120-130	325-335	1,0	100-150	576-585

The filler system designs were important for developing new type of composites for further applications into the electronic industry. Virgin polymers have many limitations for electronic industry. Polymeric composites were very favorable way for improving polymer matrix properties cheaper and easier.

In our country, polymer derivatives produce and sell abundantly but commercial prices of these materials are low and cost reliability is weak. For increasing cost efficiency and benefit of producing polymers, new composites were designed in this study. Aim of thesis is inspection of hybrid filler systems effects on thermal and physical properties of the polymer matrix based composites. In the literature, different kinds of filler loaded polymer matrixes had been studied in lots of paper. However, different types of fillers combination were not attempted in polymer that is polyolefin-based matrixes like PE, PP and etc.

The filler system designs were important for developing and understanding of heat transfer into the polymer matrix. Nano particles and their thermal properties inspect into the ceramic particles loaded polymer matrix. Metal-ceramic composites thermal and mechanical effects investigated into the polymer matrix. The effects of surface modification researched on to the thermal and mechanical properties polymer matrix composites. Although, ceramic and carbon based materials thermal and mechanical effects into the polymer matrix find out with this study.

Polymer matrix was chosen PP for new electronic packing material in this study and thermal, mechanical, viscoelastic, electrical properties was analyzed. PP had low price, low electrical conductivity and low density for light equipment applications, PP preferred for these properties.

2. EXPERIMENTS

2.1 Materials

2.1.1 Polypropylene (PP)

PP was supplied from PETKIM Petrochemical Company in Izmir-TURKEY. PP MH418 was used as a matrix material at this these. PP MH418 properties were given in Table 2.1.

Table 2.1: Chemical and physical properties of PP MH418.

Experiment Name	Unit	Value	Test Method
Melt flow index	g/10min	4.0-4.6	ASTM D1238
Fisheye test	Number	Max 6	TM 125
Dirty	Number/gr	Max 5	TM 113
Color test	Unit less	1.8	Hunter-Lab. CQ
Tensile Strength	Kg/cm ²	430	ASTM D638

2.1.2 Aluminum 2017 alloy and silicon carbide (SiC) metal-ceramic composites

Al 2017 alloy and SiC ceramic ground 9:1 portion were ground by ball milling under the inert nitrogen atmosphere for four hours. AlSiC, metal-ceramic based composite material which was sieved under 50 μ mesh size sieve.

Scanning electron microscopy (SEM) images of AlSiC was taken by ZEISS, VP300 model SEM system which was shown in Figure 2.1. Particle size distribution (PSD) of AlSiC composites was measured by Malvern Instruments, Master Sizer 3000 model dynamic light scattering system. Wet analysis cell part of the system was chosen for PSD analysis. AlSiC PSD result was given in Figure 2.2.

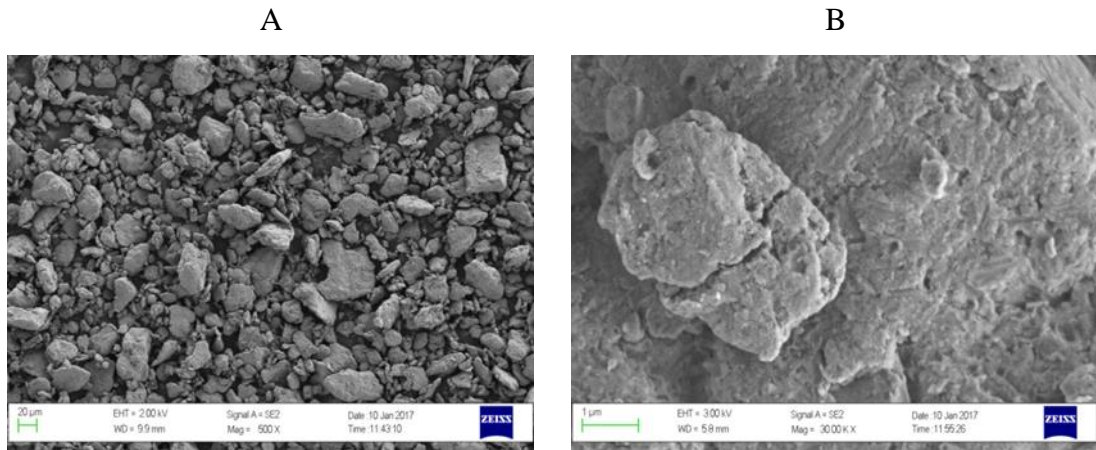


Figure 2.1: AlSiC metal-ceramic composite particles scanning electron microscopy (SEM) image was taken by ZEISS trademark VP30 model scanning electron microscope. A was a 500X magnification of particles and B was a 30.000X magnification of particles.

Particles size of AlSiC composite was measured by Malvern, Mastersizer 3000 was a model instrument. Hydro side equipment was used for dispersion of particles. D_{10} , D_{50} , and D_{90} values were obtained from Figure 2.2, respectively.

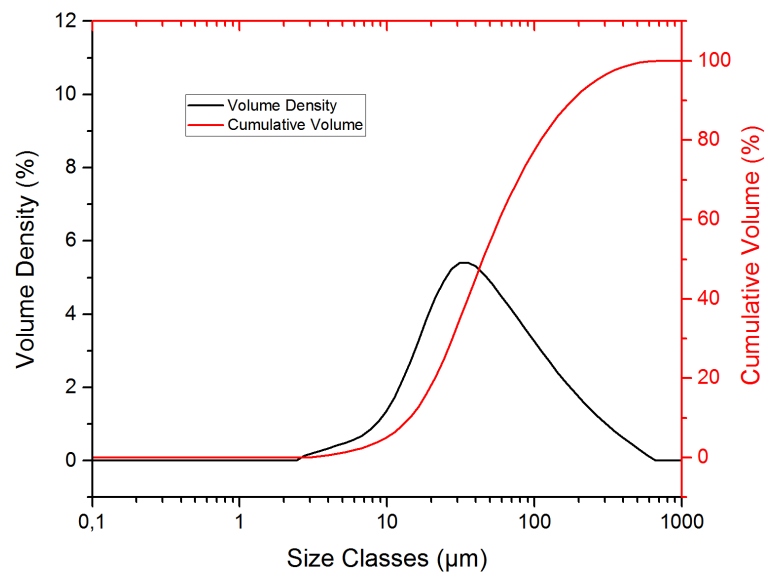


Figure 2.2: AlSiC metal-ceramic composite particles values were obtained for D_{50} , 37μ .

2.1.3 Alumina (Al_2O_3)

The alumina particles D_{50} value was under 20μ and supplied from Morgan Technical Ceramics Company California USA. Particles purity was 99,9 %. The color was white, no electrical conductivity and it had over 20W/m.K thermal conductivity. Again, the particle size of alumina was measured by Malvern, Mastersizer 3000 was a model instrument. Aero side equipment was used for dispersion of particles. D_{10} , D_{50} , and D_{90} values were obtained from Figure 2.3 D_{50} value of alumina was obtained from PSD machine 14μ . D_{90} value of alumina was obtained 20μ .

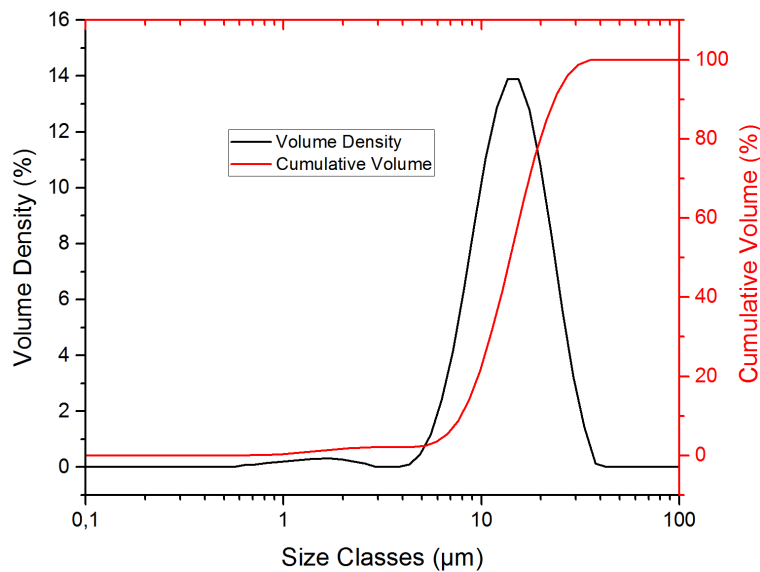


Figure 2.3: PSD of alumina particles D_{50} value was 14μ .

2.1.4 Silicon carbide (SiC)

Green SiC was supplied form ZENGMETAL Company from China. The purity of SiC was 99,9% and particle size of D_{50} value was 20μ . F320 model SiC mesh size chosen for mixing to PP matrix because of good dispersion into the matrix.

2.1.5 Coped carbon fiber (CF)

CF was supplied form ZOLTEC Company from the USA. Trademark model was Zoltek 35X for PP applications. The purity of CF was 94,9% and length of fibers was 6mm. Fiber dimension was approximately 100μ .

2.1.6 Aluminum nitride (AlN)

AlN was supplied form ZENGMETAL Company from China. The purity of AlN was 99,9% and particle size values of D_{50} was 20μ . AlN was tested by SEM. SEM images of particles were given Figure 2.4.

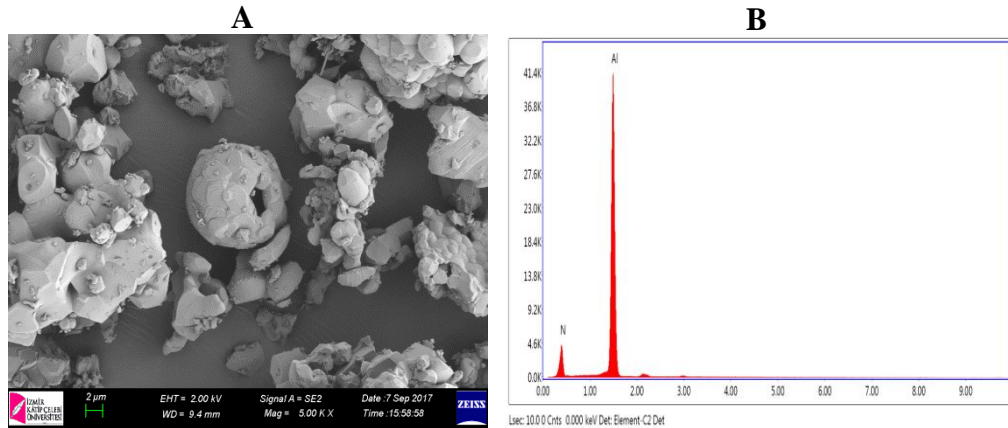


Figure 2.4: AlN ceramic particles scanning electron microscopy (SEM) image was taken by ZEISS trademark VP30 model scanning electron microscope. A was 5000X magnification of particles and B was EDAX spectroscopy (elemental composition analysis) of AlN particles.

2.1.7 Hexagonal boron nitride (HBN)

HBN was supplied form ZENGMETAL Company from China. The purity of HBN was 99,9% and D_{50} value was 20μ . HBN was tested by SEM. SEM images of particles and EDX results of the system was used for B/N ratio of the material (Figure 2.5).

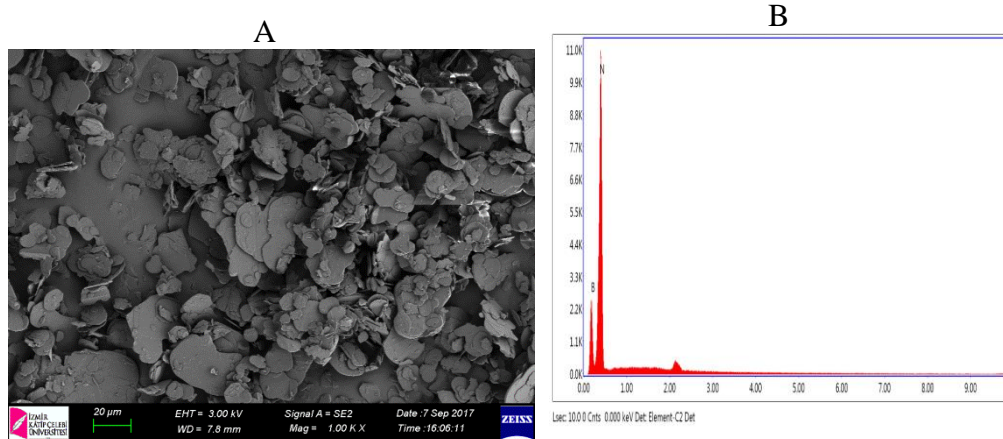


Figure 2.5: HBN ceramic particles scanning electron microscopy (SEM) image was taken by ZEISS trademark VP30 model scanning electron microscope. A was 1000X magnification of particles and B was EDAX spectroscopy (elemental composition analysis) of HBN particles.

2.1.8 Graphene (G)

Graphene was supplied from GRAFEN Future Engineering. The model code of product was GRAFEN®-iGP2 / Industrial Graphene Nanoplatelets for General Purposes. Thickness was 5 to 10nm and diameter 5 to 10 μ . The purity of graphene nano-plaques was 99.9%. Raman spectra ID/IG ratio was 0,08 (Figure 2.6).

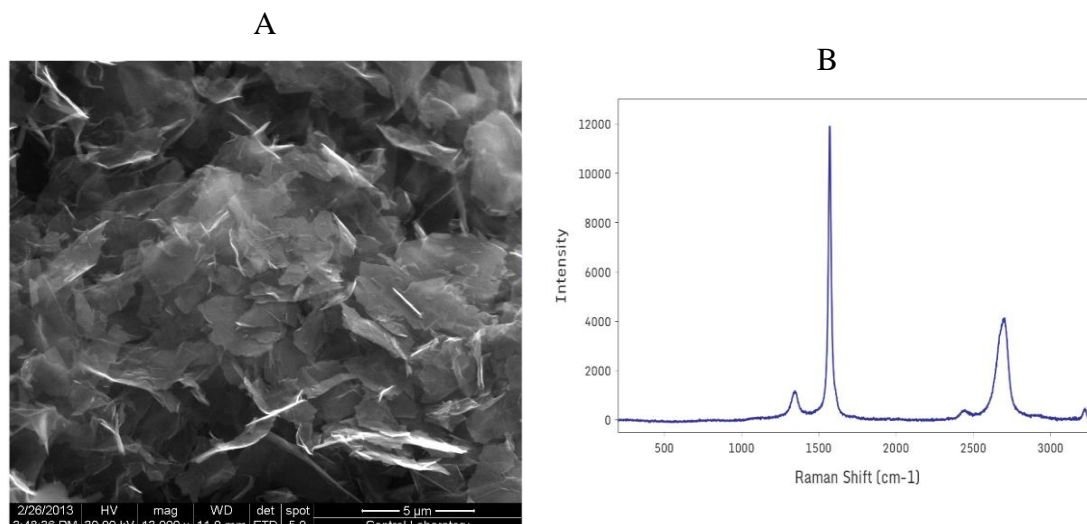


Figure 2.6: Graphene nano-plaques particles SEM image was taken by product technical data sheets. A was a 13.000X magnification of particles and B was the Raman spectrum of graphene nano-plaques particles.

2.1.9 Super thermal conductive graphite (Gr)

Super thermal conductive graphite was supplied from Momentive Performance Materials Inc. The high alignment of the graphene layers gives the product superior thermal conductivity which makes it an excellent thermal management material for heat sink applications. Through-plane thermal conductivity was 4 to 6W/m.K but in-plane thermal conductivity was over 1500W/m.K (Figure 2.7).

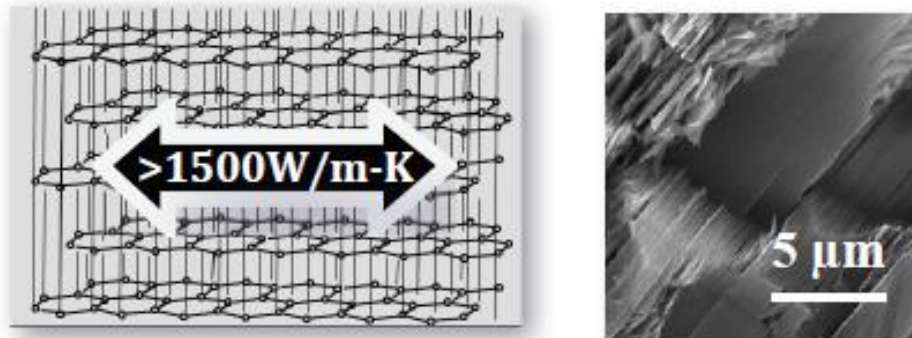


Figure 2.7: Super thermal conductive graphite particles scanning electron microscopy (SEM) image and orientation of carbon atoms into graphite were given from Momentive marketing bulletin.

2.1.10 Surface modification agents

Silane modification is an interfacial compatibility process commonly used today. This process chemically bonds the inorganic surfaces bonded to the organic surfaces by covalent bonds. The use of these chemicals, known as surface compatibilizers, in the polymer industry is very common. It is used to add inorganic filler to the filler material during production or before production to enable interaction with the polymer matrix (Figure 2.8). The silane compound attached to a core filler material interacts with the radical groups present on the other polymer chains to form a bond. In this way, high strength composite materials can be produced.

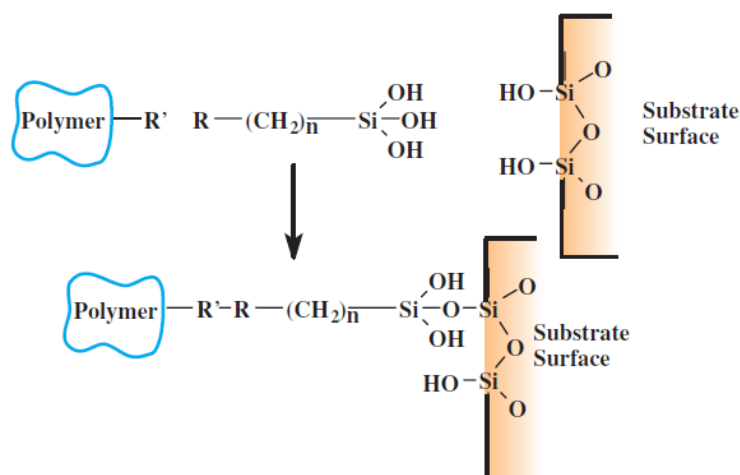
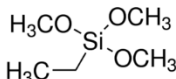
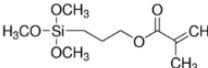
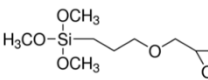
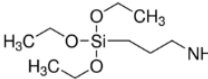
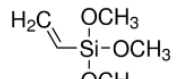


Figure 2.8: Silane modification reaction mechanism of -OH bonds included substrate surface [116].

In general studies, Deeping method; the solution prepared by dissolving the silane in an acidic water solution is to be immersed and filtered by drying the desired material to be modified. The amount of silane to be used depends on the amount of OH bonds on the surface of the material to be modified and the surface area of the material. The silane manufacturer usually gives this amount to the consumer.

In this study, five different types of surface modification agents were used for modification of 20 μ alumina particles. The detailed information of modification agents were given Table 2.2 1% of coupling agent was used to modified alumina particles [116]. Industrial dipping method was used for surface modification. Modification process was made under the same condition for all surface modification agents. The water pH was arranged to 4,0 for ionization of silane molecules into the water. 1% silane was added to solutions and stirred for 30 minutes at room temperature. 60gr alumina was added to the solution and stirred for 30 minutes too. The end of the progress, solutions were filtered and alumina particles were removed from the solution. Modified alumina particles were washed with pure water for five times and exceed (unreacted) surface modified agent molecules were removed from the alumina particles surface. The modified alumina particles dried at 105°C for 24 hours into the drier.

Table 2.2: Alumina particles silane modification agents list.

Modification No.	Surface modification agent	Molecular formula	Trade Name	Company
M0	Unmodified	-	-	-
M1	Ethyltrimethoxysilane		Z6320	Dow Corning
M2	3-(Trimethoxysilyl) propyl methacrylate		Z1030	Dow Corning
M3	(3-Glycidyloxypropyl) trimethoxysilane		Silquest O187	Momentive Per. Mat. Inc.
M4	(3-Aminopropyl) tetraethoxysilane		Silquest A1110	Momentive Per. Mat. Inc.
M5	Vinyltrimethoxysilane		Z6300	Dow Corning

Modification of particles controlled with MALVERN trade mark Nano ZS model instrument. Modified alumina particles were analyzed by Zeta potential measurement system for understanding modification results.

Table 2.3: Zeta potential of silane modified alumina particles.

Modification No.	Surface modification agent	Zeta potential (mV)
M0	Unmodified	-20.4
M1	Ethyltrimethoxysilane	-17.9
M2	3-(Trimethoxysilyl)propyl methacrylate	-25.4
M3	(3-Glycidyloxypropyl)trimethoxysilane	-6.2
M4	(3-Aminopropyl)triethoxysilane	-4.9
M5	Vinyltrimethoxysilane	-9,5

After the modification of alumina particles surface, surface electrical properties would be changed by surface agent molecules beside particles electrical mobility affected by modification. Table 2.3 gave zeta potential change of particles after the modification. Zeta potential of alumina particles changed with silane modification. Below this results, we can say that surface modification of alumina particles occur by the dipping process.

2.2 Composite Manufacturing

High-speed thermo-kinetic mixer generally used to prepare a composite prototype of which have low melting temperature polymers. This type of mixer operates at high speed to provide friction with the polymers. With the filling materials added, the polymer is well mixed on this surface. The resulting polymer pulps are cooled in the desired form to provide preparation of test samples for various tests. Its application is simple and fast, so it is widely used in preliminary tests in the plastic industry [117; 118]. This production technique is not an alternative production method to extruding. However, it is preferred by many manufacturers because of the information obtained from the test products and the fact that the waste formation is less than the extruder. Depending on the type and melting characteristics of the polymer to be used, many parts, mainly the mixing chamber, can be changed or modified as desired. The power of the engine transfers directly to the material with the helping of knives.

All samples dried at 80°C for 2h to remove moisture of filler particles and PP before addition to high-speed thermo-kinetic mixer chamber. The recipes of composites, which were given in Table 2.4, were produced by using a laboratory type high-speed thermo-kinetic mixer.

In order to produce thermal conductive composites, the total amount of composite into mixer was arranged as 70g. The high-speed thermo-kinetic mixer was GULNAR trademark and motor speed 2.000rpm. The volume of mixer chamber was 150ml and fill factor of the mixer was nearly 0,7 (sample volume / total volume). Chamber and blades were made by hardened steel.

The composite plates were produced by the help of hydraulic hot and cold press at 180°C for 210s between 40 and 120 bar pressure in the hot press, then composite

plates were cooled at 20°C for 120s at 120 bar pressure in cold press. All composite plaques were cut for mechanical analysis and respectively analysis methods. Schematic illustration of composite production method was given in Figure 2.9.

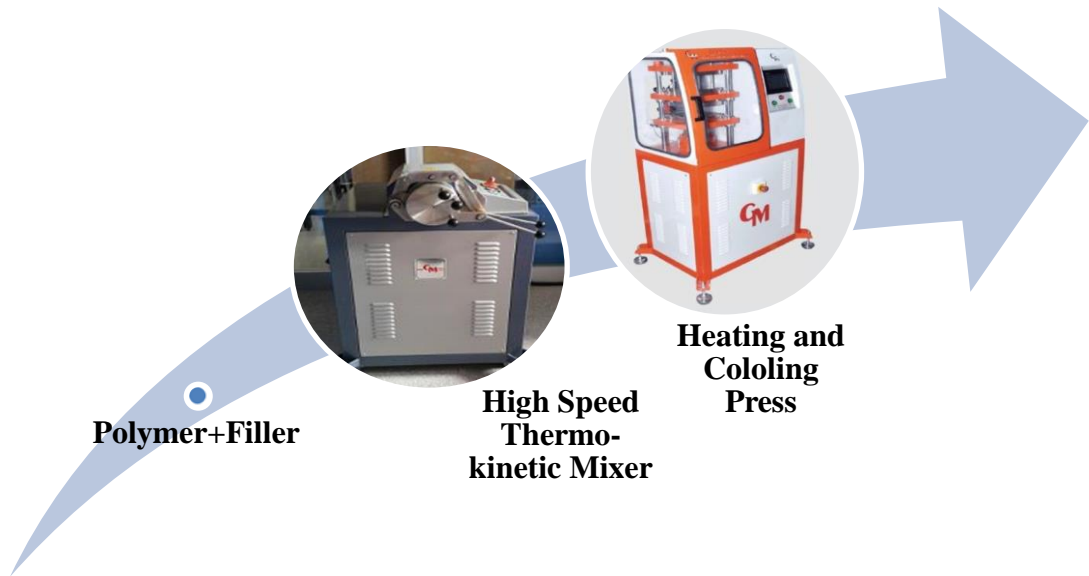


Figure 2.9: Sample preparation Equipment.

Table 2.4: Composites weight (%) recipes and and prices.

SAMPLES	PP (%)	AlSiC (%)	SiC (%)	CF (%)	G (%)	Alumina (%)	Graphite (%)	HBN (%)	AlN (%)	MAPP (%)	1Kg Price *(TL)
PP	100	-	-	-	-	-	-	-	-	-	50.0
10AlSiC-PP	90	10	-	-	-	-	-	-	-	-	65.0
20AlSiC-PP	80	20	-	-	-	-	-	-	-	-	80.0
30AlSiC-PP	70	30	-	-	-	-	-	-	-	-	95.0
40AlSiC-PP	60	40	-	-	-	-	-	-	-	-	110.0
50AlSiC-PP	50	50	-	-	-	-	-	-	-	-	125.0
60AlSiC-PP	40	60	-	-	-	-	-	-	-	-	140.0
SiC0CF-PP	50	-	50	-	-	-	-	-	-	-	75.0
SiC1CF-PP	50	-	49	1	-	-	-	-	-	-	74.0
SiC3CF-PP	50	-	47	3	-	-	-	-	-	-	73.0
SiC5CF-PP	50	-	45	5	-	-	-	-	-	-	72.0
SiC7CF-PP	50	-	43	7	-	-	-	-	-	-	71.0
AO-PP	60	-	-	-	-	40.0	-	-	-	-	70.0
AOG1-PP	60	-	-	-	0.4	39.6	-	-	-	-	78.0
AOG3-PP	60	-	-	-	1.2	38.8	-	-	-	-	94.0
AOG5-PP	60	-	-	-	2.0	38.0	-	-	-	-	110.0

Table 2.4 (cont.): Composites weight (%) recipes and prices.

SAMPLES	PP (%)	AlSiC (%)	SiC (%)	CF (%)	G (%)	Alumina (%)	Graphite (%)	HBN (%)	AlN (%)	MAPP (%)	1Kg Price *(TL)
AOG7-PP	60	-	-	-	2.8	37.2	-	-	-	-	126.0
M0-PP	50	-	-	-	-	50	-	-	-	-	75.0
M1-PP	50	-	-	-	-	50	-	-	-	-	76.0
M2-PP	50	-	-	-	-	50	-	-	-	-	76.0
M3-PP	50	-	-	-	-	50	-	-	-	-	76.0
M4-PP	50	-	-	-	-	50	-	-	-	-	76.0
M5-PP	50	-	-	-	-	50	-	-	-	-	76.0
5AlN-PP	95	-	-	-	-	-	-	-	5	-	75.0
10AlN-PP	90	-	-	-	-	-	-	-	10	-	85.0
15AlN-PP	85	-	-	-	-	-	-	-	15	-	102.6
20AlN-PP	80	-	-	-	-	-	-	-	20	-	120.0
25AlN-PP	75	-	-	-	-	-	-	-	25	-	137.6
25AlN5Gr-PP	75	-	-	-	-	-	5	-	20	-	122.6
20AlN10Gr-PP	75	-	-	-	-	-	10	-	15	-	107.6
15AlN15Gr-PP	75	-	-	-	-	-	15	-	10	-	92.6
10AlN20Gr-PP	75	-	-	-	-	-	20	-	5	-	79.6

Table 2.4 (cont.): Composites weight (%) recipes and prices.

SAMPLES	PP (%)	AlSiC (%)	SiC (%)	CF (%)	G (%)	Alumina (%)	Graphite (%)	HBN (%)	AlN (%)	MAPP (%)	1Kg Price *(TL)
5HBN-PP	95	-	-	-	-	-	-	5	-	-	70.0
10HBN-PP	90	-	-	-	-	-	-	10	-	-	85.0
15HBN-PP	85	-	-	-	-	-	-	15	-	-	52.6
10HBN5Gr-PP	85	-	-	-	-	-	5	10	-	-	87.6
10HBN10Gr-PP	80	-	-	-	-	-	10	10	-	-	90.0
10HBN15Gr-PP	75	-	-	-	-	-	15	10	-	-	82.6
10HBN20Gr-PP	70	-	-	-	-	-	20	10	-	-	95.0
10HBN20Gr1MaPP-PP	69	-	-	-	-	-	20	10	-	1	96.0
10HBN20Gr2MaPP-PP	68	-	-	-	-	-	20	10	-	2	97.0
10HBN20Gr3MaPP-PP	67	-	-	-	-	-	20	10	-	3	98.0

*Dollar exchange rate was taken as 7.0 according to August 2018

2.3 Composites Analysis

The composites were analyzed by the sophisticated analysis systems and methods. These system and methods were given below with the sub-titles.

2.3.1 Mechanical analysis

All mechanical analysis were made SHIMADZU AGX 5KN Universal test machine. The load cell of the machine was proper for polymeric composite samples, which had maximum force 5.000N.

2.3.1.1 Tensile tests

Tensile test of samples was prepared for plastic composites according to ASTM D638 [119]. Sample sizes were given appendix part of the thesis. Tensile test velocity was 50mm/min.

2.3.1.2 Flexural tests

Three-point bending test was made according to ASTM D790 and velocity of bending was 1mm/min. Test specimens prepared according to the same standard [120].

2.3.2 Scanning electron microscopy (SEM) analysis

The surfaces of the composite samples and expanded vermiculite particles were investigated using a scanning electron microscope (SEM) (Carl Zeiss 300VP, Germany) operated at 3,0 kV. A thin layer of gold was coated on the fractured surface of the composites by using an automatic sputter coater (Emitech K550X) to reduce the extent of sample arcing during SEM observation.

2.3.3 Simultaneous differential thermal (SDT) analysis

Simultaneous differential thermal analysis (SDT) was conducted on a TA instrument SDT-Q-600 at a heating rate of 10°C/min and under a nitrogen atmosphere, the flow rate of 50 mL/min, within the temperature range of ambition temperature to 600°C

[121]. Weight and heat calibration of SDT was made before analysis. For heat calibration of SDT, four different certificate standards were used.

2.3.4 Differential scanning calorimetry (DSC) analysis

Measurements of crystallinity percentage, phase change temperatures and specific heat capacities of composite neat PP were performed in a differential scanning calorimetry (DSC) instrument. TA instrument trademark, Q2000 model DSC was used for each analysis. Before all measurements, the DSC instrument was calibrated with certified Indium standard. Measurement method was designed as a heat/cool/heat procedure. Heating and cooling rate of DSC was set up 10°C/min between to 20°C to 200°C. End of the first heating cycle, 5 min isothermal step was applied to DSC oven for relaxation and for removing all mechanical stress on to the samples [121]. Then the samples were cooled constant cooling rate from 200°C to 20°C. At the second heating cycle, again samples were started to heat 20°C to 200°C. 20 ml/min nitrogen atmosphere was applied for preventing degradation and oxidation of samples into DSC chamber. Samples were weighted 10 ± 1 mg and hermetic standard aluminum pans were used for all analysis.

2.3.5 Dynamic mechanical analysis (DMA)

Viscoelastic properties such as storage modulus (E'), loss modulus (E''), and Tan delta ($\text{Tan}\delta$) of the neat PP and its composites as a function of temperature were evaluated using a dynamic mechanical analyzer (TA Instruments, Inc., DMA Q800) [122]. Analysis was performed in the Dual Cantilever mode at a fixed frequency of 1 Hz. Samples were heated from 30°C to 135°C at a heating rate of 3°C/min and the analysis was performed in the air atmosphere [121].

2.3.6 Thermal conductivity analysis

The thermal conductivity of the PP composites were investigated TCI thermal conductivity analyzer which is C-THERM Technologies trademark thermal conductivity measurement system. All samples through plane thermal conductivity measured under the same condition that was at 25°C and direct measurement method was used [123]. All measurements were repeated at 10 times and average value of through plane thermal conductivity was taken [124].

2.3.7 Surface electrical resistivity analysis

Surface Resistivity measurements were analyzed with 6517B/E Keithley trademark Electrometer/High Resistance Meter by taking ASTM-D-257-9 standard into consideration [125].

3. RESULTS AND DISCUSSION

3.1 Mechanical Analysis (Tensile and Flexural Properties)

The tensile test results of the AlSiC-PP composites were given in Figure 3.1. The tensile strength of composites decreased with the addition of AlSiC particles into the PP matrix.

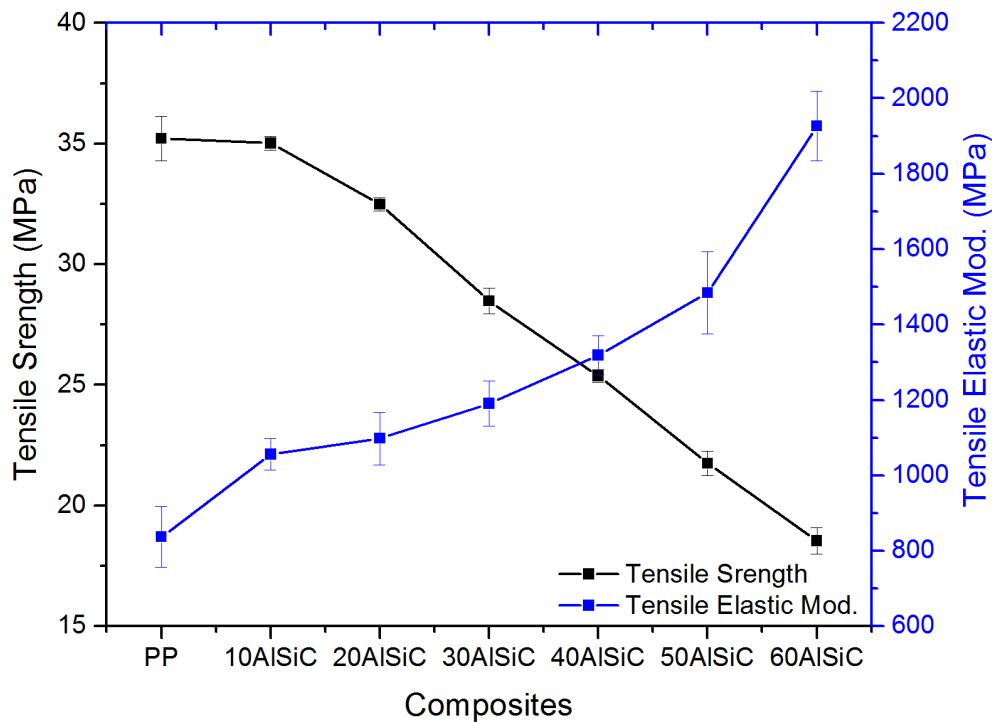


Figure 3.1: Tensile strength and tensile elastic modulus of neat PP, 10AlSiC-PP, 20AlSiC-PP, 30AlSiC-PP, 40AlSiC-PP, 50AlSiC-PP, and 60AlSiC-PP

The tensile strength of 10AlSiC-PP was nearly the same with neat PP but the tensile elastic modulus of the composite was approximately 25% higher than the neat PP. The tensile strength of composites decreased dramatically after 10% AlSiC particles addition to the PP matrix. The tensile elastic modulus of AlSiC-PP composites increased with the increasing of AlSiC particles w/w ratio into the polymer matrix. The polymer chains movements decreased into matrix respectively increasing of

particle number into the matrix. The tensile elastic modulus of filler is higher than the matrix material and this case leads to an increase in the elastic modulus of the matrix. The tensile elastic modulus of composites can be lead to restricted macromolecular mobility and deformation in the presence of filler particles [126].

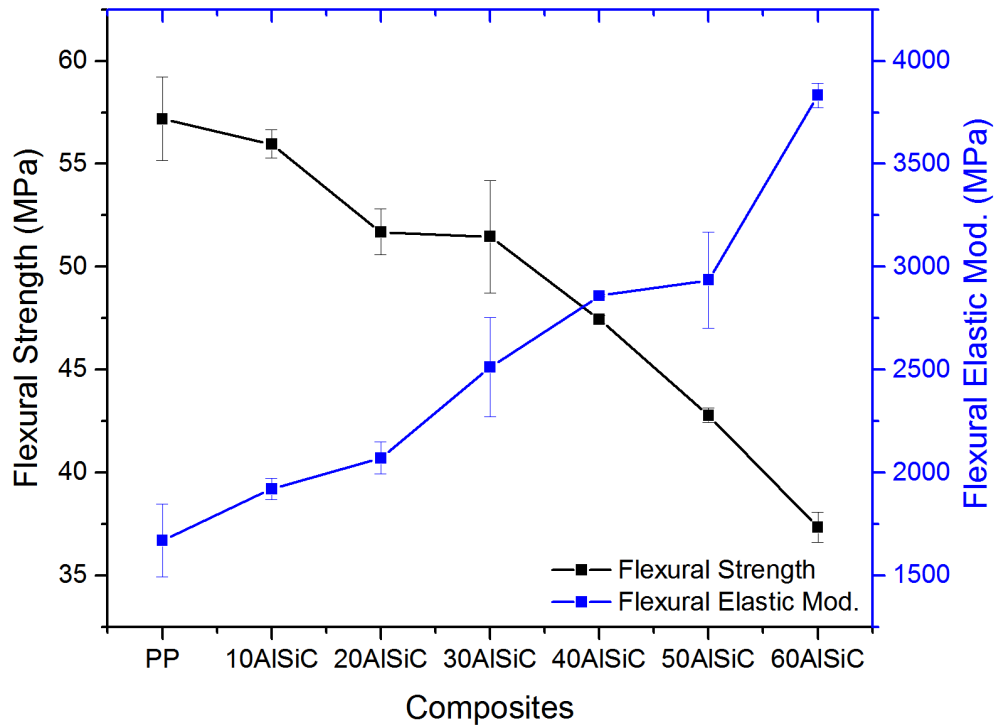


Figure 3.2: Flexural strength and flexural elastic modulus of neat PP, 10AlSiC-PP, 20AlSiC-PP, 30AlSiC-PP, 40AlSiC-PP, 50AlSiC-PP, and 60AlSiC-PP

The flexural test results of AlSiC-PP composites were given in Figure 3.2. The flexural strength of composites decreased with the addition of AlSiC particles into the PP matrix. The flexural strength of 20AlSiC-PP and 30AlSiC were nearly the same but the standard deviation of test results of 30AlSiC composite higher than the 20AlSiC-PP test results and possibly the flexural strength of composite was lower than the 20AlSiC-PP. The flexural elastic modulus of the composite increased with the addition of AlSiC particles. The flexural elastic modulus of composites increased dramatically after 50% AlSiC particles addition to PP matrix. The flexural elastic modulus of AlSiC-PP composites increases with the increasing of AlSiC particles w/w ratio into the polymer matrix. PP matrix ratio decrease into a composite, lowered the loading force transfer to AlSiC particles [121].

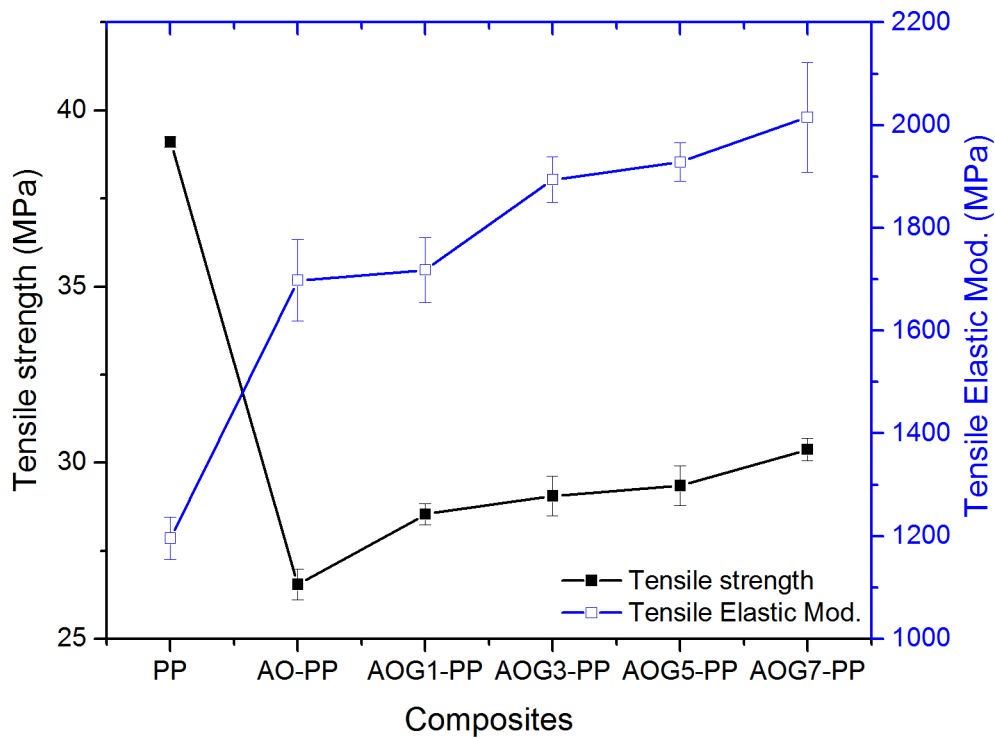


Figure 3.3: Tensile strength and tensile elastic modulus of neat PP, AO-PP, AOG1-PP, AOG3-PP, AOG5-PP, and AOG7-PP

The tensile strength and tensile elastic modulus of 40% alumina-G filler mixture added PP matrix composites were given in Figure 3.3. The tensile strength of composites dramatically decreased with the addition of alumina particles into the PP matrix. After the G plaques addition to the PP matrix composites tensile strength started to rise. AOG7-PP composite tensile strength was 12% higher than the AO-PP. The tensile elastic modulus of composites was higher than the neat PP. The tensile elastic modulus of AO-PP and AOG1-PP were the nearly same but G plaques addition to PP matrix and decreasing alumina content into the filler increased tensile elastic modulus of composites [127].

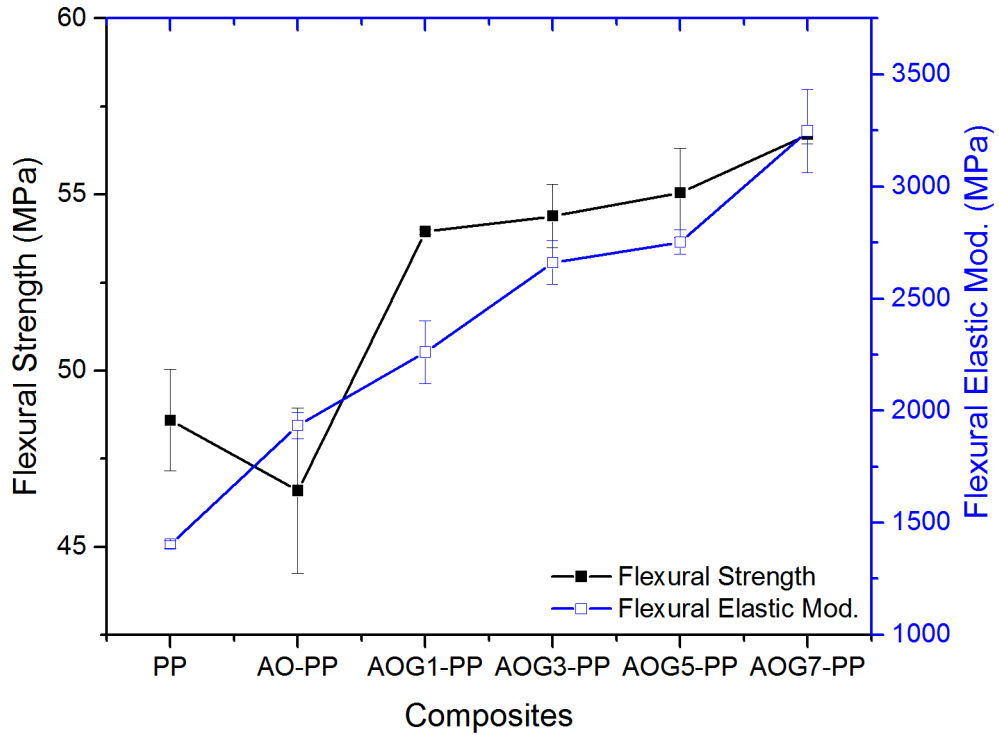


Figure 3.4: Flexural strength and flexural elastic modulus of neat PP, AO-PP, AOG1-PP, AOG3-PP, AOG5-PP, and AOG7-PP

The flexural strength and flexural modulus of 40% alumina-G filler mixture added PP matrix composites were given Figure 3.4. The flexural strength of PP decreased with the addition of 40% alumina into the matrix. After G plaques addition to filler content without changing the filler ratio into the matrix, the flexural strength of composites started to increase sharply. 1% amount of G plaques replace with alumina into the filler, increased 30% flexural strength of the composite. The only 5% flexural strength increment was able to obtain between 1 and 7% G plaques addition into the filler. The flexural modulus of composites increased with the addition of 50% alumina into PP matrix and G plaques ratio increment into filler content increased the flexural strength of the composites[7; 128].

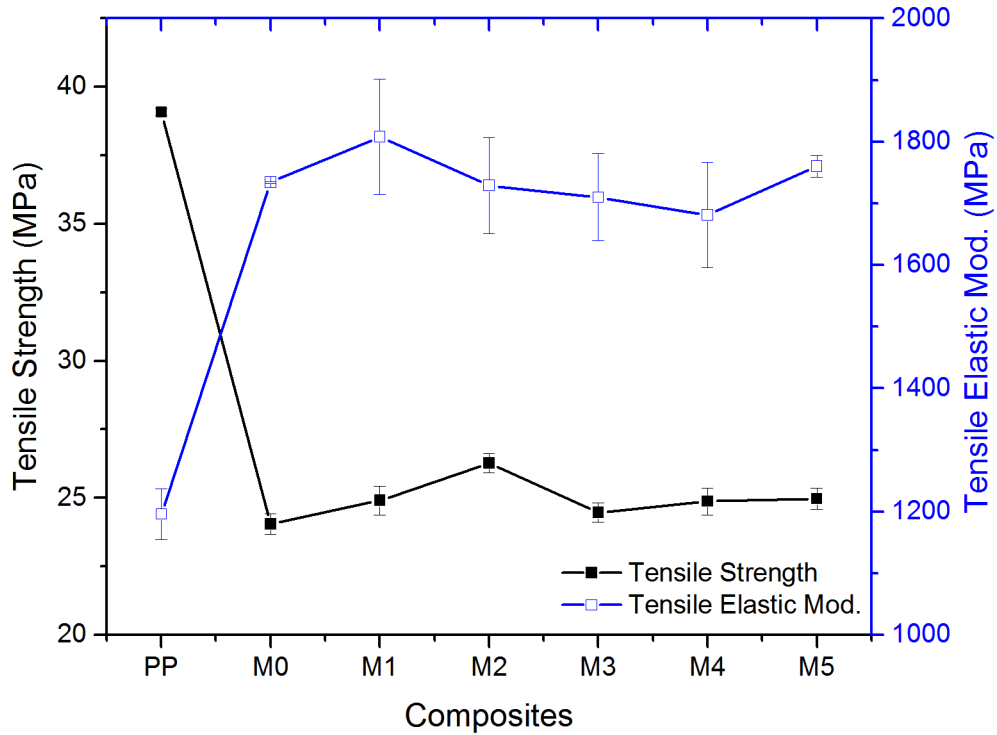


Figure 3.5: Tensile strength and tensile elastic modulus of neat PP, M0-PP, M1-PP, M2-PP, M3-PP, M4-PP, and M5-PP

The tensile strength and tensile elastic modulus of 50% silan- modified and unmodified alumina particles added PP matrix composites were given Figure 3.5. The tensile strength of composites sharply decreased with the addition of alumina particles into the PP matrix [129]. After the modified alumina addition to PP matrix composites tensile strength properties as same as unmodified alumina particle added PP matrix composites but M2-PP composite tensile strength was 5% higher than the other composites. The tensile elastic modulus of composites was higher than the neat PP. The tensile elastic modulus of M1-PP and M5-PP were higher than the other composites and the neat PP but the test variations were higher for comparing the elastic modulus differences between unmodified and modified alumina particles loaded PP matrix composites.

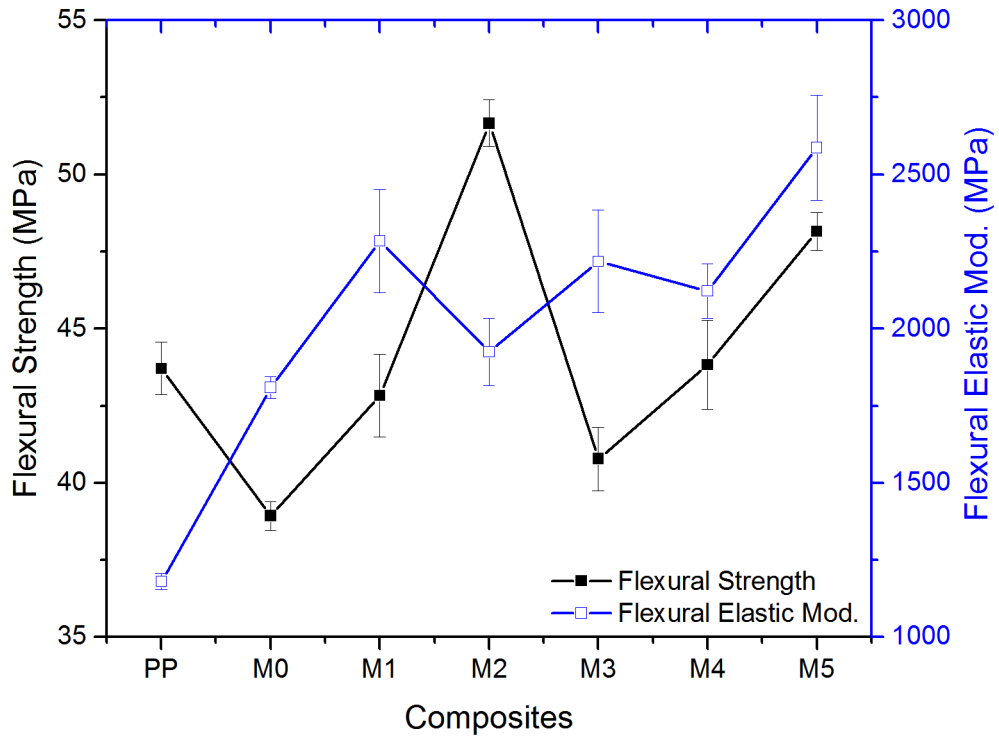


Figure 3.6: Flexural strength and flexural elastic modulus of neat PP, M0-PP, M1-PP, M2-PP, M3-PP, M4-PP, and M5-PP

The flexural strength of the silane-modified alumina particle added PP matrix composites were higher than the unmodified alumina particle added PP matrix composites (Figure 3.6). M2-PP composite flexural strength was higher than the other composites and neat PP. The unmodified alumina particle added composite flexure strength was the lowest one of the composites and neat PP. M3-PP and M1-PP composites were almost the same as the neat. The flexural strength of M5-PP was 10% higher than the neat PP. The flexural strength value was important to understand the achievement of surface modification of the filler particles [130]. According to these results, the surface modification occurred successfully on to the filler surface. The flexural elastic modulus increased with the addition of alumina particles into the PP matrix[131]. M5-PP had the highest elastic modulus. M1-PP, M3-PP, and M4-PP almost had same elastic modulus although M2-PP elastic modulus were higher than M0-PP and the neat PP.

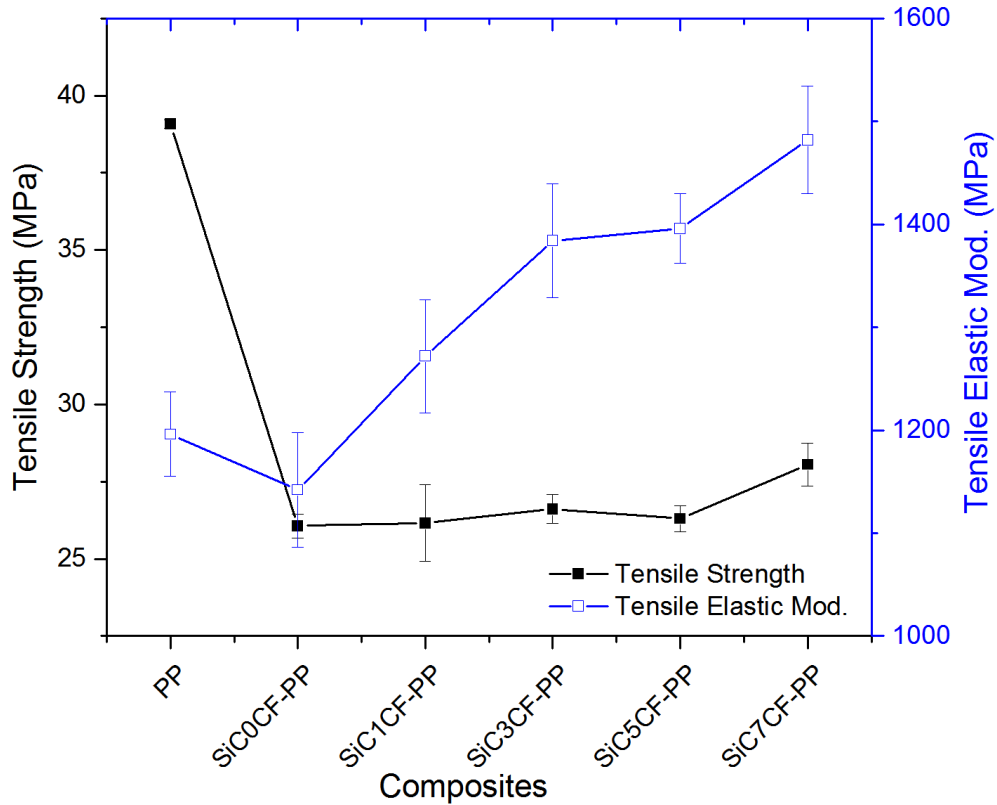


Figure 3.7: Tensile strength and tensile elastic modulus of neat PP, SiC0CF-PP, SiC1CF-PP, SiC3CF-PP, SiC5CF-PP, and SiC7CF-PP

The tensile strength and tensile elastic modulus of 50% silicon carbide particles added PP matrix composites were given in Figure 3.7. The tensile strength of composites sharply decreased with the addition of silicon carbide particles into the PP matrix. After the CF addition to silicon carbide ceramic filler, the composites tensile strength didn't change meaningfully [132]. However, over the 5% CF addition to PP matrix, the tensile strength of composite increased 10%. SiC0CF-PP composite had the lowest tensile elastic modulus value. 50% silicon carbide addition to the PP matrix decreased the elastic modulus of the composites. CF addition to the PP matrix with reducing weight percentage of silicon carbide ratio same as adding the value of CF was increased tensile elastic modulus of composites[133].

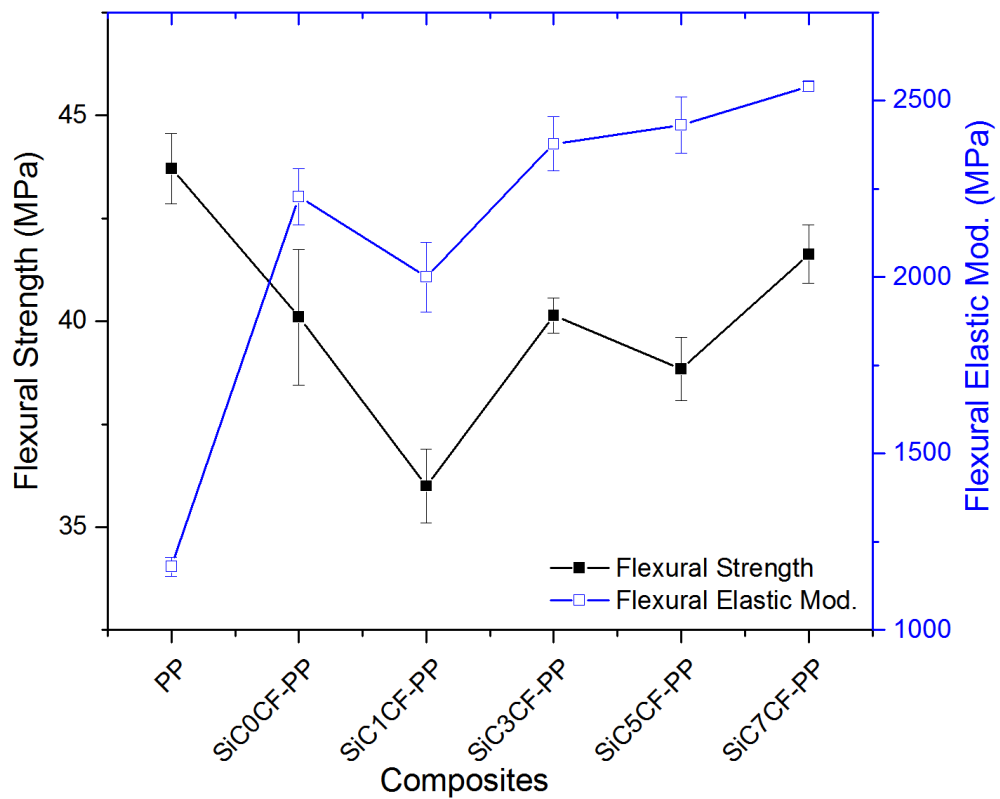


Figure 3.8: Flexural strength and flexural elastic modulus of neat PP, SiC0CF-PP, SiC1CF-PP, SiC3CF-PP, SiC5CF-PP, and SiC7CF-PP

The flexural strength of CF and SiC particle added PP matrix composites were lower than the neat PP (Figure 3.8). SiC1CF-PP composite flexural strength was the lowest than the other composites and neat PP. With increasing CF into the composite the flexural strength increased [134]. However, this increment was not linear or meaningful. Flexural elastic modulus of composites increased with the addition to filler to PP matrix although CF replacement with the SiC, flexural elastic modulus increased [135].

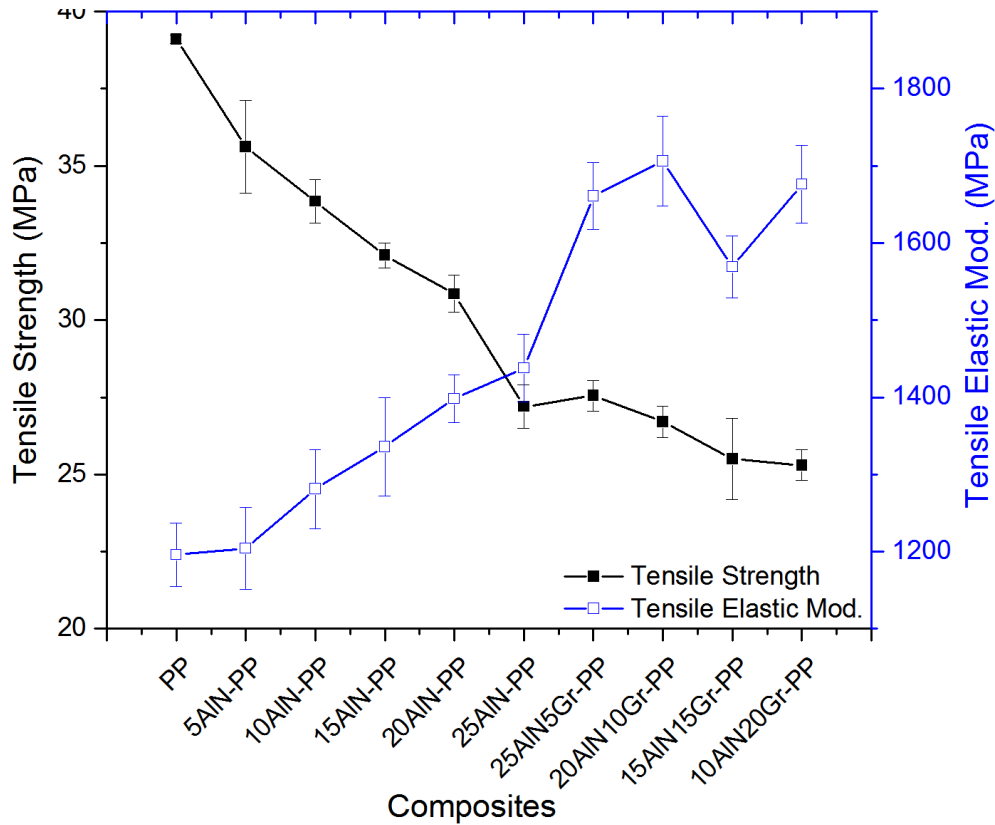


Figure 3.9: Tensile strength and tensile elastic modulus of neat PP, 5AlN-PP, 10AlN-PP, 15AlN-PP, 20AlN-PP, 25AlN-PP, 25AlN5Gr-PP, 20AlN10Gr-PP, 15AlN15Gr-PP, and 10AlN20Gr-PP

According to Figure 3.9, the tensile strength of composite decreased with increasing AlN particles into PP matrix. After Gr addition to AlN loaded PP matrix, the tensile strength of hybrid composite decreased too. Tensile elastic modulus of AlN added PP matrix composite increased with increasing filler content [129]. Gr addition to AlN loaded PP matrix composite, increased to the tensile elastic modulus of composites. 15AlN15Gr-PP tensile elastic modulus was lower than the other Gr included composites. However, error variation of test was higher than the other composites. The mixing process of the composite could cause tensile elastic modulus decrement.

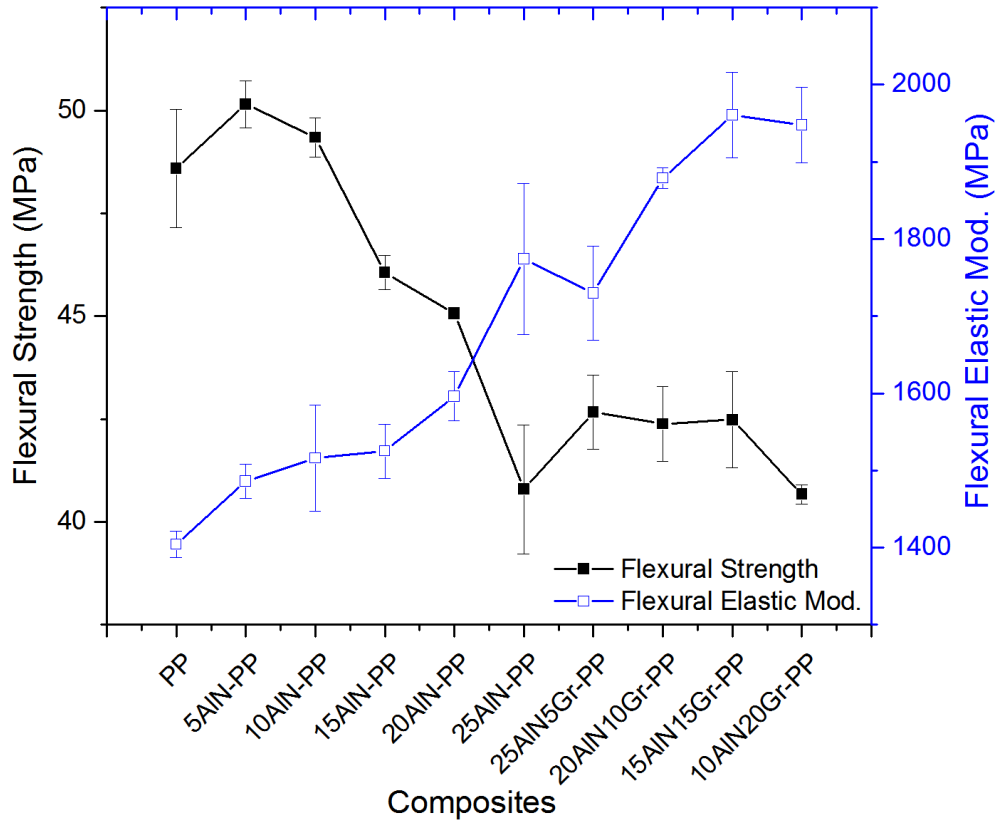


Figure 3.10: Flexural strength and flexural elastic modulus of neat PP, 5AlN-PP, 10AlN-PP, 15AlN-PP, 20AlN-PP, 25AlN-PP, 25AlN5Gr-PP, 20AlN10Gr-PP, 15AlN15Gr-PP, and 10AlN20Gr-PP

The flexural strength of 5% AlN added PP matrix composites increased. Over the 10% AlN addition to PP matrix decreased tensile strength of the composites. 25% AlN addition to PP matrix decreased flexural strength of composite almost 20% than neat PP. Gr addition into the PP matrix nearly 5% increased to tensile strength of 25AlN-PP composite but over the 20% Gr addition to 10% AlN added PP matrix decreased the flexural strength of the composite. The flexural elastic modulus of composites increased with AlN and Gr addition to the matrix (Figure 3.10). 25% AlN addition to PP matrix increased flexural modulus of composite nearly 20%. Gr addition to PP matrix increased flexural modulus of composite almost 40%. Gr addition to matrix was more efficient than the AlN addition [136].

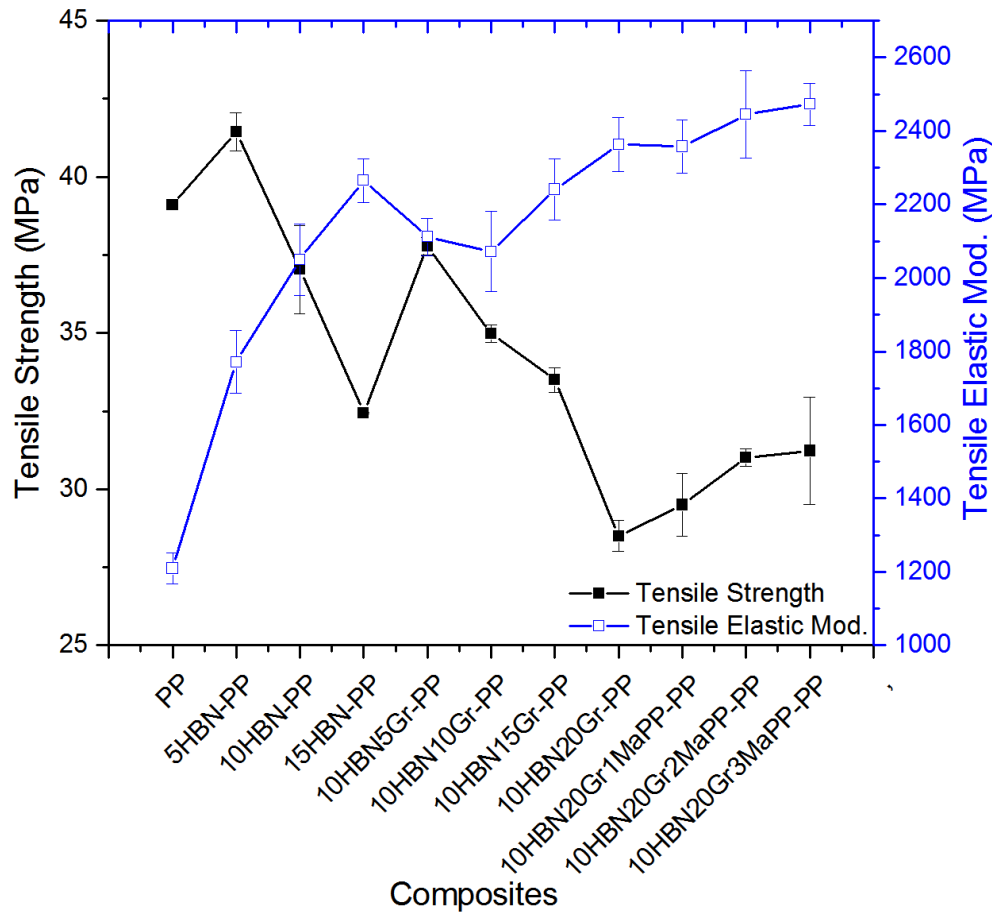


Figure 3.11: Tensile strength and tensile elastic modulus of neat PP, 5HBN-PP, 10HBN-PP, 15HBN-PP, 10HBN5Gr-PP, 10HBN10Gr-PP, 10HBN15Gr-PP, 10HBN20Gr-PP, 10HBN20Gr1MaPP-PP, 10HBN20Gr2MaPP-PP, and 10HBN20Gr3MaPP-PP

Figure 3.11 showed that three different part of studies of HBN and Gr added PP matrix composites. The first part of the study, the only 5, 10, and 15% HBN addition to PP matrix and the tensile strength of composite increased until the 5% HBN addition [137]. The tensile elastic modulus of composites increased. The second part of mechanical tests was included HBN and Gr hybrid filler combinations. The tensile strength of composite increased sharply 5% Gr addition into the PP matrix but after increasing Gr content into the composite tensile strength of composites decreased. The tensile elastic modulus of HBN and Gr hybrid filler combinations included composites were increased by Gr ratio increase into PP matrix. The last part of the study was 10% HBN and 20% Gr added PP matrix with the addition 1,2, and 3%

maleic anhydride grafted polypropylene (MaPP). The MaPP addition to the matrix was increased tensile strength and tensile elastic modulus of composites [138].

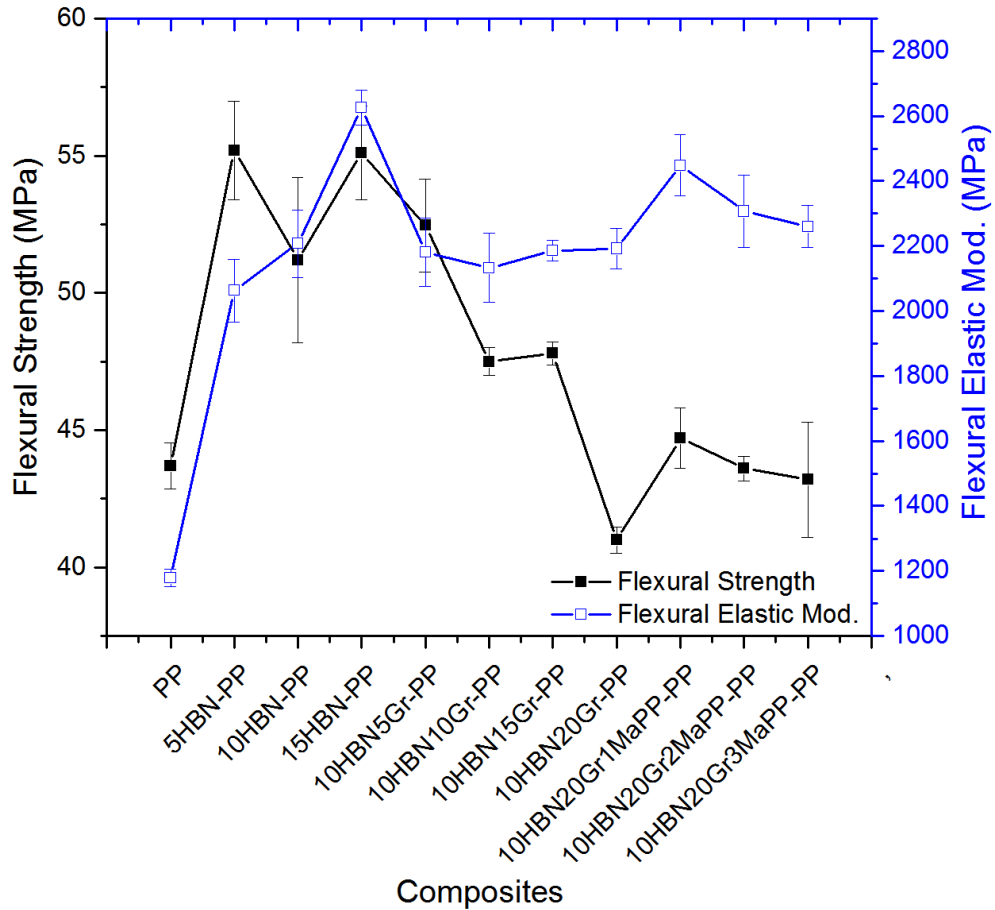


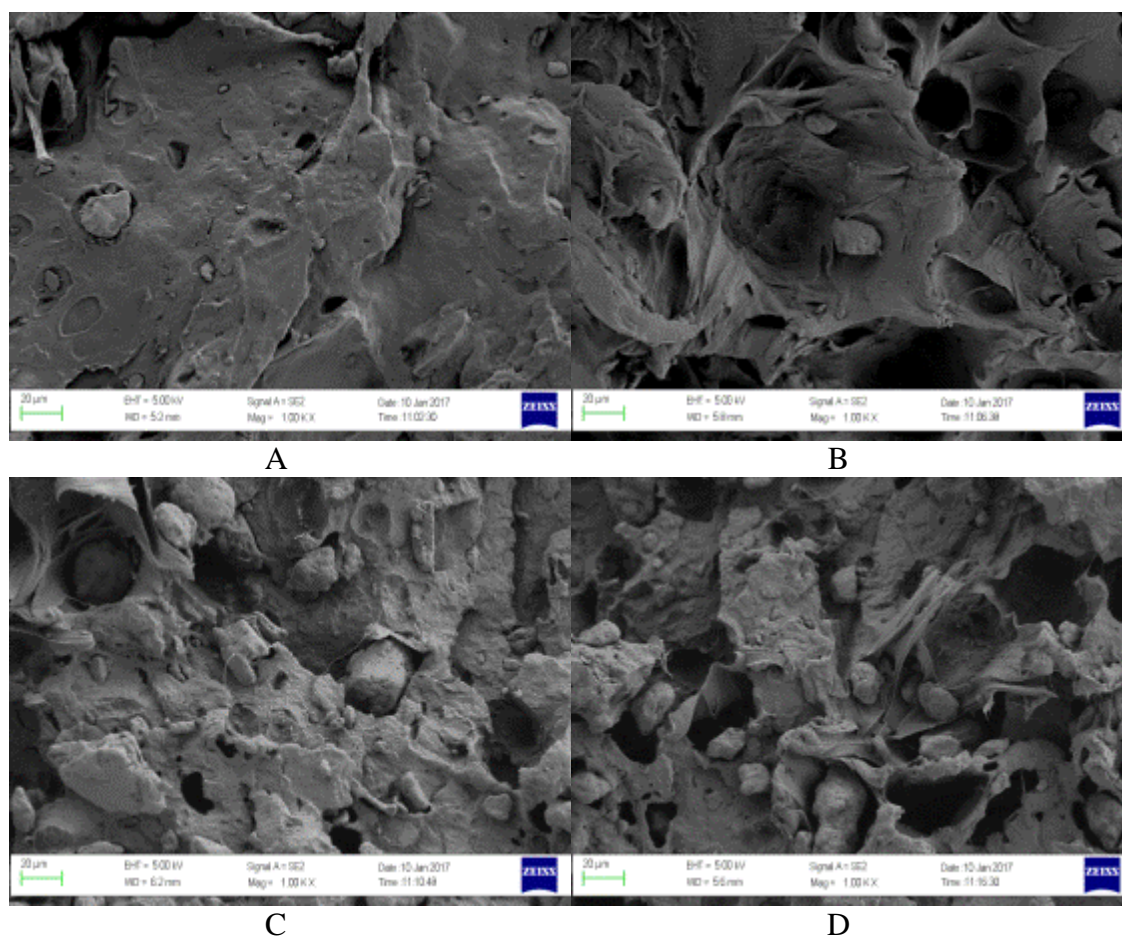
Figure 3.12: Flexural strength and flexural elastic modulus of neat PP, 5HBN-PP, 10HBN-PP, 15HBN-PP, 10HBN5Gr-PP, 10HBN10Gr-PP, 10HBN15Gr-PP, 10HBN20Gr-PP, 10HBN20Gr1MaPP-PP, 10HBN20Gr2MaPP-PP, and 10HBN20Gr3MaPP-PP

Figure 3.12 showed that three different part of a study of HBN and Gr added PP matrix composites. The first part of the study, the only 5, 10, and 15% HBN addition to PP matrix and the flexural strength of composites increased. The flexural elastic modulus of composites increased. The second part of mechanical tests was included HBN and Gr hybrid filler combinations. The flexural strength of composite decreased sharply with Gr addition into the PP matrix. The flexural elastic modulus of HBN and Gr hybrid filler combinations included composites were almost the same

for different Gr ratio in to the PP matrix. The last part of the study was 10% HBN and 20% Gr added PP matrix with the addition of 1,2, and 3% maleic anhydride grafted polypropylene (MaPP). 1% MaPP addition to PP matrix was increased the flexural strength and flexural elastic modulus of the composite. However, increasing of MaPP ratio into PP matrix decreased the flexural strength and flexural elastic modulus of composites [138].

3.2 SEM Analysis

SEM analysis results of AlSiC metal-ceramic composites added PP matrix was given Figure 3.13. SEM images showed that AlSiC particles ratio increase image A to F. AlSiC particles distribution was good and particles dimensions were 1μ to 100μ in the large distribution area. AlSiC particles were amorphous and spherical form. Filler-matrix interaction was pure.



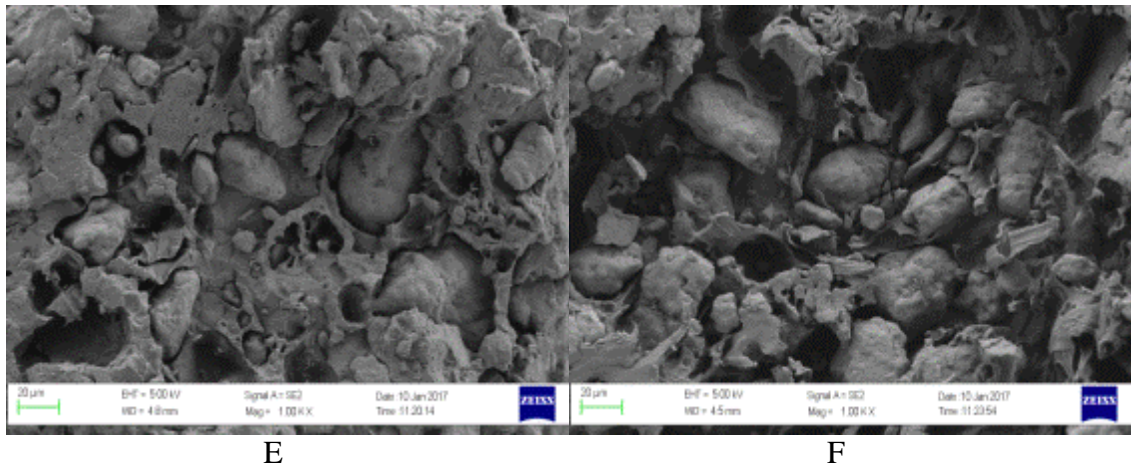
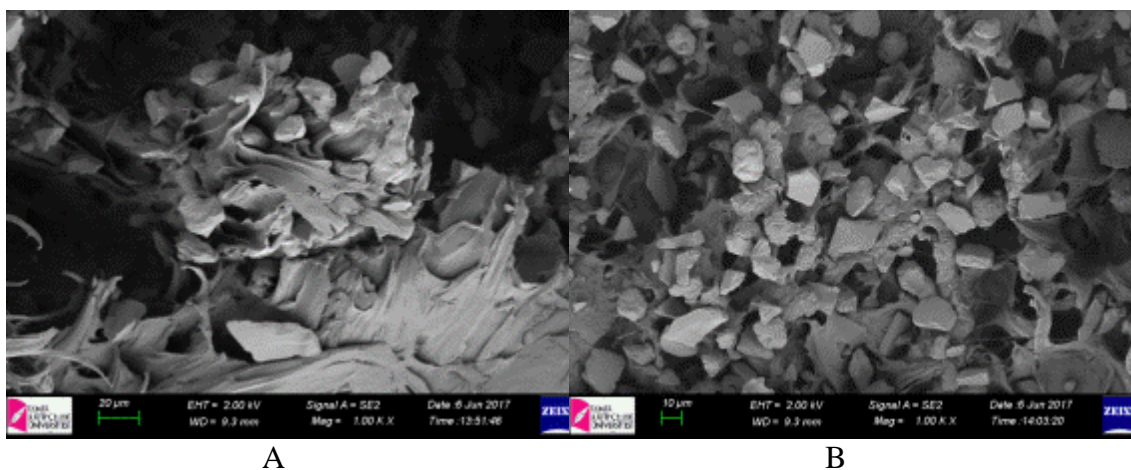


Figure 3.13: 1000X SEM images A)10AlSiC-PP, B)20AlSiC-PP, C)30AlSiC-PP, D)40AlSiC-PP, E)50AlSiC-PP, and F)60AlSiC-PP

SEM analysis results of 40% alumina and G hybrid PP composites were given Figure 3.14. SEM images showed that alumina particles matrix interaction not so good but alumina particles distribution into matrix good. Alumina particles size distribution good and particles had sharp edges and smooth surface properties. After the G addition to matrix, alumina matrix interaction did not change but polymer molecules orientation get better. G plaques orientation into the matrix was seen over 5000X magnification values better. AOG7-PP image was the best picture to see G plaques easily into PP matrix. (3000X images were given in Appendix)



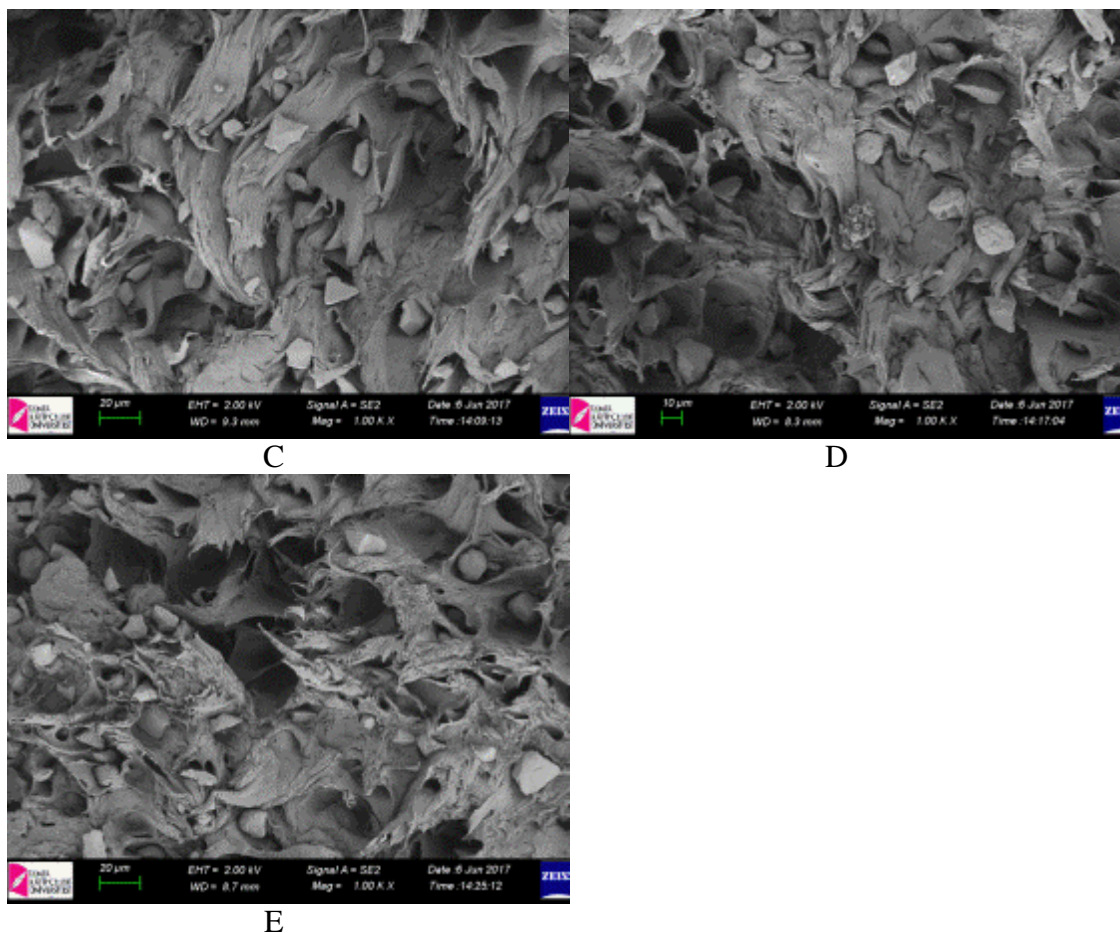


Figure 3.14: 1000X SEM images of, A)AO-PP, B)AOG1-PP, C)AOG3-PP, D)AOG5-PP and E)AOG7-PP

Silan-modified alumina particles loaded PP matrix tensile specimens broken surfaces SEM images were showed in Figure 3.15. Unmodified alumina particles loaded PP matrix image was A which was seen that matrix filler interaction weak. The ethyltrimethoxysilane (M1) modified alumina particles and the PP matrix interaction was good. PP matrix holed on to the alumina particles. Some part of matrix and alumina particles left from the PP matrix as agglomeration. The 3-(Trimethoxysilyl) propyl methacrylate (M2) modified alumina particles and the PP matrix interaction was weak and alumina particles left to matrix easily. (3-Glycidyoxypropyl) trimethoxysilane (M3) modified alumina particles and the PP matrix interaction better than M2-PP composite however not as good as M1-PP. (3-Aminopropyl) tetraethoxysilane (M4) modified alumina particles and the PP matrix interaction was very good and matrix holed on to the alumina particles. Vinyltrimethoxysilane (M5)

modified alumina particles and the PP matrix interaction was very good and matrix holed on to the alumina particles. According to these results, M1, M3, M4, and M5 modification occurred well but M2 did not show to the proper effect on the PP matrix.

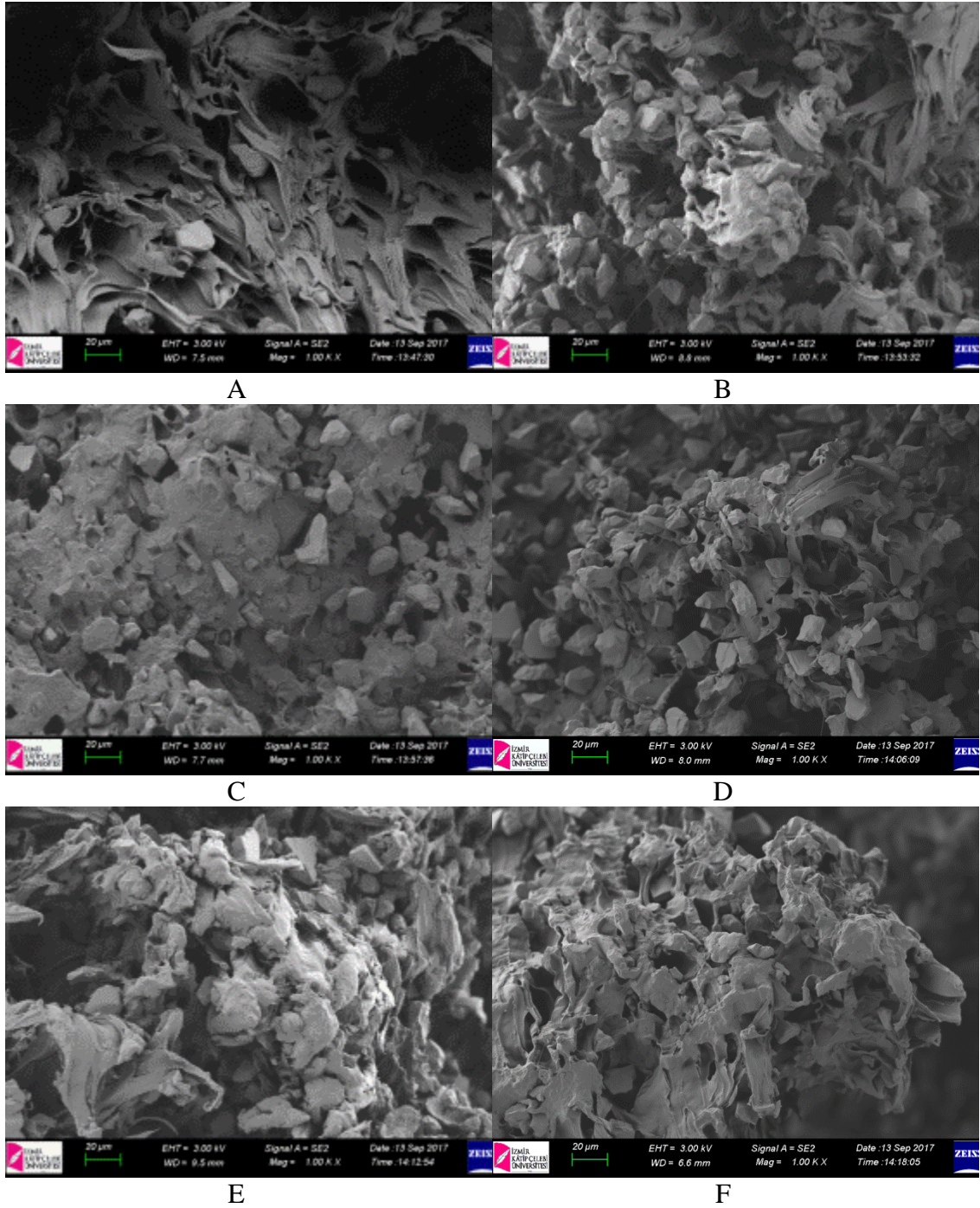
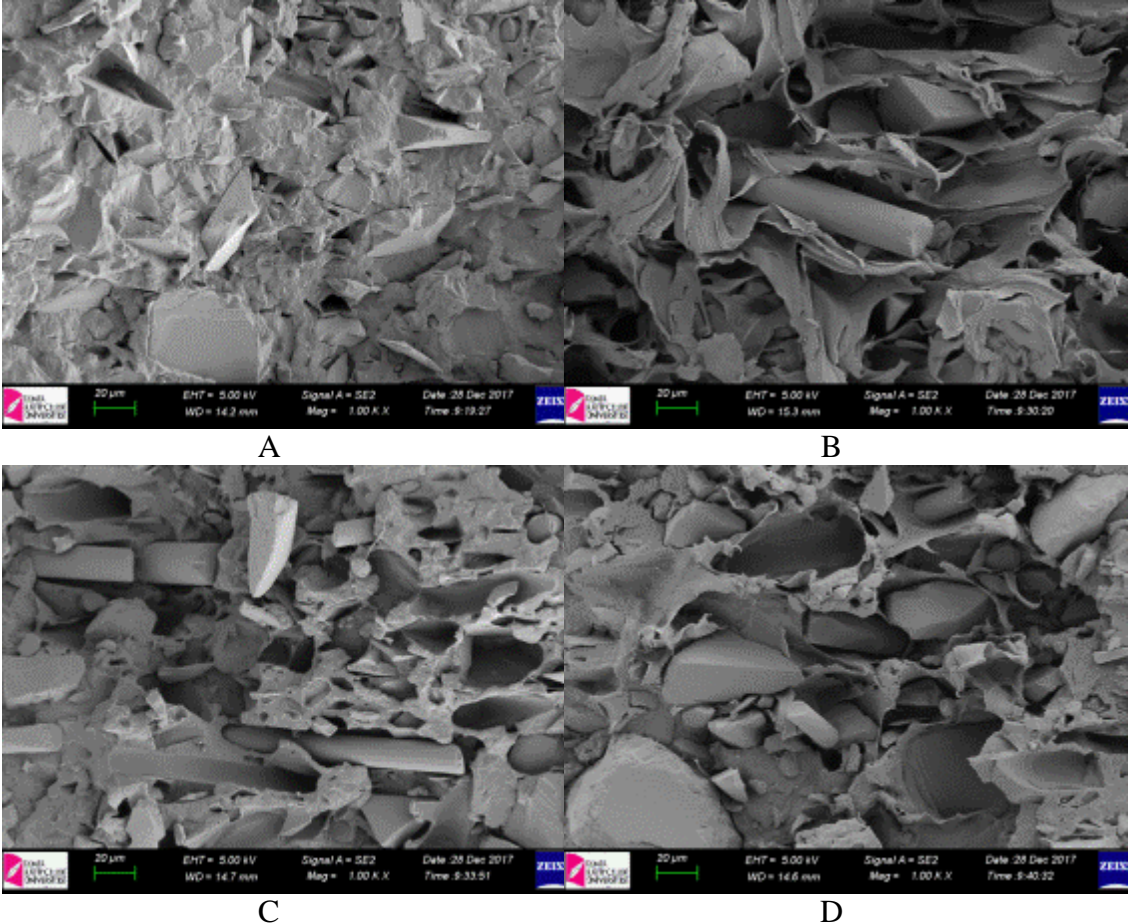
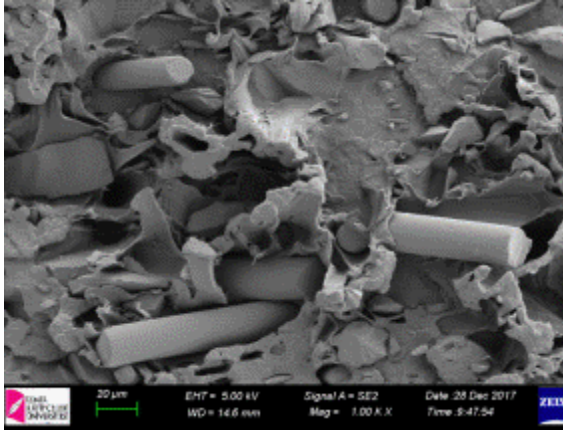


Figure 3.15: 1000X SEM images of, A)M0-PP, B)M1-PP, C)M2-PP, D)M3-PP, E)M4-PP and F)M5-PP

SEM analysis results of 50% SiC and CF hybrid PP composites were given Figure 3.16. SEM images showed that SiC particles and matrix interaction not good but SiC particles distribution into matrix was good. SiC particles size distribution good and particles had sharp edges and smooth surfaces. After the CF addition to matrix, SiC matrix interaction did not change but polymer molecules orientation get better. CF plaques orientation into the matrix was seen over 5000X magnification values better. From the B, C, D, and F images included CF into the PP matrix. CF orientation was same direction and CF matrix interaction weak As seen in the SEM images, fiber-like voids are formed at places where CF is separated from the PP matrix.

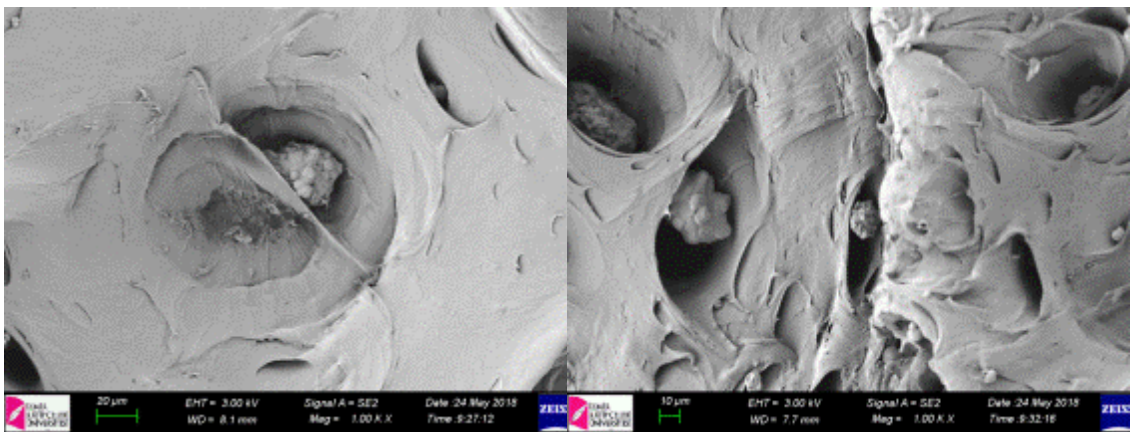




E

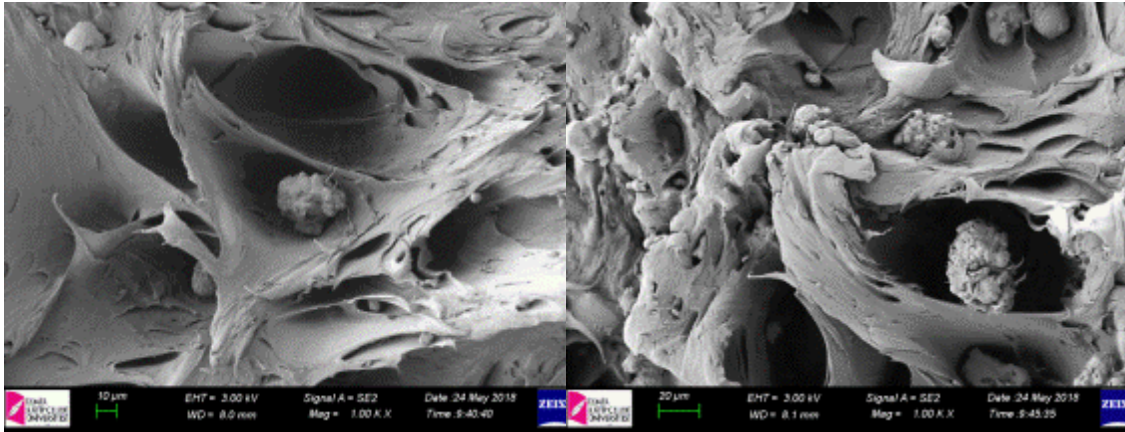
Figure 3.16: 1000X SEM images of, A) SiC0CF-PP, B) SiC1CF-PP, C) SiC3CF-PP, D) SiC5CF-PP and E) SiC7CF-PP

SEM analysis results of AlN and AlN-Gr hybrid PP composites were given in Figure 3.17. A, B, C, D, and E SEM images showed that respectively 5,10,15, 20 and 25% AlN added PP matrix tensile samples broken surfaces. AlN and PP matrix interaction pure and AlN particles distribution was not good. AlN particles shapes were spherical. Gr addition to PP matrix, the filler matrix interaction and particles distribution into the matrix became better. Gr particles shape and size distribution random but PP matrix interface was better than the AlN particles. Image L showed that Gr particles which became multi G plaques layers into PP matrix.



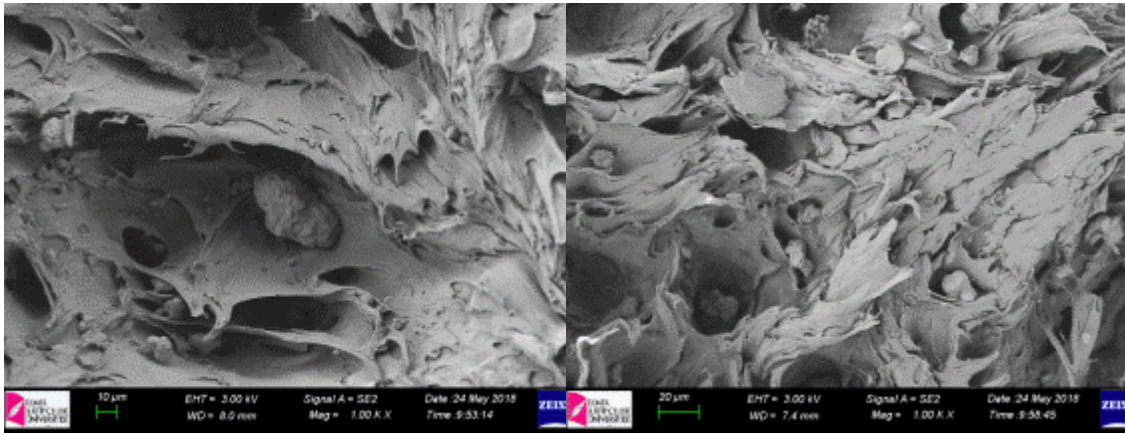
A

B



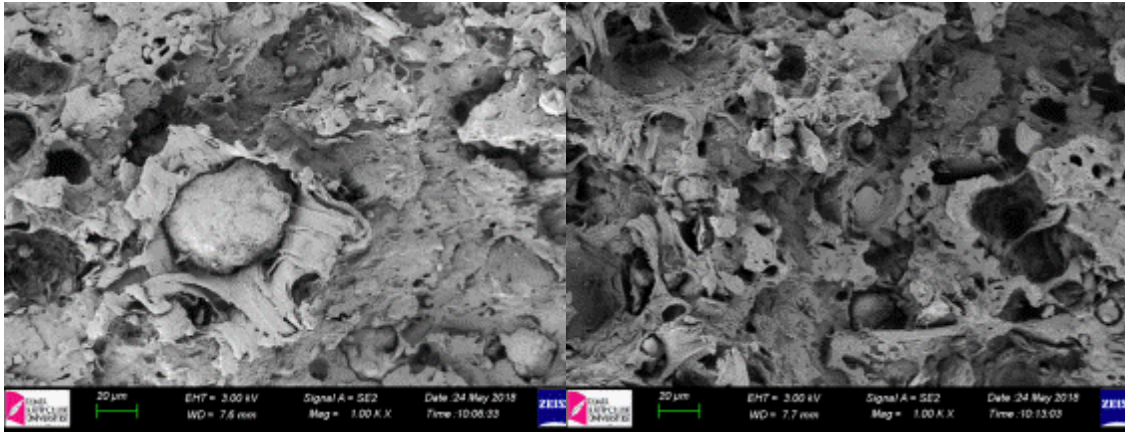
C

D



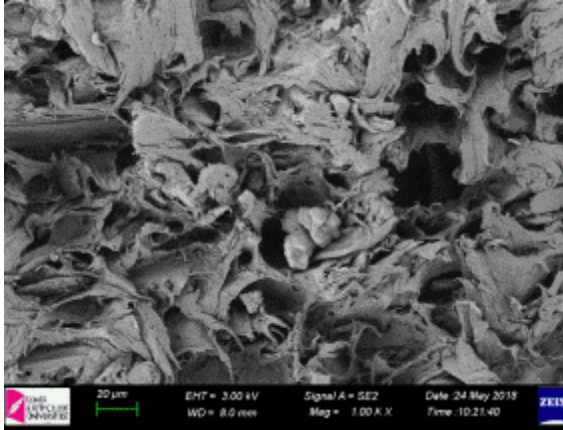
E

F



G

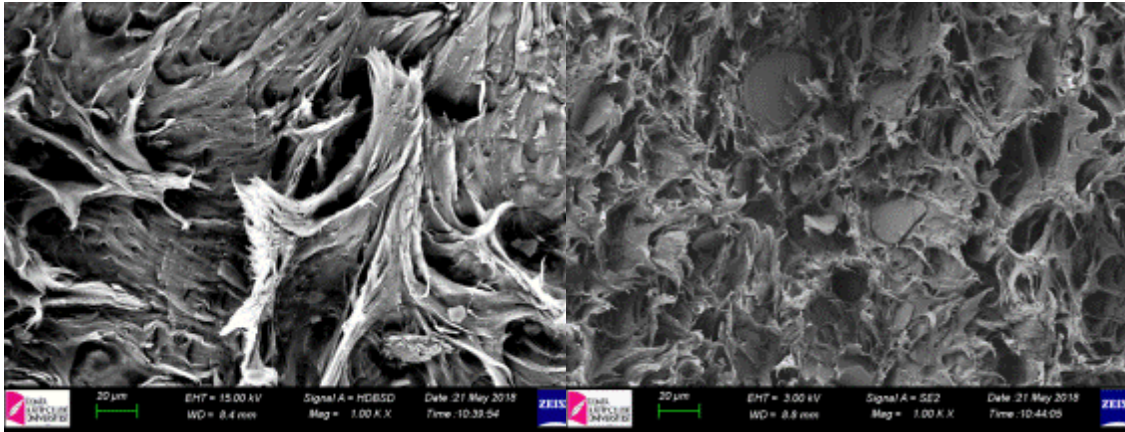
H



L

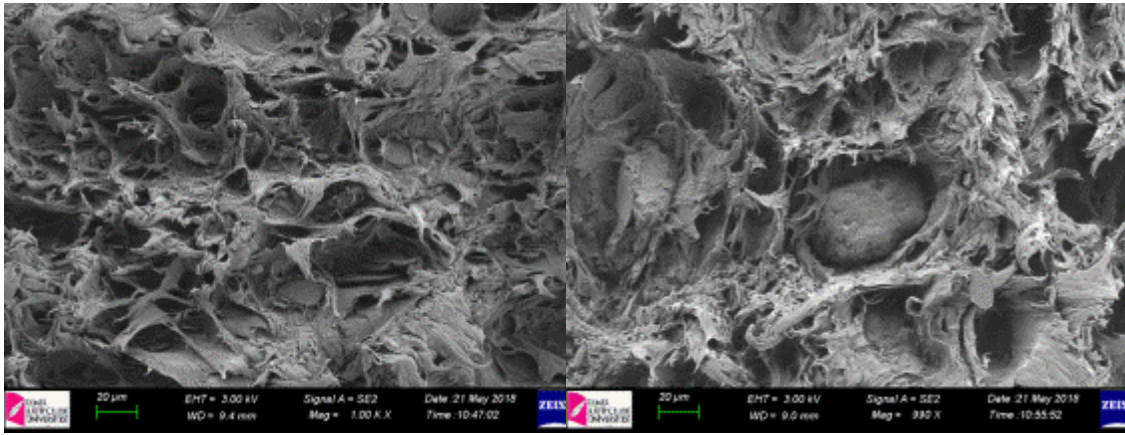
Figure 3.17: 1000X SEM images of, A) 5AlN-PP, B) 10AlN-PP, C) 15AlN-PP, D) 20AlN-PP, E) 25AlN-PP, F) 25AlN5Gr-PP, G) 20AlN10Gr-PP, H) 15AlN15Gr-PP, and L) 10AlN20Gr-PP

SEM analysis results of HBN and HBN-Gr hybrid PP composites were given Figure 3.18. A, B, and C SEM images showed that respectively 5,10, and 15% HBN added PP matrix tensile samples broken surfaces. HBN particles distributed into the PP matrix were good and HBN particles had micro plaque shapes were seen clearly. HBN and the PP matrix interaction was weak. After the Gr addition to 10%, HBN included the PP matrix, Gr and HBN random orientation was seen from image D, E, F, and G. The PP matrix filler interaction was pure and Gr particle size bigger than the HBN particles. HBN particles smooth surface properties and Gr structures could be separated from images easily. 10% HBN, 20% Gr, and MaPP included the PP matrix could be seen from H, L, and K named SEM images. The PP matrix and filler interface was good. HBN and Gr particles showed the same interaction properties with the PP matrix. It means that, molecular polarity of HBN and Gr particles were nearly same with the PP matrix.



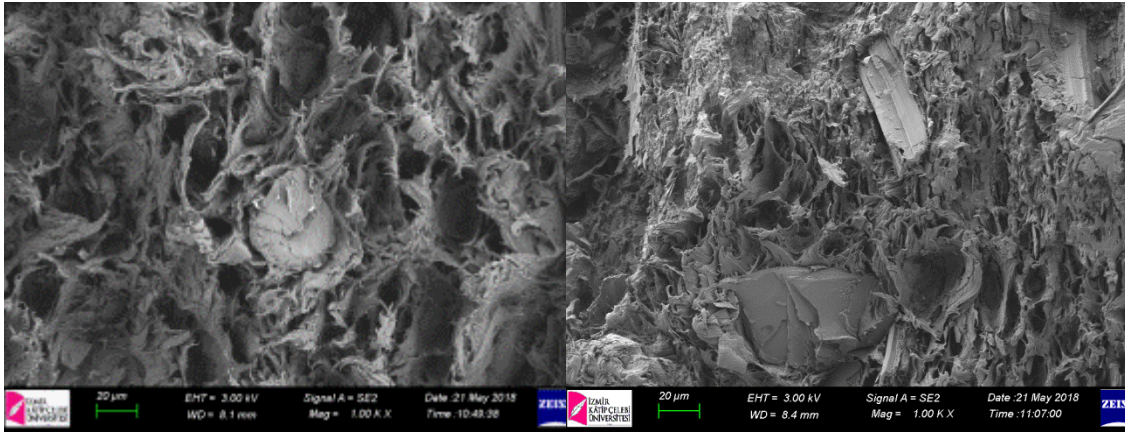
A

B



C

D



E

F

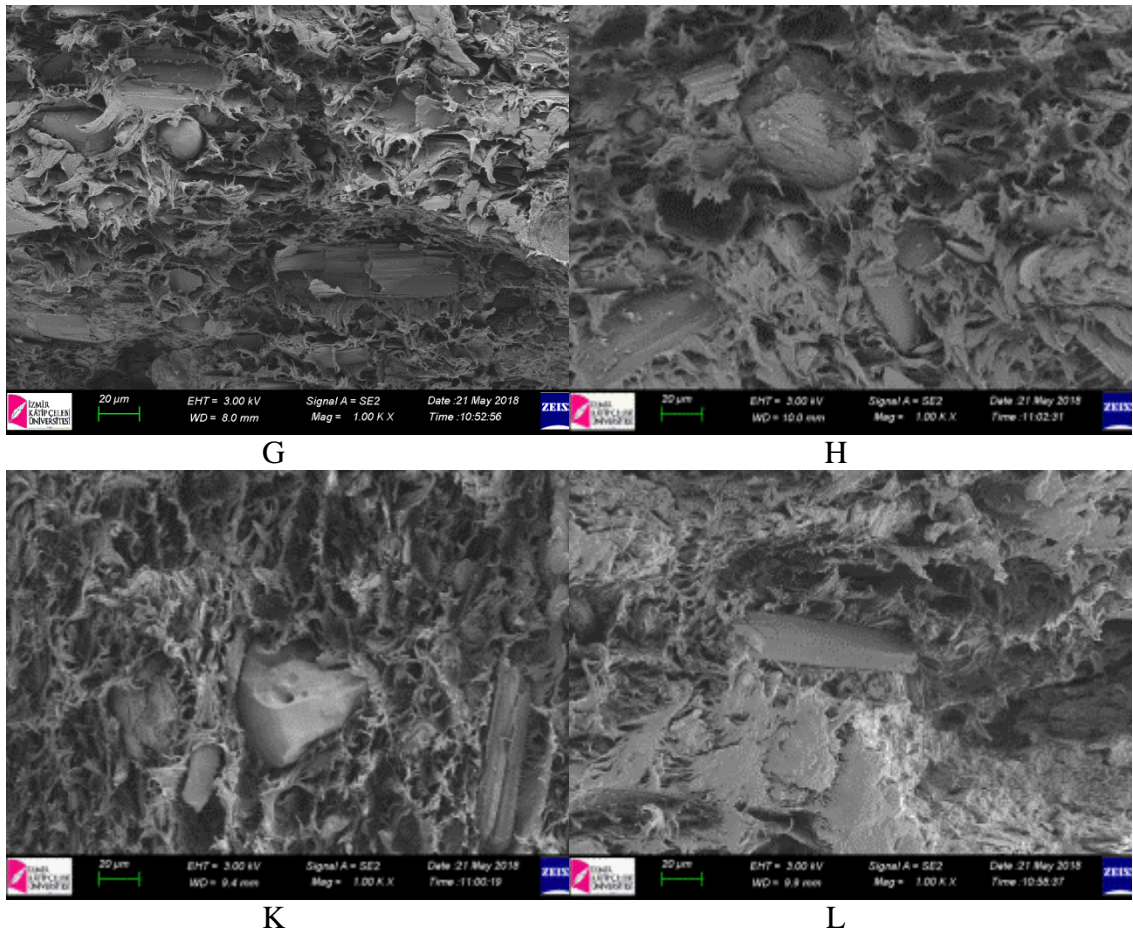


Figure 3.18: 1000X SEM images of, A)5HBN-PP, B)10HBN-PP, C)15HBN-PP, D)10HBN5Gr-PP, E)10HBN10Gr-PP, F)10HBN15Gr-PP, G)10HBN20Gr-PP, H)10HBN20Gr1MaPP-PP, K)10HBN20Gr2MaPP-PP, and L)10HBN20Gr3MaPP-PP

3.3 SDT Analysis

Table 3.1: Thermal degradation; onset temperature, degradation temperature (T_d), offset temperature, melting temperature (T_m), and residue

Sample	Degradation			T_m (°C)	% Residue
	Onset Temp. (°C)	T_d (°C)	Offset Temp. (°C)		
PP	436,6	460.7	477.6	167.1	2.25
10AISiC-PP	444.2	470.5	484.5	169.2	10.65

Table 3.1 (cont.): Thermal degradation; onset temperature, degradation temperature (T_d), offset temperature, melting temperature (T_m), and residue

Sample	Degradation			T_m (°C)	% Residue
	Onset Temp. (°C)	T_d (°C)	Offset Temp. (°C)		
20AlSiC-PP	449.1	473.9	487.8	170.6	20.30
30AlSiC-PP	441.7	474.2	488.3	169.8	30.05
40AlSiC-PP	438.7	473.7	491.9	168.2	40.10
50AlSiC-PP	435.1	474.3	490.9	170.2	49.8
60AlSiC-PP	436.1	476.8	492.1	167.8	59.5
SiC0CF-PP	441.3	469.2	482.6	172.1	48.2
SiC1CF-PP	448.5	468.5	487.4	172.0	49.0
SiC3CF-PP	450.0	469.7	482.1	172.8	49.2
SiC5CF-PP	449.9	468.9	481.7	170.5	49.5
SiC7CF-PP	450.7	469.5	487.3	171.2	49.4
AO-PP	441.3	463.7	476.3	165.1	40.8
AOG1-PP	407.1	439.7	467.2	171.6	40.2
AOG3-PP	453.2	469.1	481.2	170.1	40.8
AOG5-PP	453.2	470.1	481.9	171.6	41.0
AOG7-PP	454.7	471.9	483.2	169.8	40.5
M0-PP	437.0	463.9	475.0	172.2	48.9
M1-PP	439.0	464.5	476.9	172.0	49.0
M2-PP	385.0	437.0	462.4	172.9	47.8
M3-PP	441.9	465.8	478.2	173.0	49.6
M4-PP	441.1	464.6	476.2	170.1	49.3
M5-PP	440.3	465.0	479.6	174.7	49.0
5AlN-PP	436.1	464.3	476.7	173.3	5.1
10AlN-PP	438.0	463.5	479.9	170.1	10.6
15AlN-PP	440.8	458.6	474.6	169.8	15.4
20AlN-PP	439.7	465.4	477.5	174.3	20.5

Table 3.1 (cont.): Thermal degradation; onset temperature, degradation temperature (T_d), offset temperature, melting temperature (T_m), and residue

Sample	Degradation			T_m (°C)	% Residue
	Onset Temp. (°C)	T_d (°C)	Offset Temp. (°C)		
25AlN-PP	441.5	465.0	477.9	167.3	26.1
25AlN5Gr-PP	404.8	428.2	448.8	170.1	30.1
20AlN10Gr-PP	443.7	467.3	483.5	173.7	30.5
15AlN15Gr-PP	446.6	468.8	481.3	169.6	30.1
10AlN20Gr-PP	398.7	458.3	475.0	171.5	29.9
5HBN-PP	386.4	434.9	450.7	169.1	6.7
10HBN-PP	432.7	464.7	479.7	167.3	10.5
15HBN-PP	375.8	447.3	451.6	166.6	15.2
10HBN5Gr-PP	445.6	466.4	480.2	175.2	14.9
10HBN10Gr-PP	435.6	467.5	481.5	167.5	20.9
10HBN15Gr-PP	448.4	470.8	483.8	170.0	26.1
10HBN20Gr-PP	422.8	463.5	478.8	170.1	30.8
10HBN20Gr1MaPP-PP	453.0	470.5	484.4	172.8	30.5
10HBN20Gr2MaPP-PP	453.0	470.6	483.9	172.1	30.8
10HBN20Gr3MaPP-PP	450.4	470.7	483.6	170.8	30.2

SDT analysis results were given in Table 3.1. All calculation was made under TA instrument advantage software.

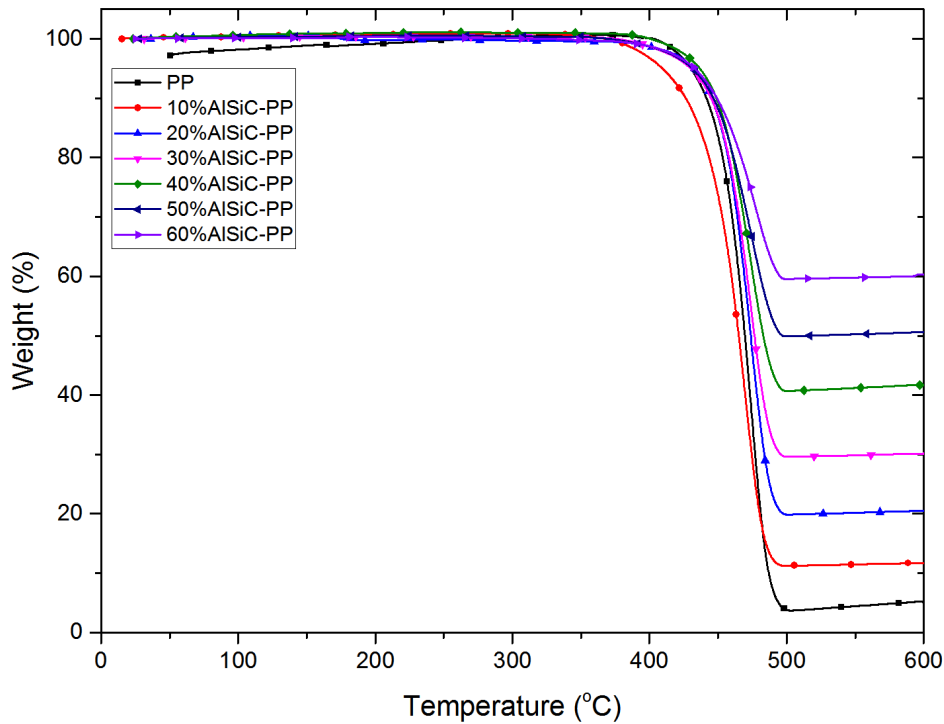


Figure 3.19: TGA thermogram of neat PP, 10AlSiC-PP, 20AlSiC-PP, 30AlSiC-PP, 40AlSiC-PP, 50AlSiC-PP, and 60AlSiC-PP

10 to 60% AlSiC metal-ceramic composite particle loaded PP matrix composites TGA analysis results were given in Figure 3.19. The addition of AlSiC into the PP increased the thermal degradation temperature of all composites except 10 AlSiC. The amount of residues after thermal decomposition was found to vary with the weight of PP compared to Table 3.1. Thermal stability of PP matrix enhanced by addition of AlSiC filler metal matrix composites. Polymer chains motions were restricted by filler loading in to the polymer matrix that decreased to degradation temperature of composites [139].

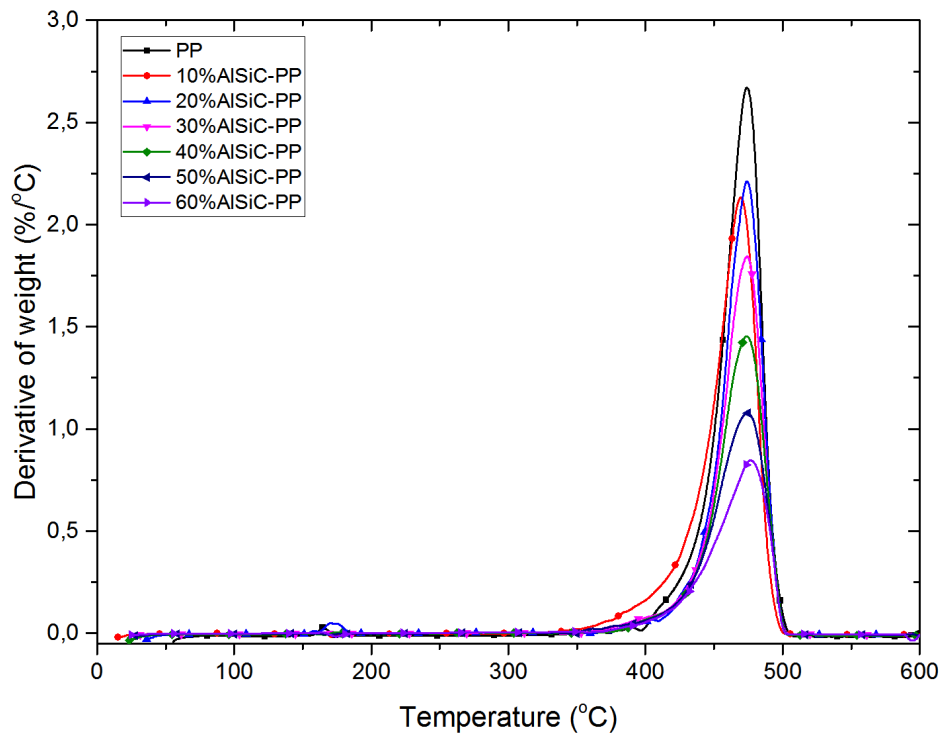


Figure 3.20: DTG thermogram of neat PP, 10AlSiC-PP, 20AlSiC-PP, 30AlSiC-PP, 40AlSiC-PP, 50AlSiC-PP, and 60AlSiC-PP

When the DTG curve, which is the derivative of the temperature of the TGA graph, is taken into account, the difference between the decomposition starting temperatures of the composites and the neat PP is better. There was no big difference in the offset temperature, which the breakdown was over. It was thought that the melting temperature of PP is between 160°C and 180°C in DTG graph. The judging from the decay rates of the composites, 10AlSiC-PP and 20AlSiC-PP were found to be approximately the same but proportional to the amount of PP in the degradation rates of the other composites (Figure 3.20).

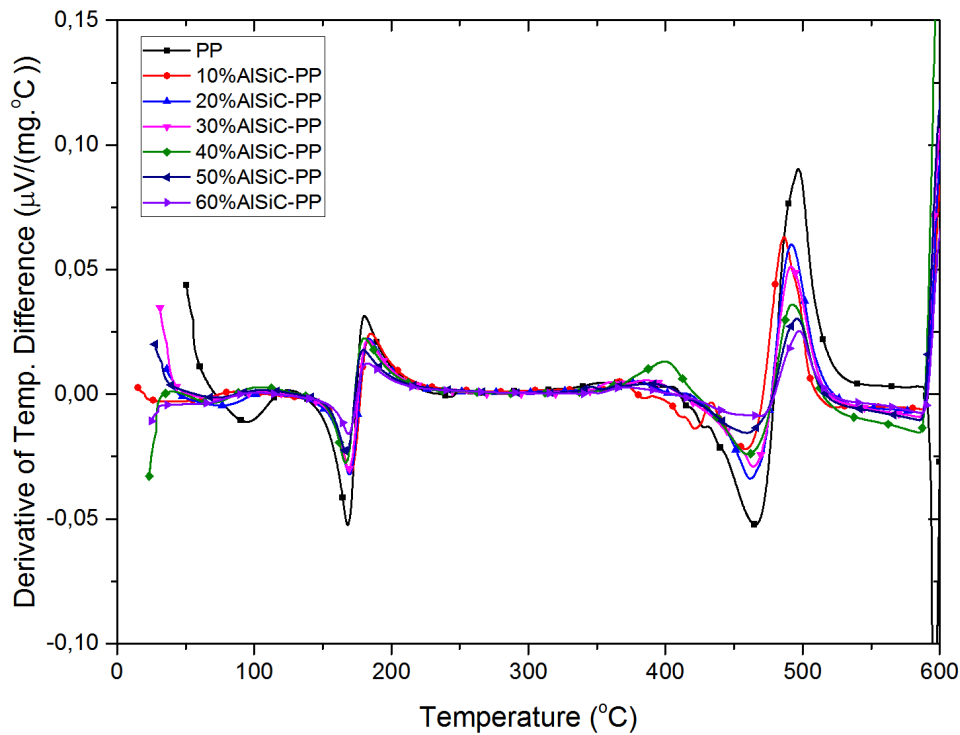


Figure 3.21: DTA thermogram of neat PP, 10AlSiC-PP, 20AlSiC-PP, 30AlSiC-PP, 40AlSiC-PP, 50AlSiC-PP, and 60AlSiC-PP

Differential thermal analysis (DTA) showed two specific reaction in to the composite with increasing temperature (Figure 3.21). The first reaction occurred between 160°C to 180°C. The PP matrix melting temperature was almost 167°C and we identified this reaction as a phase change reaction of PP matrix. The second reaction started at 460°C and finished at 500°C also this reaction temperature similar to decomposition point of PP matrix. DTA signal ratios were parallel to PP partition in to the composites. 10AlSiC-PP composite's DTA signal started change before 400°C and showed a different property from the other composites. Some different reaction pathway could be occurred on this temperature region. Although 40AlSiC-PP composite was thermal, reaction showed differences in this region. The neat PP could not get to thermal balance as fast as composites and showed different properties below 100°C.

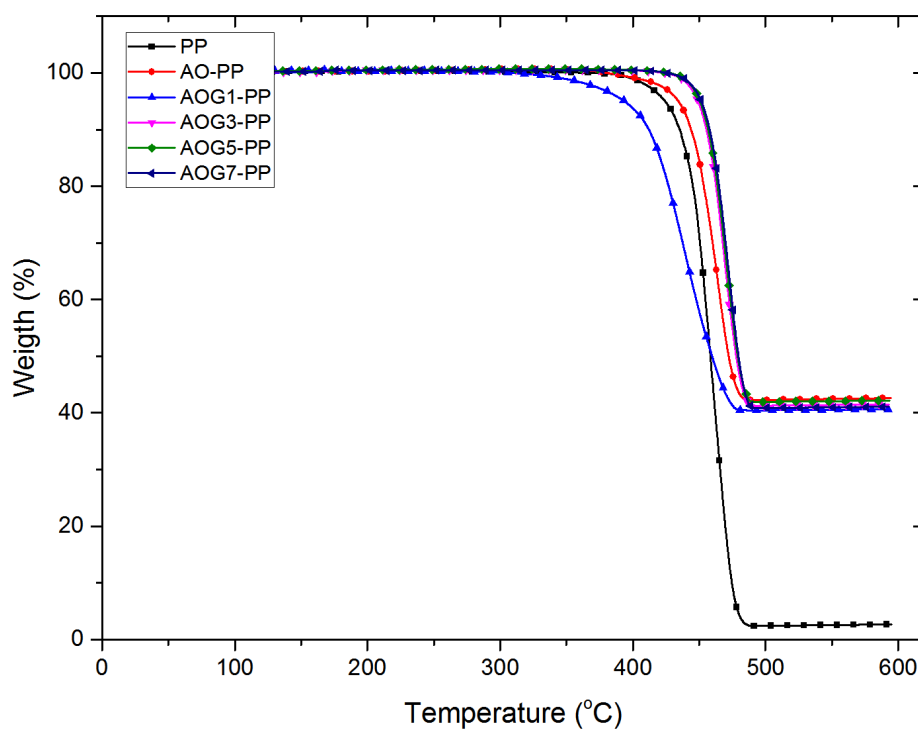


Figure 3.22: TGA thermogram of neat PP, AO-PP, AOG1-PP, AOG3-PP, AOG5-PP and AOG7-PP

40% alumina and alumina-G hybrid filler loaded PP matrix composites TGA analysis results were given in Figure 3.22. The addition of alumina into the PP matrix increased the thermal degradation temperature of composite AO-PP [140]. With addition to G plaques in to the filler and 1, 3, 5, and 7% respectively to the PP matrix, the composites thermal degradation temperatures increased except AOG1-PP composite. At the thermogravimetric analysis thermogram, total residue of thermal degradation of composites was same and around 40%. Total amount of filler did not changed for understanding G plaques effects into the alumina loaded PP matrix.

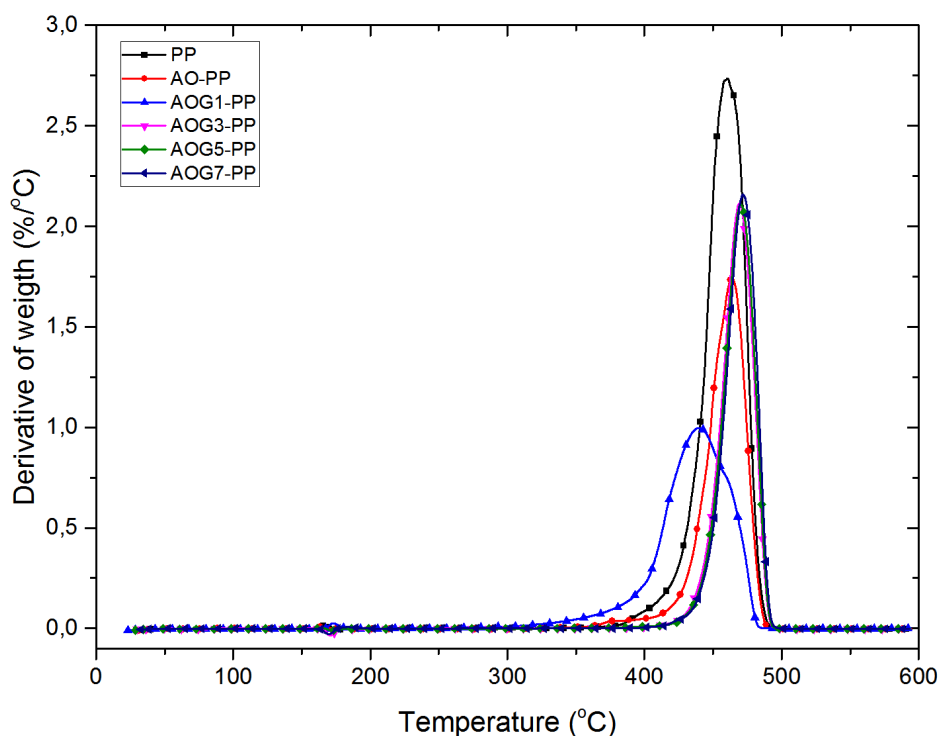


Figure 3.23: DTG thermogram of neat PP, AO-PP, AOG1-PP, AOG3-PP, AOG5-PP and AOG7-PP

The DTG results (Figure 3.23) showed that thermal degradation rate of PP was higher than all composites but maximum thermal degradation temperature of composite shifted right side of thermogram, which could be explained by thermal stability increment of the composites. Thermal degradation velocity and rates of AOG3-PP, AOG5-PP, and AOG7-PP were the same. However, AO-PP and AOG1-PP degradation velocity and rate was smaller than the neat PP and the other composites. G plaques might be increased the orientation of polymer chains order in to the matrix except low ratios. In the literature, G plaques loaded composites thermal properties have been studied before but has not worked with a ceramic mixture in the PP matrix. This study became as a first for researching effects of G plaques into the alumina loaded PP matrix.

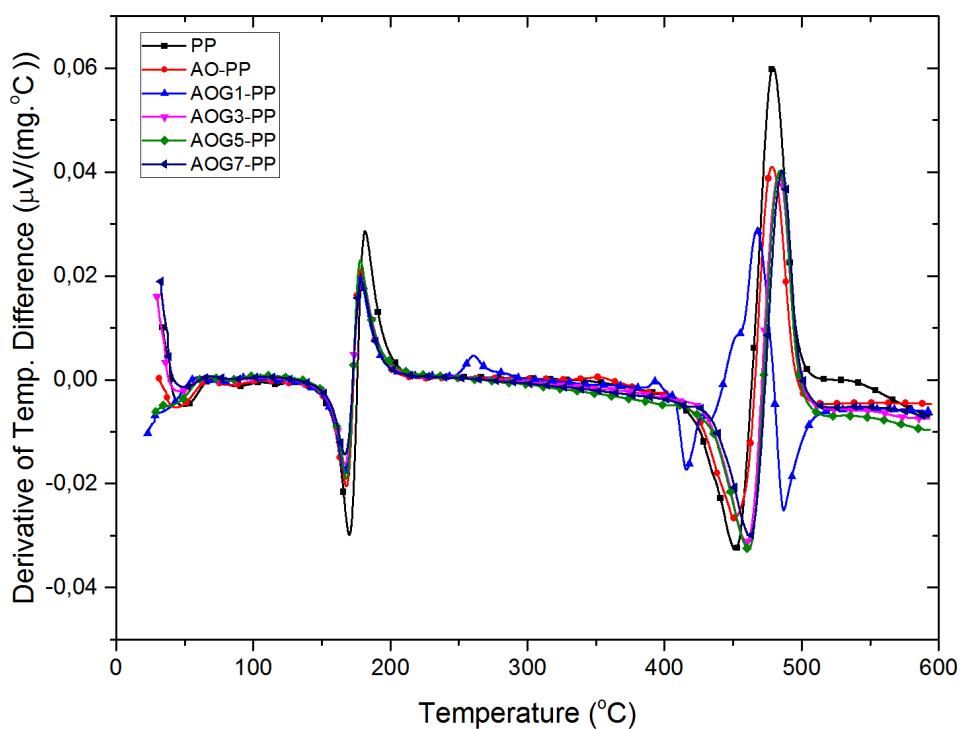


Figure 3.24: DTA thermogram of neat PP, AO-PP, AOG1-PP, AOG3-PP, AOG5-PP and AOG7-PP

DTA showed two specific reactions in to the composite with increasing temperature. The first reaction occurred between 160°C to 180°C (Figure 3.24). PP matrix melting temperature was almost 167°C and we identified this reaction as a phase change reaction of PP matrix. The second reaction started at 460°C and finished at 500°C, also this reaction temperature similar to decomposition point of PP matrix. AOG1-PP composite's DTA signal started change before 250°C to 300°C and showed a different property from the other composites. Some different thermal degradation pathway could be occurred on this temperature region. AOG1-PP was different energetic reactions between 400°C to 520°C. DTA signals sharpness increase over 3% G plaques addition to filler content.

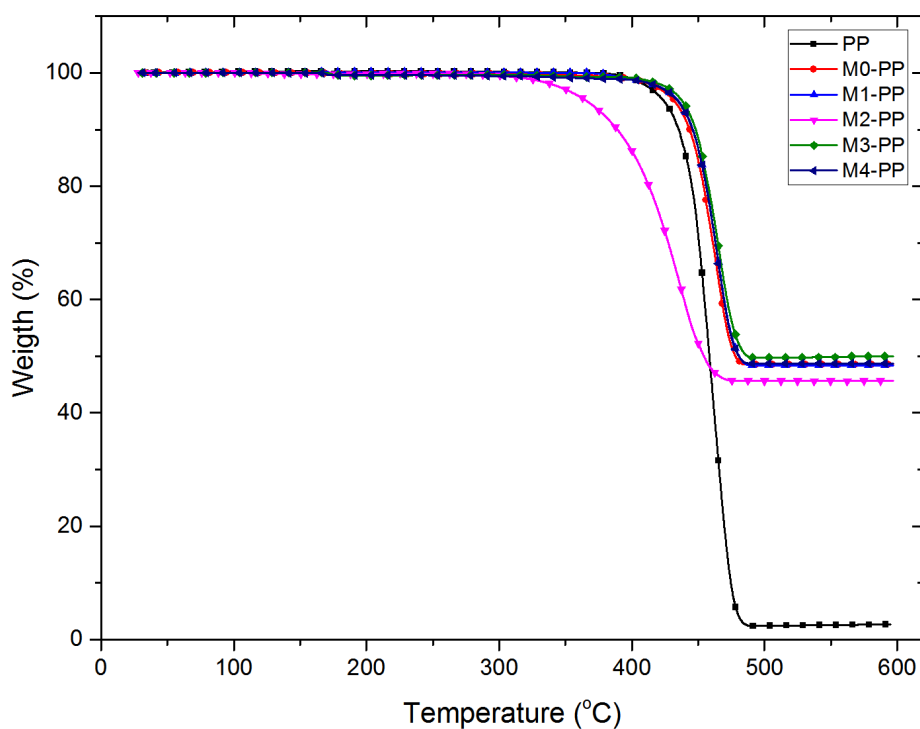


Figure 3.25: TGA thermogram of neat PP, M0-PP, M1-PP, M2-PP, M3-PP, M4-PP and M5-PP

50% unmodified alumina and silan-modified alumina particle loaded PP matrix composites TGA thermogram was given in Figure 3.25. The addition of unmodified alumina into the PP matrix increased the thermal degradation temperature of composite which was M0-PP. Thermal stability increased with the surface modification of alumina particles addition to the PP matrix [141]. However M2 (3-(Trimethoxysilyl) propyl methacrylate) modification decreased to PP matrix decomposition temperature significantly. For understanding of these unacceptable result DTA curve was examined thoroughly.

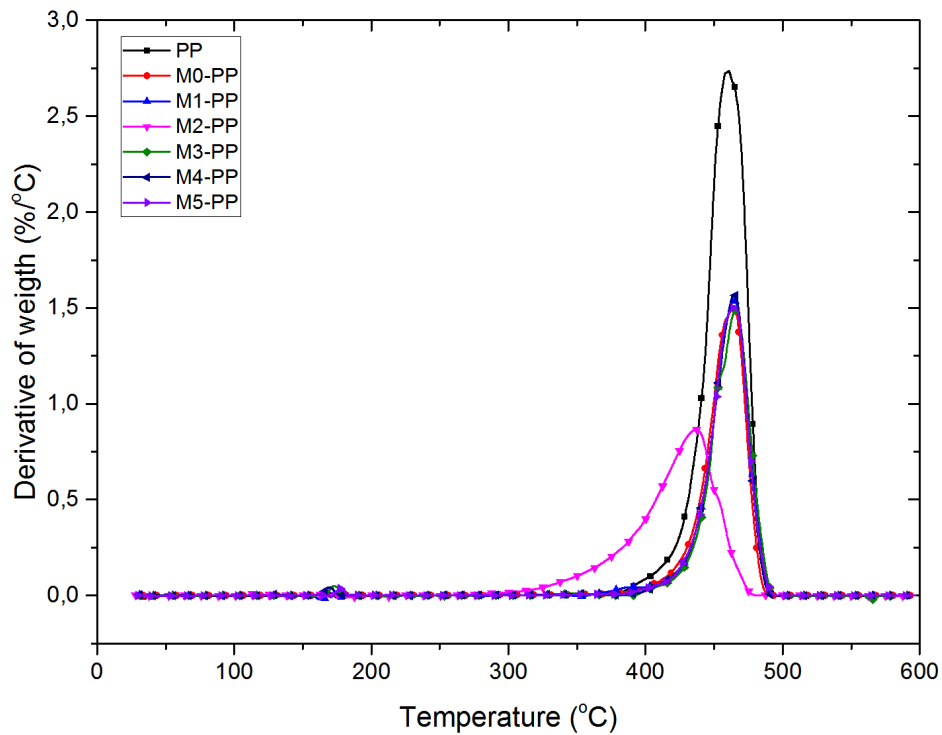


Figure 3.26: DTG thermogram of neat PP, M0-PP, M1-PP, M2-PP, M3-PP, M4-PP and M5-PP

The DTG results (Figure 3.26) showed that thermal degradation rate of PP was higher than all composites but maximum thermal degradation temperature of M0-PP, M1-PP, M3-PP, M4-PP, and M5-PP composites shifted right side of thermogram, which might be explained by thermal stability increment of the composites [142; 143]. Thermal degradation velocity and rates of M0-PP, M1-PP, M3-PP, M4-PP, and M5-PP were the nearly same. However, M2-PP degradation velocity and rate was smaller and large temperature interval than the neat PP and the other composites.

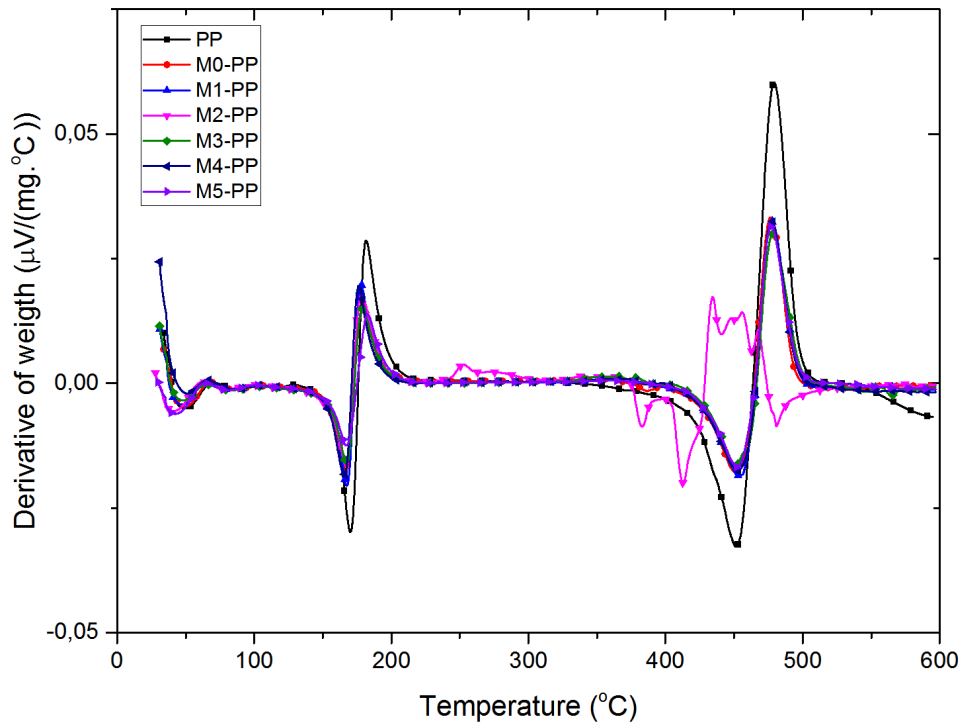


Figure 3.27: DTA thermogram of neat PP, M0-PP, M1-PP, M2-PP, M3-PP, M4-PP and M5-PP

Figure 3.27 gave the DTA signals of 50% unmodified alumina and modified alumina loaded PP matrix composites between ambient temperatures to 600°C. DTA results showed two specific reactions in to the composite with increasing temperature. The first reaction occurred between 160°C to 180°C. PP matrix melting temperature was almost 167°C and we identified this reaction as a phase change reaction of PP matrix. The second reaction started at 440°C and finished at almost 500°C, also this reaction temperature similar to decomposition point of PP matrix. M2-PP composite's DTA signal started to change before 250°C to 300°C and showed a different property from the other composites. Some different thermal degradation pathway could be occurred on this temperature region. M2-PP was different energetic reactions between 380°C to 480°C. DTA signals sharpness and similarities were the same other composites.

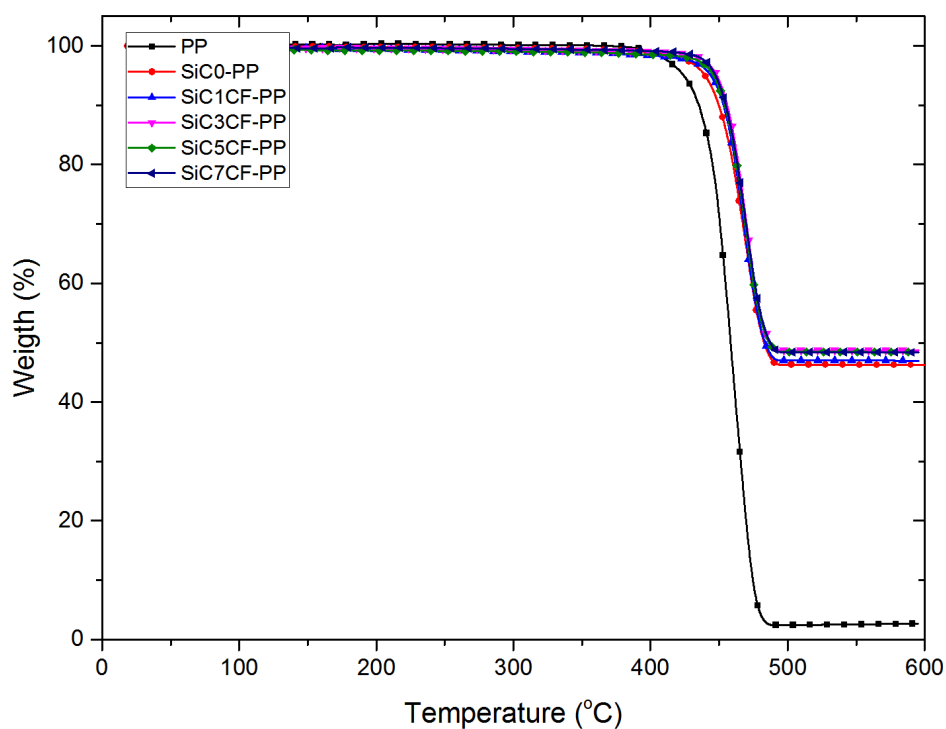


Figure 3.28: TGA thermogram of neat PP, SiC0CF-PP, SiC1CF-PP, SiC3CF-PP, SiC5CF-PP and SiC7CF-PP

According to Figure 3.28, the thermal stability of composites increased with addition of 50% SiC and SiC-CF combined filler into the PP matrix. Total amount of filler content was same and 50% so TGA thermogram filler residues were same for all composites. CF addition to matrix improved thermal degradation temperature for almost 10°C. In the literature, Huaili Q. et al. works showed that ceramic based materials loading to PP matrix increased thermal degradation temperature of PP matrix [144].

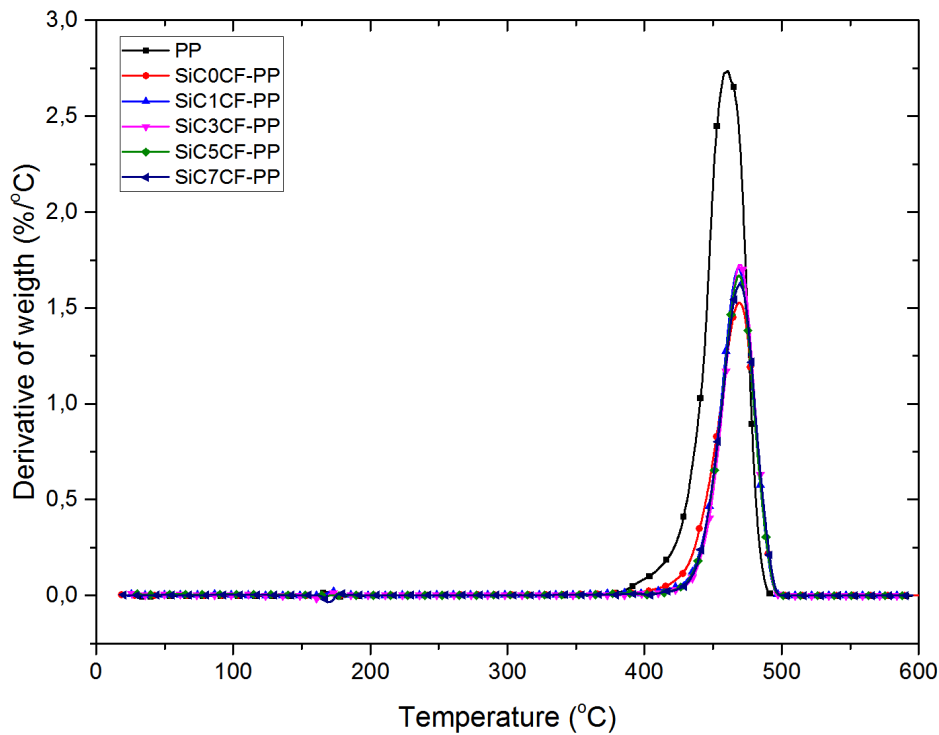


Figure 3.29: DTG thermogram of neat PP, SiC0CF-PP, SiC1CF-PP, SiC3CF-PP, SiC5CF-PP and SiC7CF-PP

The DTG results (Figure 3.29) showed thermal degradation rate of PP was higher than all composites. The thermal degradation temperature of composites shifted right side of thermogram, which might be explained by thermal stability increment of the composites. CF improved thermal stability and increased thermal degradation velocity and rates of composites [145]. In the literature, SiC and CF loaded PP matrix composites similar works have not worked yet. Due to the this reason, thermal properties of composites was discussed onto the CF loaded PP matrix and derivatives.

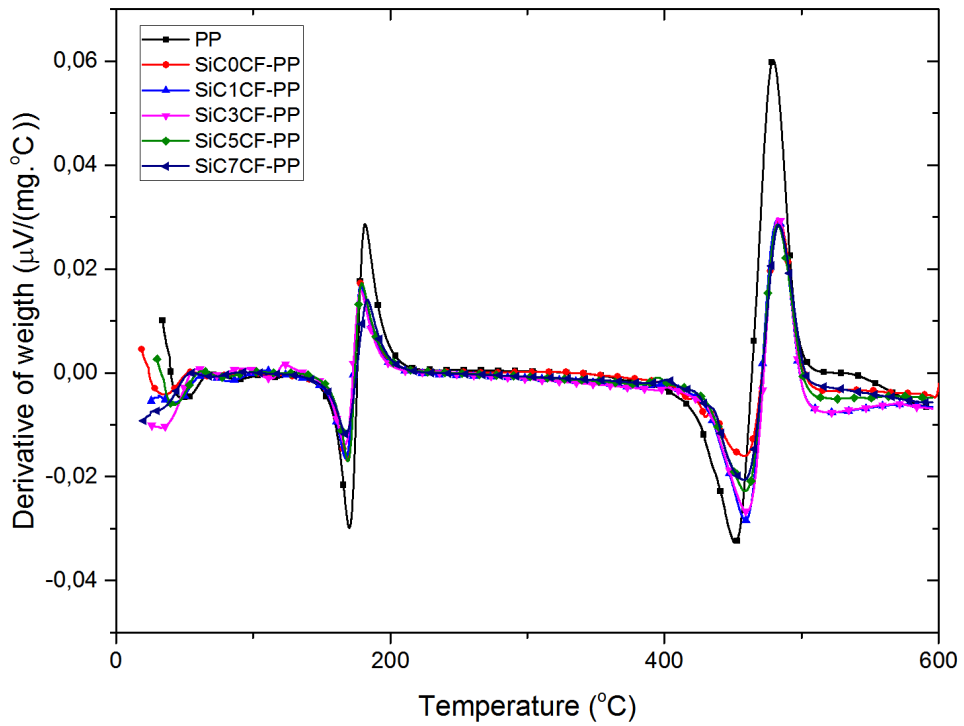


Figure 3.30: DTA thermogram of neat PP, SiC0CF-PP, SiC1CF-PP, SiC3CF-PP, SiC5CF-PP and SiC7CF-PP

Figure 3.30 gave the DTA signals of 50% SiC and SiC-CF loaded PP matrix composites between room temperature to 600°C. DTA showed two specific reactions in to the composite with increasing temperature. The first reaction occurred between 160°C to 180°C. PP matrix melting temperature was almost 167°C and we identified this reaction as a phase change reaction of PP matrix. The second reaction started at 450°C and finished at almost 500°C so this reaction temperature similar to decomposition point of PP matrix. DTA signals sharpness and similarities were the same all composites.

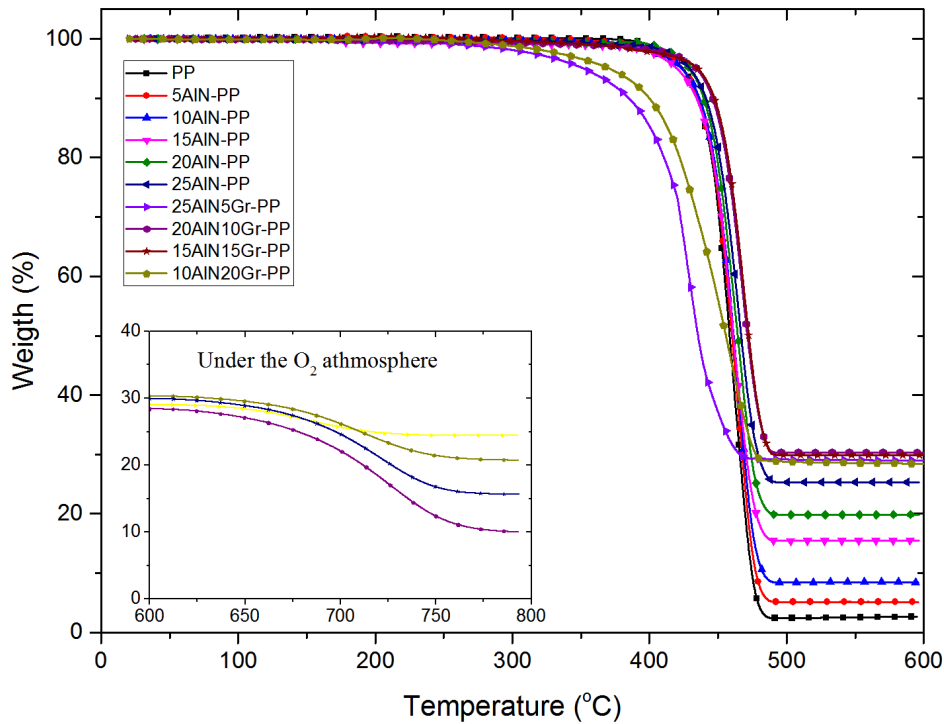


Figure 3.31: TGA thermogram of neat PP, 5AlN-PP, 10AlN-PP, 15AlN-PP, 20AlN-PP, 25AlN-PP, 25AlN5Gr-PP, 20AlN10Gr-PP, 15AlN15Gr-PP, and 10AlN20Gr-PP

TGA thermogram of AlN and AlN-Gr loaded PP matrix composites were given in Figure 3.31. Test temperature extended for Gr included composite to 800°C and oxygen atmosphere applied the between 600°C to 800°C for corrected ratio of Gr content into the composites. Thermal residue of composites showed similarity to addition ratio of filler. Thermal degradation temperature of composite increased with AlN addition to PP matrix [146]. However, Gr addition was decreased thermal degradation temperature of 25AlN5Gr-PP and 10AlN20Gr. Over 10% Gr addition increased thermal degradation temperature. AlN and Gr loaded PP matrix composites have not been studied in the literature before so results of studies were discussed ceramic based material loaded PP composites. However, that discussion was not reflected original studies data properly.

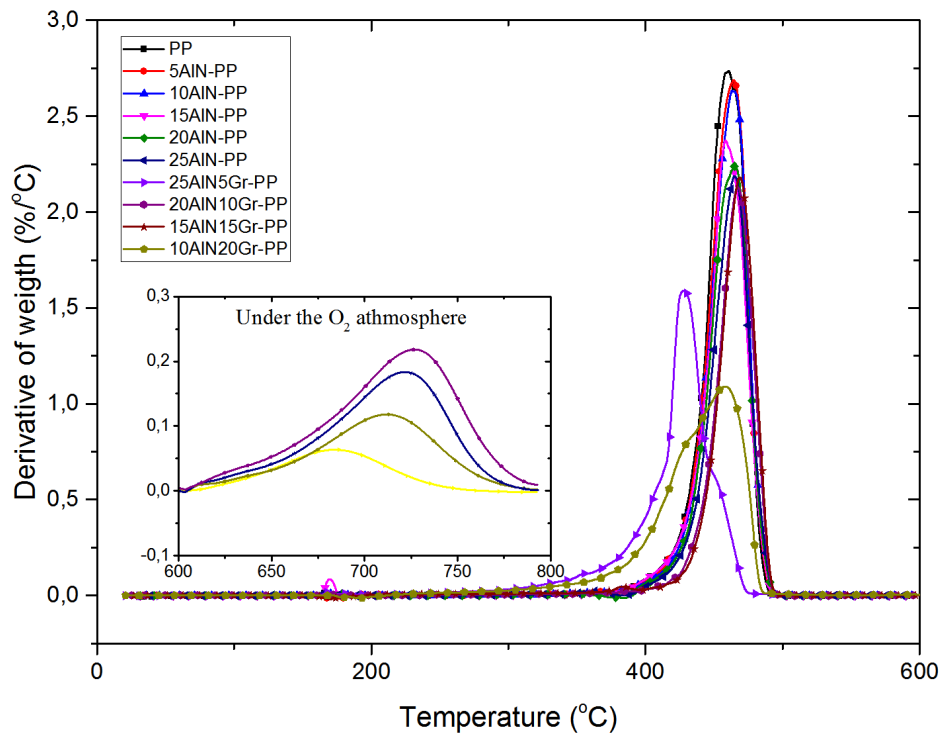


Figure 3.32: DTG thermogram of neat PP, 5AlN-PP, 10AlN-PP, 15AlN-PP, 20AlN-PP, 25AlN-PP, 25AlN5Gr-PP, 20AlN10Gr-PP, 15AlN15Gr-PP, and 10AlN20Gr-PP

According to DTG results (Figure 3.32), thermal degradation velocity and rates were the almost same for neat PP, 5AlN-PP, and 10AlN-PP composites but top of thermal degradation shifted right side of the thermogram nearly 10°C. The thermal degradation rates and velocities nearly same for Gr added PP matrix composites except 25AlN5Gr-PP and 10AlN20Gr-PP. 25AlN5Gr-PP maximum thermal degradation temperature was lower than neat PP and the other composites. 10AlN20Gr-PP thermal degradation onset and offset points' difference was higher than neat PP and the other composites. 10AlN20Gr-PP and 25AlN5Gr-PP composites thermal degradation mechanisms were different from neat PP and the other composites. The thermal degradation temperature increased with ratio of Gr over the 600°C. This shift might be explained with carbon content increment. If, oxygen gas flow rate were small for the burning process of sample, burning of time of sample would be extended.

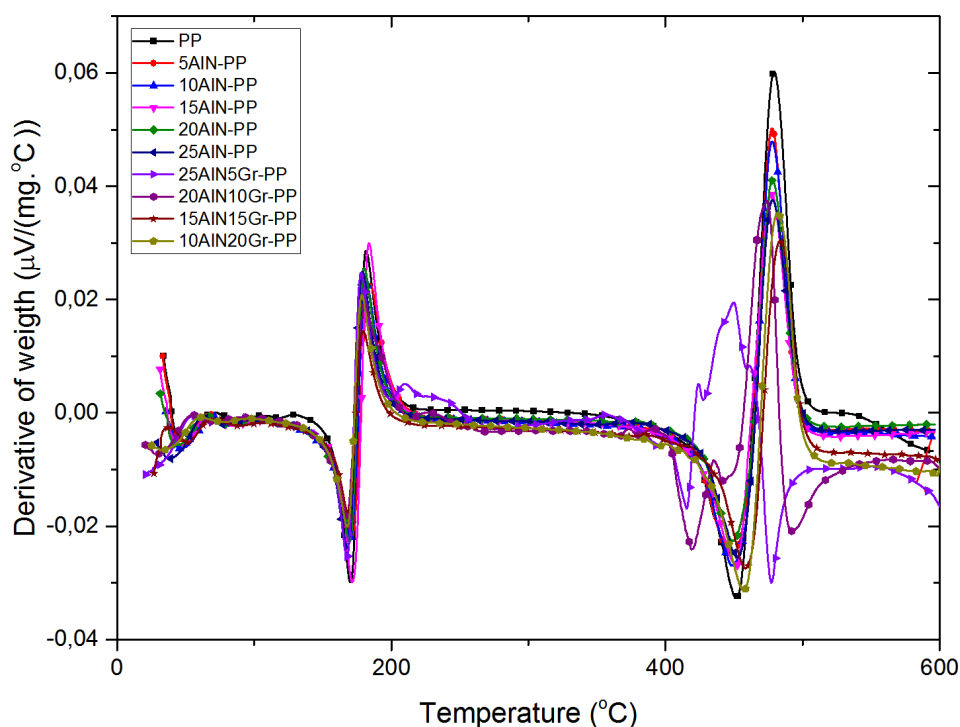


Figure 3.33: DTA thermogram of neat PP, 5AIN-PP, 10AIN-PP, 15AIN-PP, 20AIN-PP, 25AIN-PP, 25AIN5Gr-PP, 20AIN10Gr-PP, 15AIN15Gr-PP, and 10AIN20Gr-PP

Figure 3.33 gave the DTA signals of AIN and ALN-Gr hybrid filler loaded PP matrix composites between room temperature to 600°C. DTA showed two specific reactions in to the composite with increasing temperature. The first reaction occurred between 160°C to 180°C. PP matrix melting temperature was almost 167°C and we identified this reaction as a phase change reaction of PP matrix. The second reaction started at 450°C and finished at almost 480°C so this reaction temperature similar to decomposition point of PP matrix. The melting part of PP matrix DTA signals sharpness were same but melting temperature of composites were not similar for the all of the composites. 25AIN5Gr-PP and 20AIN10Gr-PP thermal degradation pathway was different to neat PP and the other composites. 25AIN5Gr-PP started to change its chemical structure at 410°C and these reaction sequences went on 480°C. 20AIN10Gr-PP started to change its chemical structure at 420°C and these reaction sequences went on 490°C but the last part of degradation mechanism was same as neat PP and the other composites

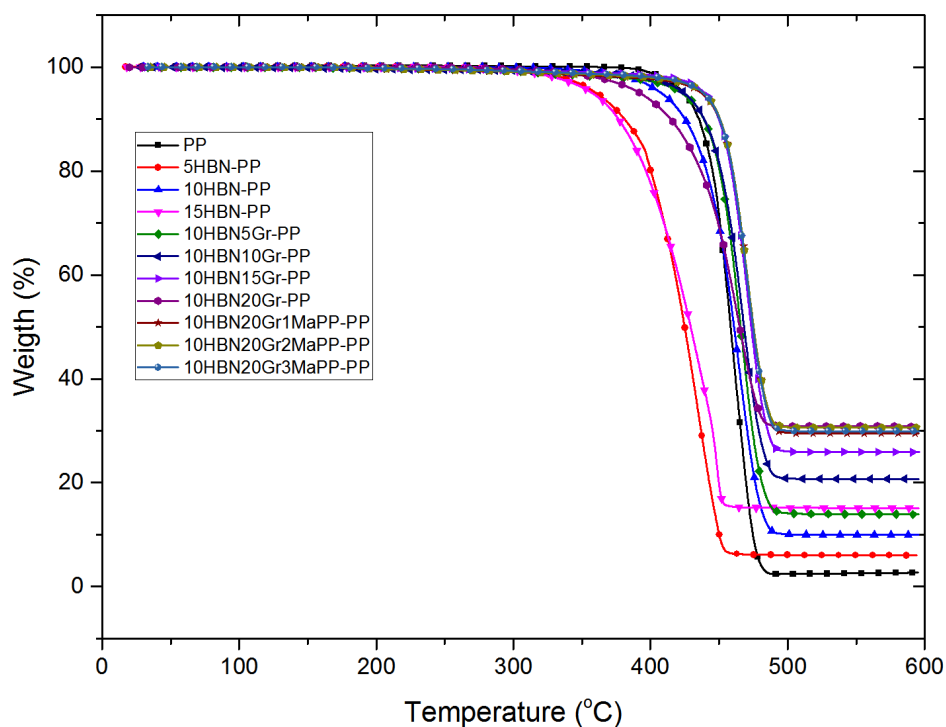


Figure 3.34: TGA thermogram of neat PP, 5HBN-PP, 10HBN-PP, 15HBN-PP, 10HBN5Gr-PP, 10HBN10Gr-PP, 10HBN15Gr-PP, 10HBN20Gr-PP, 10HBN20Gr1MaPP-PP, 10HBN20Gr2MaPP-PP, and 10HBN20Gr3MaPP-PP

TGA thermogram of HBN, HBN-Gr and HBN-Gr-MaPP loaded PP matrix composites were given in Figure 3.34. HBN addition to PP matrix Thermal residue of composites showed similarity to addition ratio of filler. Thermal degradation temperature decreased with HBN addition to PP matrix. Thermal degradation temperature of composites increased with addition of over 15% Gr to the PP matrix. Thermal degradation temperature increased with addition of 1, 2, and 3% MaPP into the 10% HBN and 20% Gr included PP matrix. HBN loaded PP matrix composites properties have not been investigated enough and HBN-Gr hybrid filler mixtures have not been manufactured by high-speed thermo-kinetic mixer. However only Gr added polymer matrix based composites were investigated in literature. While manufactured composites results were comparing to literature data, some differences were seen. For example, Rajatendu et al. have been worked on graphite loaded polymer matrix composite and observed that Gr addition to polymer matrix increased polymer mechanical and thermal properties with increasing addition ratio of Gr

[136]. However in our study showed that Gr addition to HBN loaded PP matrix decreased thermal stability of composites until over the 10% Gr addition to PP matrix.

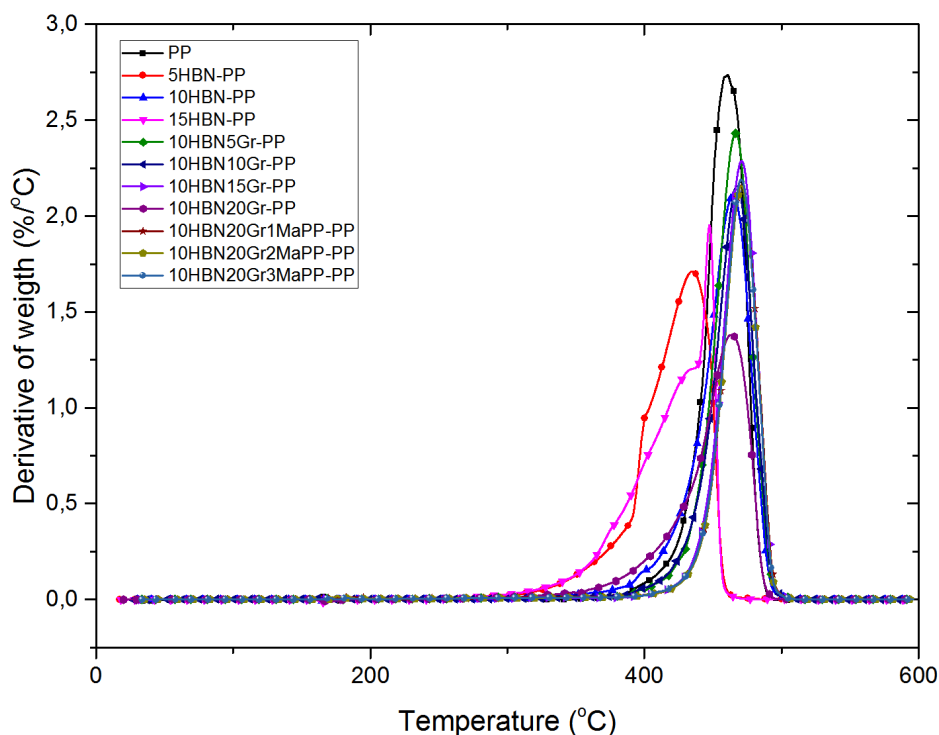


Figure 3.35: DTG thermogram of neat PP, 5HBN-PP, 10HBN-PP, 15HBN-PP, 10HBN5Gr-PP, 10HBN10Gr-PP, 10HBN15Gr-PP, 10HBN20Gr-PP, 10HBN20Gr1MaPP-PP, 10HBN20Gr2MaPP-PP, and 10HBN20Gr3MaPP-PP

According to DTG results (Figure 3.35), thermal degradation velocity and rates were the almost same for 10HBN10Gr-PP, 10HBN15Gr-PP, 10HBN20Gr-PP, 10HBN20Gr1MaPP-PP, 10HBN20Gr2MaPP-PP, and 10HBN20Gr3MaPP-PP. HBN added PP matrix composites DTG curves were different than the other composites. HBN-Gr loaded and MaPP modified PP matrix composites thermal degradation shifted to right side of the thermogram nearly 10 to 15°C. 5 and 10% HBN added PP composites thermal degradation mechanisms were different from the other composite and each other. However 10% HBN added PP matrix composite was similar thermal degradation pathway the other composites and neat PP.

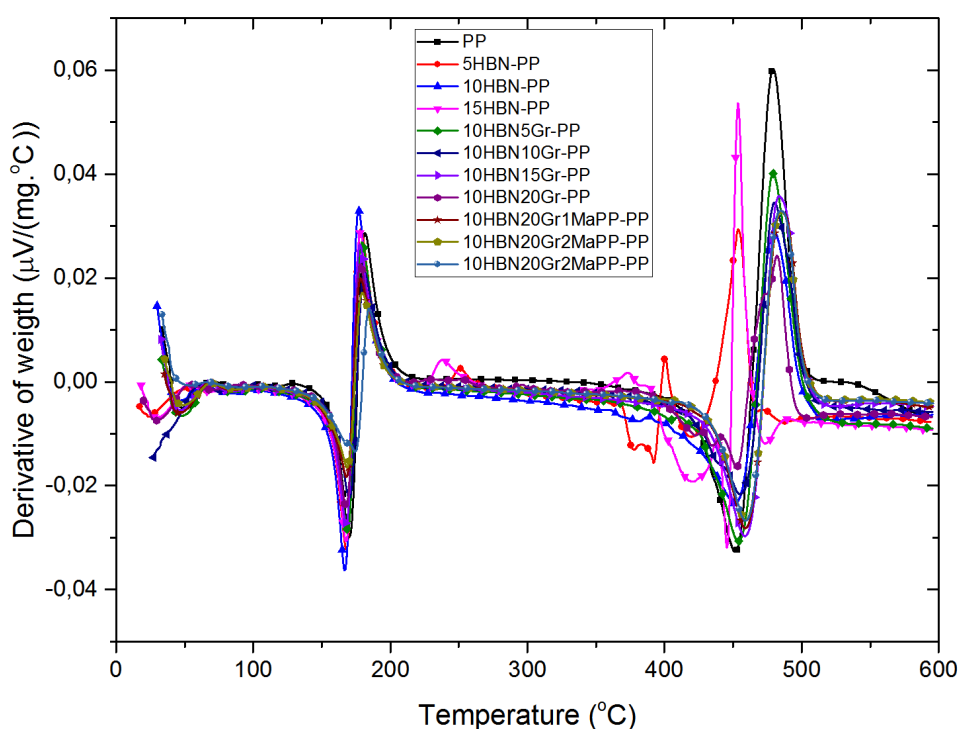


Figure 3.36: DTA thermogram of neat PP, 5HBN-PP, 10HBN-PP, 15HBN-PP, 10HBN5Gr-PP, 10HBN10Gr-PP, 10HBN15Gr-PP, 10HBN20Gr-PP, 10HBN20Gr1MaPP-PP, 10HBN20Gr2MaPP-PP, and 10HBN20Gr3MaPP-PP

Figure 3.36 gave the DTA signals of HBN, HBN-Gr and HBN-Gr-MaPP loaded PP matrix composites between room temperature to 600°C. DTA showed two specific reactions in to the composite with increasing the temperature. The first reaction occurred between 160°C to 180°C. PP matrix melting temperature was almost 167°C and we identified this reaction as a phase change reaction of PP matrix. The second reaction started at 450°C and finished at almost 500°C so this reaction temperature similar to decomposition point of PP matrix. The melting part of PP matrix DTA signals sharpness were same but melting temperature of composites were not similar for the all of the composites. HBN loaded PP matrix thermal decomposition pathways were not similar the other composites and neat PP. 5HBN-PP composite chemical change started at 230°C and finished over the 500°C. 15HBN-PP composite chemical change started at 250°C and ended below the 500°C.

3.4 DSC Analysis

Table 3.2: DSC analysis results of all composites.

Sample	Cooling Cycle			ΔH_c (J/g)	Second Heating Cycle			ΔH_m (J/g)	%Crys.	C_p at 25°C
	Onset Temp. (°C)	T_c (°C)	Offset Temp. (°C)		Onset Temp. (°C)	T_m (°C)	Offset Temp. (°C)			
PP	123.2	119.9	113.6	98.88	157.7	163.5	168.9	84.12	40.64	2.326
10AlSiC-PP	121.8	118.2	112.6	92.89	147.0	163.4	169.0	94.69	50.8	2.255
20AlSiC-PP	122.8	118.8	113.6	82.40	143.2	163.1	168.1	73.84	44.6	2.071
30AlSiC-PP	123.6	120.4	114.0	77.14	142.3	163.1	168.3	75.12	51.8	1.756
40AlSiC-PP	123.9	120.8	116.1	62.70	147.5	162.9	167.3	60.93	49.1	1.370
50AlSiC-PP	124.0	120.7	116.4	51.00	150.9	161.5	166.2	49.24	47.6	1.359
60AlSiC-PP	125.0	122.2	118.0	41.40	152.0	161.6	166.2	40.28	48.6	1.058
SiC0CF-PP	134.4	131.5	126.4	54.25	147.4	165.2	167.8	55.08	53.2	1.071
SiC1CF-PP	133.0	130.2	125.8	54.14	150.4	164.9	167.0	53.79	52.0	0.743
SiC3CF-PP	133.0	130.4	125.4	51.98	154.0	165.0	167.2	51.99	50.2	0.896
SiC5CF-PP	134.4	131.9	126.2	50.60	147.9	165.6	168.9	53.24	51.4	1.179
SiC7CF-PP	132.4	130.0	124.8	51.71	152.1	165.1	168.1	53.04	51.2	1.143
Al-PP	125.2	124.5	117.2	60.39	156.7	162.6	167.9	57.93	46.6	2.381

Table 3.2 (cont): DSC analysis results of all composites.

Sample	Cooling Cycle			ΔH_c (J/g)	Second Heating Cycle			ΔH_m (J/g)	%Crys.	C_p at 25°C
	Onset Temp. (°C)	T_c (°C)	Offset Temp. (°C)		Onset Temp. (°C)	T_m (°C)	Offset Temp. (°C)			
AIG1-PP	125.7	131.9	135.4	63.08	148.5	166.1	170.4	59.93	48.3	1.734
AIG3-PP	128.2	133.2	137.7	59.89	150.7	166.4	170.5	58.92	47.4	2.067
AIG5-PP	128.9	133.9	137.9	60.79	148.9	166.5	170.7	61.48	49.5	2.128
AIG7-PP	127.5	133.7	138.0	57.28	149.4	167.6	172.1	56.49	45.5	1.836
M0-PP	116.8	122.2	124.3	52.89	158.7	163.3	168.4	44.29	42.8	1.283
M1-PP	116.4	122.8	125.2	52.86	158.9	163.8	168.7	46.53	45.0	1.234
M2-PP	117.7	122.5	126.1	53.27	159.4	163.8	168.3	46.08	44.5	1.144
M3-PP	119.8	123.8	126.6	52.22	157.9	163.2	166.74	48.41	46.8	0.947
M4-PP	117.5	123.9	125.7	51.61	160.1	164.0	168.5	46.58	45.0	1.210
M5-PP	116.5	123.0	126.0	50.14	159.6	164.3	168.8	43.58	42.1	1.078
5AIN-PP	128.4	125.4	119.3	103.4	156.1	164.3	167.4	101.6	51.66	0.938
10AIN-PP	127.5	124.8	118.6	93.38	154.9	165.1	168.9	91.22	48.96	0.642
15AIN-PP	125.7	121.5	113.4	83.05	158.6	167.3	173.2	77.44	44.01	0.135

Table 3.2 (cont): DSC analysis results of all composites.

Sample	Cooling Cycle			ΔH_c (J/g)	Second Heating Cycle			ΔH_m (J/g)	%Crys.	C_p at 25°C
	Onset Temp. (°C)	T_c (°C)	Offset Temp. (°C)		Onset Temp. (°C)	T_m (°C)	Offset Temp. (°C)			
20AlN-PP	128.2	125.5	119.4	86.38	157.3	164.4	168.8	80.00	48.31	0.487
25AlN-PP	126.9	123.9	119.8	75.90	159.6	163.8	167.4	72.24	46.53	0.085
25AlN5Gr-PP	135.0	131.1	126.8	73.71	147.3	165.5	167.9	67.71	46.73	0.187
20AlN10Gr-PP	135.0	131.0	127.1	74.09	148.0	165.0	167.4	70.50	48.65	0.099
15AlN15Gr-PP	134.7	131.1	126.4	72.34	148.2	165.9	169.4	67.57	46.63	0.233
10AlN20Gr-PP	135.0	131.7	126.4	73.87	147.02	165.6	168.3	72.09	49.75	0.541
5HBN-PP	136.2	131.8	125.9	98.09	147.6	166.6	171.5	98.05	49.86	0.937
10HBN-PP	138.4	133.9	128.2	97.52	150.7	166.3	170.8	94.28	50.60	1.222
15HBN-PP	139.2	133.9	123.1	93.71	148.9	168.5	176.2	82.17	46.70	1.199
10HBN5Gr-PP	136.4	133.1	128.3	92.02	144.8	166.5	170.6	90.20	51.26	1.090
10HBN10Gr-PP	135.7	131.0	120.3	80.79	143.6	168.0	174.4	75.20	45.41	0.836
10HBN15Gr-PP	136.9	132.2	124.5	78.72	148.6	166.6	171.0	79.03	50.91	0.634
10HBN20Gr-PP	136.2	132.1	124.4	71.39	147.7	166.3	171.8	67.20	46.37	0.897

Table 3.2 (cont): DSC analysis results of all composites.

Sample	Cooling Cycle			ΔH_c (J/g)	Second Heating Cycle			ΔH_m (J/g)	%Crys.	C_p at 25°C
	Onset Temp. (°C)	T_c (°C)	Offset Temp. (°C)		Onset Temp. (°C)	T_m (°C)	Offset Temp. (°C)			
10HBN20Gr1M aPP-PP	136.4	132.7	126.8	75.11	149.2	165.7	168.8	71.78	49.54	1.021
10HBN20Gr2M aPP-PP	136.4	133.0	126.3	73.42	147.6	165.4	168.8	69.25	47.79	1.077
10HBN20Gr3M aPP-PP	135.6	132.5	128.5	72.30	154.9	164.8	167.8	70.77	48.84	NA

$$X_c(\%) = \frac{\Delta H_m}{\Phi_{PP} \Delta H_m^0} \times 100$$

Equation 3.1: Percentage crystallinity of PP was calculated from ΔH_m^0 value of PP which was 100% crystalline PP's melting enthalpy 206.9 J/g [147]

The cooling cycle, onset temperature, crystallization temperature (T_c), offset temperature and enthalpy of crystallinity (ΔH_c) were given Table 3.2. The second heating cycle; onset temperature, melting temperature (T_m), offset temperature and enthalpy of melting (ΔH_m) were given in Table 3.2. Besides heat capacity, c_p of composites was obtained from DSC thermogram at 25°C and the percentage of crystallinity was calculated from Equation 3.1.

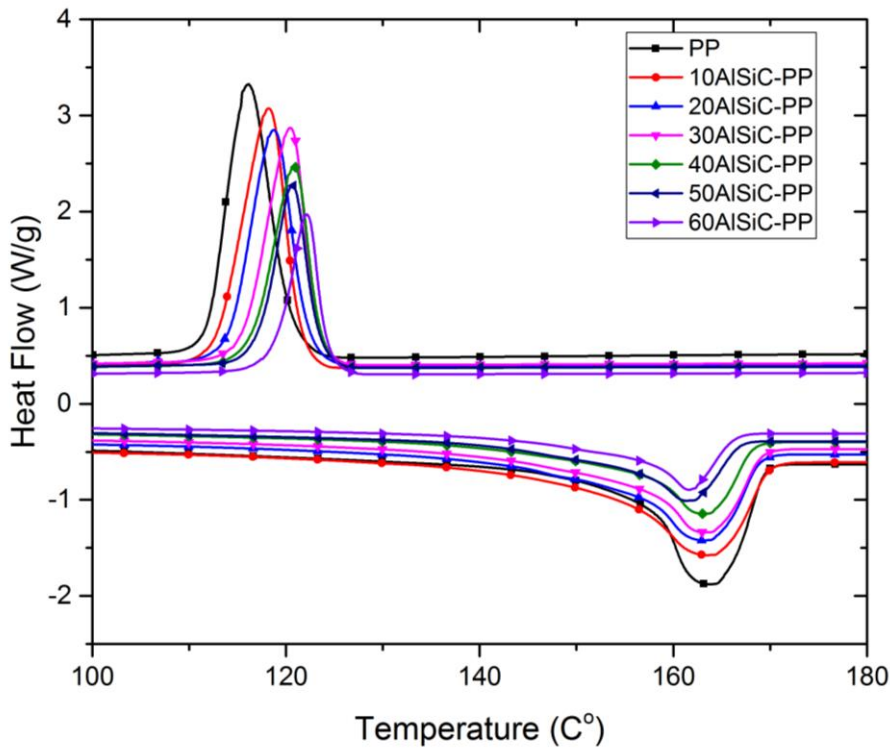


Figure 3.37: DSC thermogram of neat PP, 10AlSiC-PP, 20AlSiC-PP, 30AlSiC-PP, 40AlSiC-PP, 50AlSiC-PP, and 60AlSiC-PP

According to figure 3.37 and table 3.2, the onset temperature of melting decreased almost 10°C with AlSiC addition to PP matrix but offset temperature of composites and neat PP did not change. T_m of samples decreased almost 2°C with AlSiC addition to PP matrix. In addition, T_c values of composites increased nearly 2°C with AlSiC

addition to PP matrix [148]. T_c onset and offset temperatures increase with AlSiC ratio into the matrix [149]. Crystallinity percentage of the PP matrix increased between 10 to 25% than the neat PP. AlSiC particles increased the crystallinity of the PP matrix composites. The c_p of composite decreased with the addition of AlSiC into the the PP matrix. c_p has directly affected composites thermal conductivity behaviors [150]. ΔH_c values of composites decreased with increasing AlSiC particles into the PP matrix.

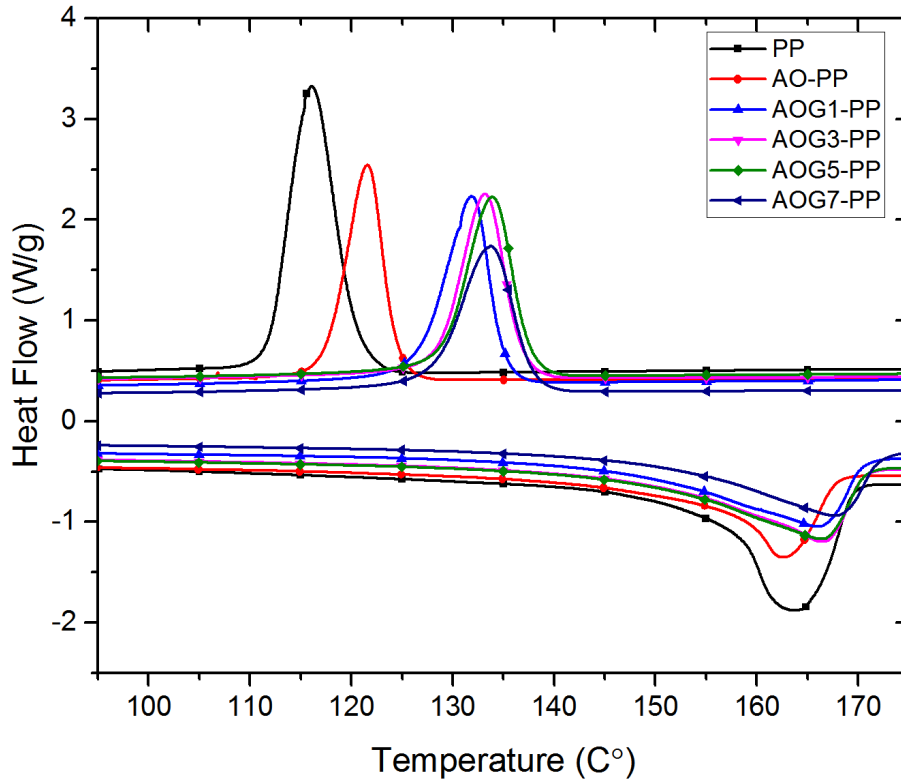


Figure 3.38: DSC thermogram of neat PP, AO-PP, AOG1-PP, AOG3-PP, AOG5-PP, and AOG7-PP

According to Figure 3.38 and Table 3.2, the onset temperature of melting decreased almost 3°C with 40% alumina or 40% alumina-G addition to PP matrix although offset temperature of G added composites shifted 3°C right side of the thermogram. T_m of the AO-PP decreased almost 1°C. AOG1-PP, AOG3-PP, AOG5-PP, and AOG7-PP composites T_m increased between 2 to 5°C than neat PP [151]. In addition, T_c values of AO-PP increased nearly 5°C than neat PP. AOG1-PP, AOG3-PP, AOG5-PP, and AOG7-PP composites T_c were increased nearly 18°C than neat PP [152]. The onset and offset temperatures increased automatically with the T_c change.

The crystallinity percentage of PP matrix increased between 10 to 20% than the neat PP. Alumina and alumina-G particles loading was increased the crystallinity of PP matrix composites [152]. G plaques could be increased crystalline regions in to the PP matrix and melting progress of composites onset-offset temperature distance increased. The c_p of composite did not change meaningfully according to Table 3.2. ΔH_c value of AO-PP decreased with addition G-particles into the PP matrix and almost 4% increased ΔH_c values.

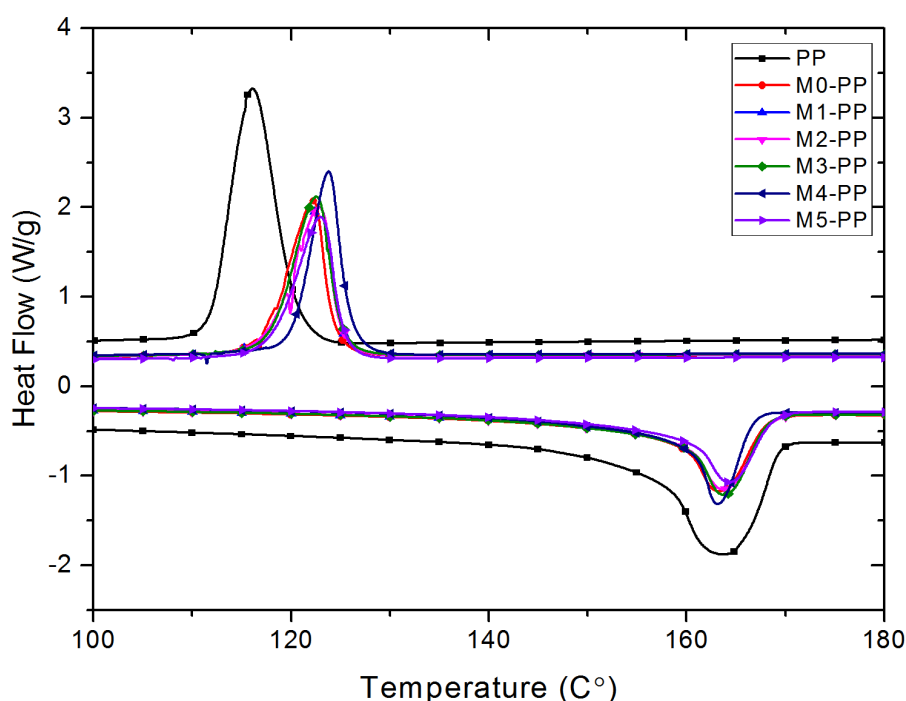


Figure 3.39: DSC thermogram of neat PP, M0-PP, M1-PP, M2-PP, M3-PP, M4-PP and M5-PP

According to Figure 3.39 and Table 3.2, the onset temperature of melting decreased almost 2°C with 50% alumina or 50% modified alumina addition to PP matrix although offset temperature of the composites as same as the neat PP. T_m of the all composites almost same with the neat PP. In addition, T_c values of the composites increased nearly 4°C than the neat PP. The onset temperature of T_c increased 3°C although offset temperature of T_c increased 3°C. The crystallinity percentage of the PP matrix increased between 10 to 15% than the neat PP. Unmodified alumina particle filled PP composites crystallinity was lower than the modified alumina particles loaded PP matrix [153]. Surface modification of alumina particles increased crystallinity of the PP matrix composites. Modified alumina particles surface could

be catalyze crystalline side formation in to the PP matrix [154]. The sharpness of composites melting peak increased and melting progress of composites onset-offset temperature distance decreased. The c_p of composites nearly 40% decreased but M3-PP c_p value decreased nearly 60%. ΔH_c values of composites were nearly the same.

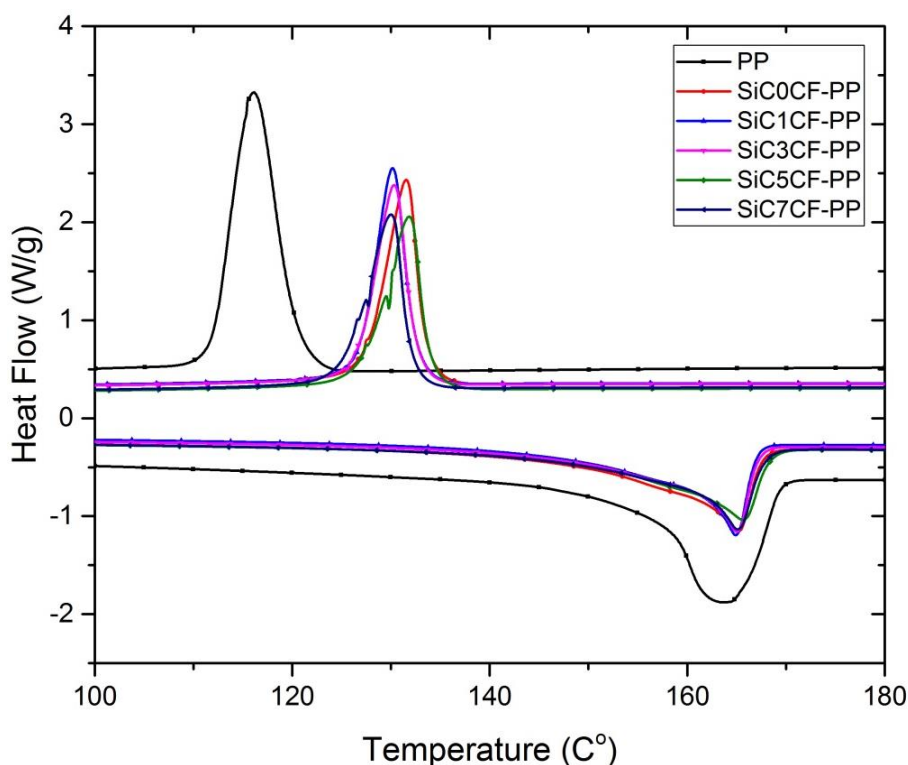


Figure 3.40: DSC thermogram of neat PP, SiC0CF-PP, SiC1CF-PP, SiC3CF-PP, SiC5CF-PP, and SiC7CF-PP

Figure 3.40 and Table 3.2 showed that detailed information about SiC and SiC-CF loaded PP matrix composites thermal properties under nitrogen atmosphere. The onset temperature of melting decreased between 3 to 10°C with the addition 50% SiC or 50% SiC-CF to the PP matrix although offset temperature of the composites as same as the neat PP. T_m of the all composites almost 2°C higher than the neat PP. T_c values of the composites increased nearly 11°C than the neat PP. The onset temperature of T_c increased 10°C although offset temperature of T_c increased 12°C. The crystallinity percentage of the PP matrix composites increased over 25% than the neat PP. The crystallinity of SiC particles filled PP matrix composites was 4% higher than the SiC-CF loaded PP matrix average crystallinity value. CF addition decreased the crystallinity of PP matrix composites [145]. SiC particles surface could be catalyze crystalline side formation in to the PP matrix better than CF [129]. The

sharpness of composites melting peak decreased and melting progress of composites onset-offset temperature distance increased. The c_p of composites nearly 50% decreased but SiC/CF-PP's c_p value decreased over 60%. ΔH_c values of composites decreased with addition CF to the PP matrix. CF could be inhibited crystalline orientation inside of the PP matrix.

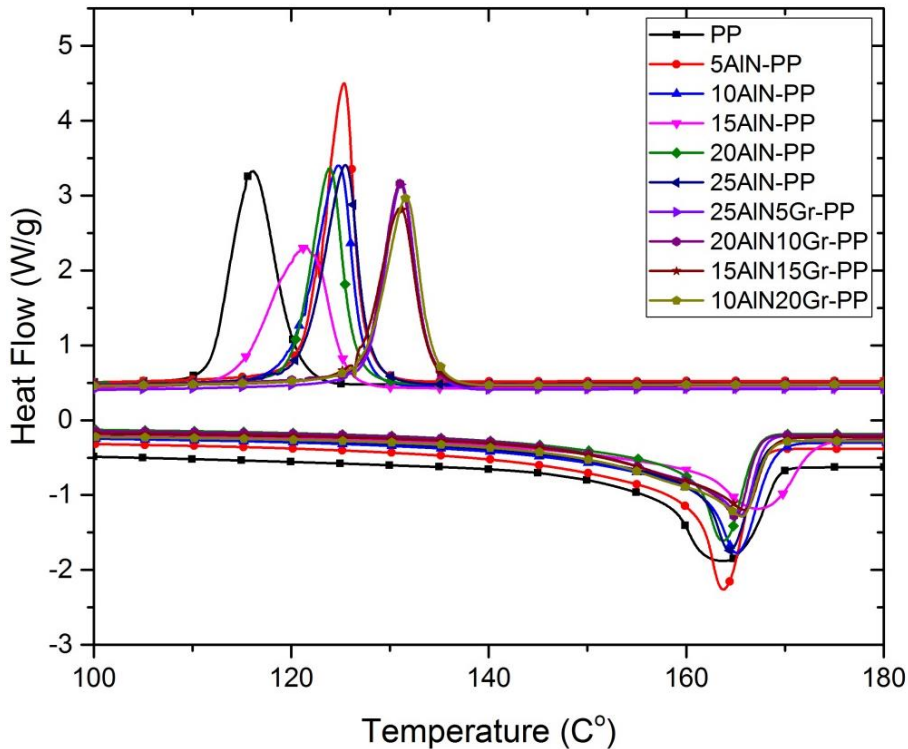


Figure 3.41: DSC thermogram of neat PP, 5AlN-PP, 10AlN-PP, 15AlN-PP, 20AlN-PP, 25AlN-PP, 25AlN5Gr-PP, 20AlN10Gr-PP, 15AlN15Gr-PP, and 10AlN20Gr-PP

Figure 3.41 and Table 3.2 showed that detailed information about AlN and AlN-Gr loaded PP matrix composites thermal properties under the nitrogen atmosphere. The onset temperature of melting decreased AlN addition to PP matrix but over the 15% AlN addition the onset temperature started to rise. Gr addition decreased the onset temperature of melting almost 10°C. The melting offset temperature of the composites was nearly same as neat PP. T_m of the composites almost 2-6°C higher than the polymer matrix. 15AlN-PP melting temperature was higher than the other composites. AlN addition to PP matrix increased T_c values nearly 6°C than the neat PP although Gr addition to matrix increased 16°C than the neat PP [155]. The onset temperature of T_c increased almost 5°C also offset temperature of T_c increased 6°C with the addition of AlN into the PP matrix. The onset temperature of T_c increased

almost 12°C also offset temperature of T_c increased nearly 13°C with the addition of AlN-Gr into the PP matrix. Crystallinity percentage of PP matrix composites increased between 10 to 25% than neat PP with addition AlN into the PP matrix. AlN particles filled PP composites crystallinity was as same as the AlN-Gr loaded PP matrix average crystallinity value. Gr addition did not change the crystallinity of PP matrix composites. 5% AlN loaded composite crystallinity was higher than the all of the composites and the neat PP. Sharpness of composites melting peak increased and melting progress of composites onset-offset temperature distance decreased. The c_p of composites overly 70% decreased but 20AlN10Gr-PP's c_p value decreased over 95%. This value could not be seen proper according to the other composites c_p values however, accuracy of the DSC machine 0.2% for c_p measurement and reproducibility of c_p test results were ± 0.05 for indium peak. ΔH_c value of 5AlN-PP increased almost 5% than the neat PP but ΔH_c values decreased increasing AlN ratio into PP matrix.

AlN and Gr hybrid filler combination added PP matrix applications have not been researched literature before so DSC results were discussed with Gr added polymer matrix composites. Nevertheless, for discussing similarities or differences of literature studies were not enough for seeing synergetic effects of hybrid filler system using in to polymer matrix.

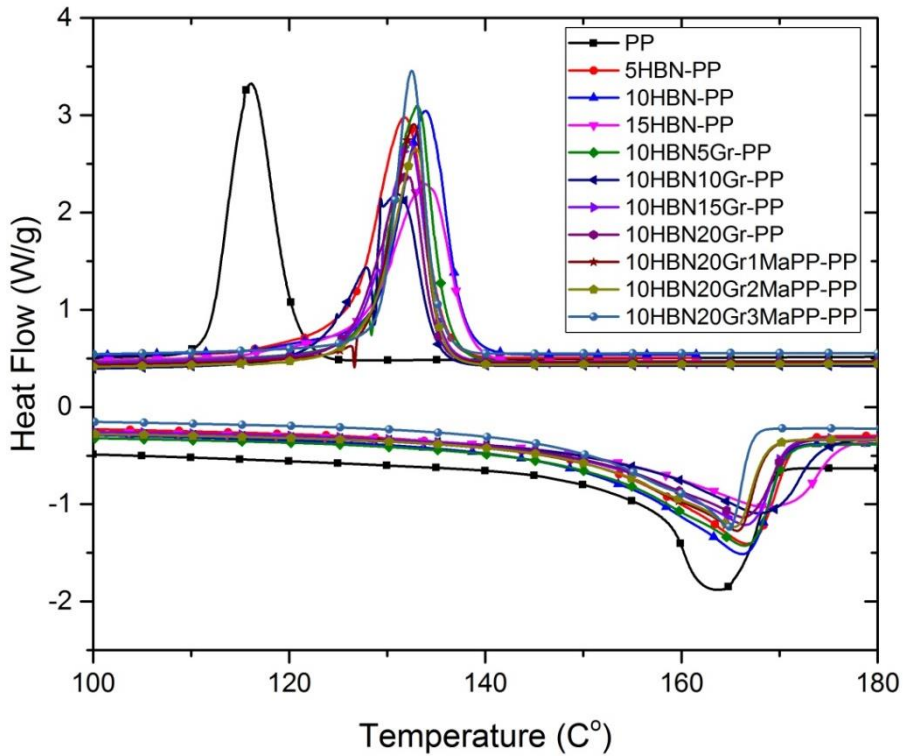


Figure 3.42: DSC thermogram of neat PP, 5HBN-PP, 10HBN-PP, 15HBN-PP, 10HBN5Gr-PP, 10HBN10Gr-PP, 10HBN15Gr-PP, 10HBN20Gr-PP, 10HBN20Gr1MaPP-PP, 10HBN20Gr2MaPP-PP, and 10HBN20Gr3MaPP-PP

Figure 3.42 and Table 3.2 showed that detailed information about HBN, HBN-Gr, and HBN-Gr-MaPP loaded PP matrix composites thermal properties under the nitrogen atmosphere. The onset temperature of melting decreased HBN, HBN-Gr, and HBN-Gr-MaPP addition to PP matrix. Gr addition to PP matrix decreased the melting onset temperature more than 5HBN-PP, 10HBN-PP and 15HBN-PP composites. 3% MaPP addition to PP matrix arrived the melting onset temperature of the neat PP [156]. HBN addition to PP matrix increased T_m values of composites. Gr addition to 10% HBN added PP matrix did not change T_m values of composites meaningfully. HBN addition to PP matrix increased T_c values nearly 13°C than the neat PP although Gr addition to matrix did not change T_c values of composites according to HBN added PP matrix composites. The onset temperature of T_c increased almost 13°C also, offset temperature of T_c increased 12°C with the addition of HBN into the PP matrix. The onset temperature of T_c increased almost 12°C also; offset temperature of T_c increased nearly 13°C with the addition of HBN-Gr into the PP matrix. MaPP addition into the 10% HBN and 20% Gr included PP matrix did not change T_c or T_m values of composites. Crystallinity percentage of HBN, HBN-Gr,

and HBN-Gr-MaPP added PP matrix composites increased between 15 to 25% than neat PP. HBN particles filled PP composites crystallinity decreased according to HBN partition into the PP matrix. 5HBN-PP and 10HBN5Gr-PP composites crystallinities were higher than the other composites. The low concentration of HBN particles increased crystallinity of PP matrix as 5AlN-PP composite. Gr addition did not change the crystallinity of PP matrix according to HBN or MaPP included ones. The c_p of composites overly for 50% decreased but the most decreasing occurred 10HBN15Gr-PP's c_p . ΔH_c value of 5HBN-PP almost the same as neat PP but ΔH_c values decreased increasing HBN and Gr ratio into PP matrix.

HBN and Gr hybrid filler combination loaded PP matrix composites have not been studied literature before. Due to that, DSC results were discussed with Gr added polymer matrix composites. However, for discussing differences of literature studies were not enough for understanding synergetic effects of hybrid filler system using in to polymer matrix.

3.5 DMA Analysis

Viscoelastic properties of composites investigated with DMA system and results were evaluated from TA instrument software analysis program.

Table 3.3: Glassy transition temperature (T_g) of neat PP and composites obtained from storage modulus (E'), loss modulus (E''), and $\text{Tan}\delta$ values.

Samples	T_g (°C) (According to Loss Mod.)	T_g (°C) (According to Storage Mod.)	T_g (°C) (According to $\text{Tan}\delta$ Mod.)
PP	65.54	76.52	80.70
10AlSiC-PP	71.84	82.85	87.06
20AlSiC-PP	73.59	84.58	85.22
30AlSiC-PP	72.33	80.98	85.75
40AlSiC-PP	75.17	85.85	84.85
50AlSiC-PP	71.00	83.98	81.83

Table 3.3 (cont): Glassy transition temperature (T_g) of neat PP and composites obtained from storage modulus (E'), loss modulus (E''), and $\text{Tan}\delta$ values.

Samples	T_g (°C) (According to Loss Mod.)	T_g (°C) (According to Storage Mod.)	T_g (°C) (According to $\text{Tan}\delta$ Mod.)
60AlSiC-PP	75.14	82.73	82.95
SiC0CF-PP	64.03	75.48	75.61
SiC1CF-PP	63.39	74.78	74.82
SiC3CF-PP	63.62	76.17	74.92
SiC5CF-PP	63.79	76.47	76.28
SiC7CF-PP	65.84	75.22	76.53
Al-PP	77.12	87.12	87.52
AlG1-PP	80.61	87.41	87.60
AlG3-PP	72.57	102.09	101.84
AlG5-PP	72.29	97.43	95.98
AlG7-PP	67.67	85.13	87.13
M0-PP	65.48	82.30	88.88
M1-PP	68.78	83.65	81.71
M2-PP	72.96	82.16	82.29
M3-PP	70.57	81.68	81.87
M4-PP	68.90	84.88	82.60
M5-PP	70.52	83.83	84.33
5AlN-PP	66.94	81.39	82.96
10AlN-PP	66.38	78.46	84.18
15AlN-PP	64.77	79.34	82.10
20AlN-PP	66.93	77.66	80.95
25AlN-PP	66.00	77.69	80.66
25AlN5Gr-PP	67.11	81.87	80.97
20AlN10Gr-PP	66.77	80.24	82.75
15AlN15Gr-PP	66.45	79.07	85.51
10AlN20Gr-PP	69.49	80.13	83.47

Table 3.3 (cont): Glassy transition temperature (T_g) of neat PP and composites obtained from storage modulus (E'), loss modulus (E''), and $Tan\delta$ values.

Samples	T_g (°C) (According to Loss Mod.)	T_g (°C) (According to Storage Mod.)	T_g (°C) (According to $Tan\delta$ Mod.)
5HBN-PP	68.13	80.26	81.21
10HBN-PP	67.33	81.13	80.91
15HBN-PP	68.09	80.04	80.02
10HBN5Gr-PP	68.07	80.22	81.95
10HBN10Gr-PP	67.4	81.11	81.35
10HBN15Gr-PP	68.66	80.24	82.54
10HBN20Gr-PP	69.07	81.80	81.86
10HBN20Gr1MaPP-PP	68.26	80.44	82.08
10HBN20Gr2MaPP-PP	66.22	81.00	81.54
10HBN20Gr3MaPP-PP	67.97	80.36	81.19

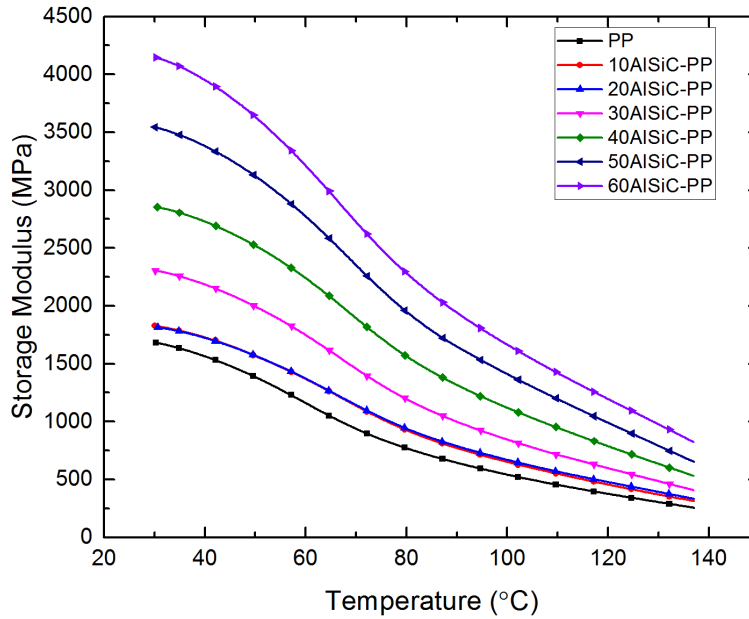


Figure 3.43: Storage Modulus of neat PP, 10AlSiC-PP, 20AlSiC-PP, 30AlSiC-PP, 40AlSiC-PP, 50AlSiC-PP, and 60AlSiC-PP

According to Figure 3.43, the neat PP had a low E' value than the other composites. AlSiC content increment into the PP matrix was increased to E' of composites [157]. 10AlSiC-PP and 20AlSiC-PP composites had nearly same E' values. E' values dramatically decreased over the 30 to 80°C. However, E' values linearly decrease over the 80°C. The elasticity of polymer matrix changed between the ambitions temperatures to 140°C. All composites and neat PP T_g values calculated from bending side of E' graphs and observed that T_g values increased 6 to 9°C than the neat PP [158]. 40AlSiC-PP composite T_g was the highest value and the neat PP.

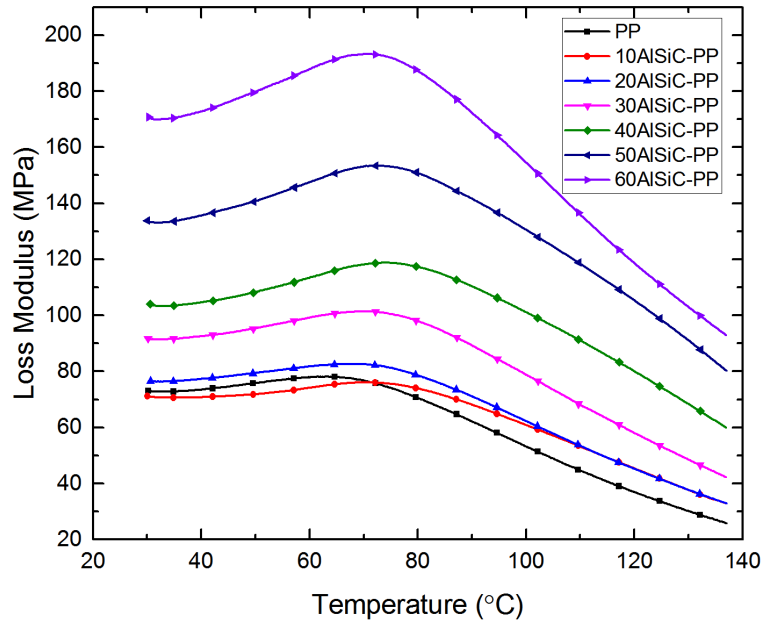


Figure 3.44: Loss Modulus of neat PP, 10AlSiC-PP, 20AlSiC-PP, 30AlSiC-PP, 40AlSiC-PP, 50AlSiC-PP, and 60AlSiC-PP

The AlSiC particle loaded PP matrix composites and neat PP's E'' values were given in Figure 3.44. E'' values of composites higher than the neat PP [72]. Deformation of PP matrix increased around 60°C but upper 70°C temperature, deformation of matrix started to decrease. Polymer chains orientation increased and macro molecular order of matrix decreased at the top of the E'' values. This means that amorphous phase of polymer increased and crystalline phase disappear over 60°C. 10AlSiC-PP and 20AlSiC-PP composites E'' values were nearly same and close to neat PP. However, differences of 10AlSiC-PP and 20AlSiC-PP composites observed over 80°C. If, the upper value of E'' accepted T_g , AlSiC was increased T_g values of PP matrix between 6 to 10°C. 40AlSiC-PP and 60AlSiC-PP composites had the highest T_g values than the other AlSiC loaded PP matrix composites.

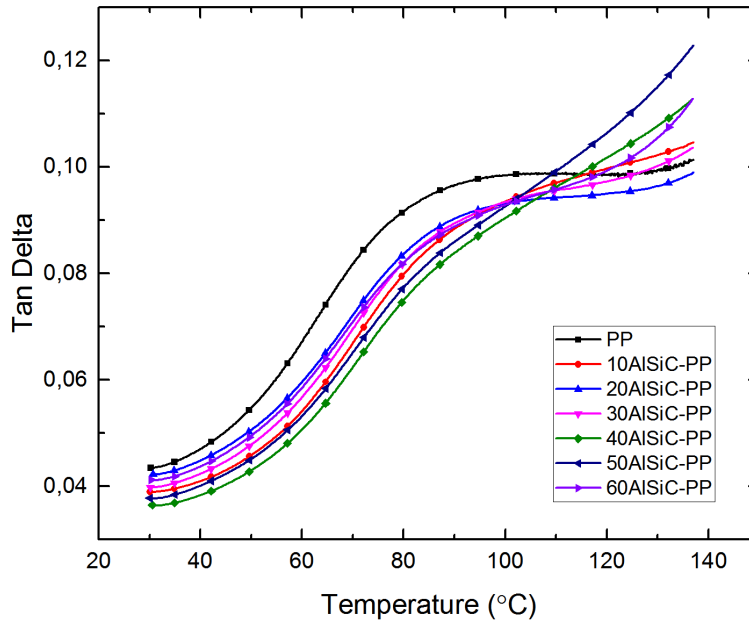


Figure 3.45: $\text{Tan}\delta$ of neat PP, 10AlSiC-PP, 20AlSiC-PP, 30AlSiC-PP, 40AlSiC-PP, 50AlSiC-PP, and 60AlSiC-PP

$\text{Tan}\delta$ values of neat PP and AlSiC loaded PP matrix composites were given in Figure 3.45. The neat PP $\text{Tan}\delta$ value was higher than the AlSiC loaded PP matrix composites. 20AlSiC-PP and 60AlSiC-PP composites $\text{Tan}\delta$ values were higher than the other AlSiC loaded PP matrix composites. $\text{Tan}\delta$ of neat PP and AlSiC loaded PP matrix composites dramatically increased the between 40 to 80°C after the 80°C this increment slowed down but climbed to over values. Polymer chains deformation was higher below at 80°C that could be referred crystalline phase of composites high. The crystallinity of PP matrix decreased over the 80°C. According to $\text{Tan}\delta$ values of neat PP and AlSiC loaded composites T_g values were given at Table 3.3. 10AlSiC-PP composite T_g value was higher than the neat PP and AlSiC loaded PP matrix the other composites. However all AlSiC loaded PP matrix composites T_g value were higher than the neat PP.

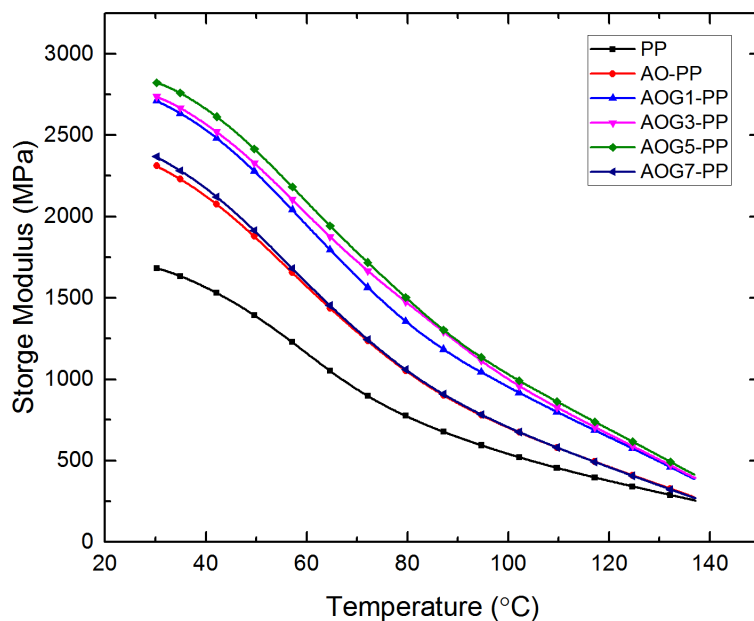


Figure 3.46: Storage Modulus of neat PP, AO-PP, AOG1-PP, AOG3-PP, AOG5-PP and AOG7-PP

According to Figure 3.46, the neat PP had a low E' value than the other composites. Alumina and alumina-G content increment into the PP matrix was increased to E' of composites [159]. AO-PP and AOG1-PP composites had nearly same E' values. AOG5-PP composite E' value was higher than the other alumina and alumina-G loaded composites. E' values decreased with different rate before nearly 70°C and after around 70°C. However, E' values decreased slowly than before 70°C. The elasticity of polymer matrix changed between the ambitions temperatures to 140°C. All composites and neat PP T_g values calculated from bending side of E' graphs and observed that T_g values increased between 11 to 25°C than the neat PP [7]. T_g of the AOG3-PP composite was the highest one. However, this amount of increment on the T_g did not observed in to the literature. The over load of G plaques into the PP matrix did not change T_g of composites as AOG3-PP composite.

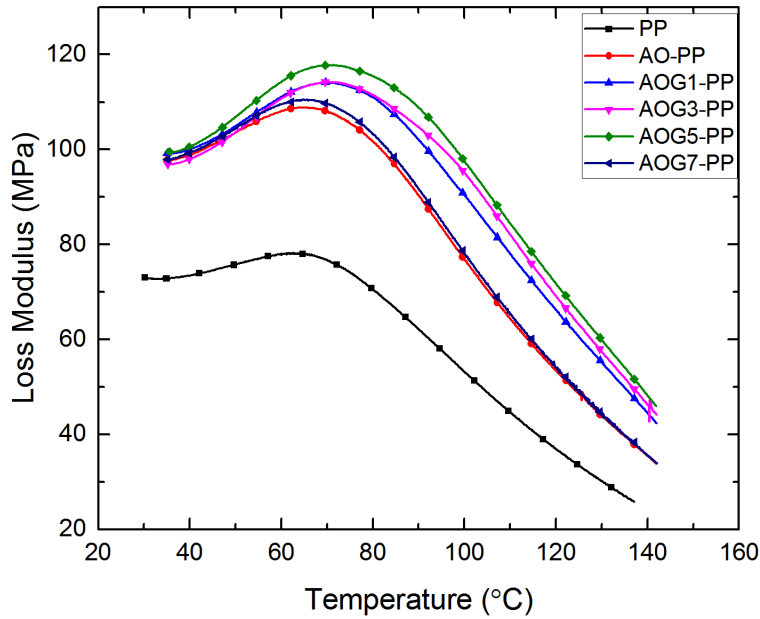


Figure 3.47: Loss Modulus of neat PP, AO-PP, AOG1-PP, AOG3-PP, AOG5-PP and AOG7-PP

The alumina and alumina-G particles loaded PP matrix composites and neat PP's E'' values were given in Figure 3.47. E'' values of composites higher than the neat PP. Plasticity of PP matrix increased around 60°C but upper 70°C temperature, deformation of matrix started to decrease. Polymer chains orientation increased and macro molecular order of matrix decreased at the top of the E'' values. Amorphous phase of polymer increased and crystalline phase disappear over the 60°C. AOG1-PP and AOG7-PP composites E'' values were almost same. AOG5-PP composite E'' value was the highest value of the other composites and neat PP. G plaques increment in to the PP matrix increased to E'' values, over 5% additions in to the filler. If, the upper value of E'' accepted T_g , alumina and alumina G plaques addition was increased T_g values of PP matrix between 2 to 15°C. AOG1-PP and AO-PP composites had the highest T_g values than the other alumina-G loaded PP matrix composites [160].

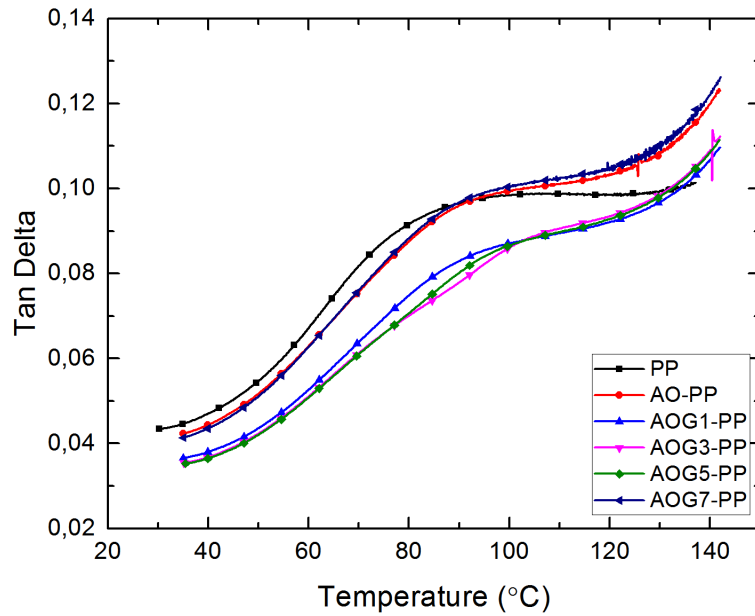


Figure 3.48: Tan δ of neat PP, AO-PP, AOG1-PP, AOG3-PP, AOG5-PP and AOG7-PP

Tan δ values of the neat PP and alumina-G plaques loaded PP matrix composites were given in Figure 3.48. The neat PP Tan δ value was higher than the alumina and alumina G loaded PP matrix composites. AO-PP and AOG7-PP composites Tan δ values were higher than the other alumina-G filler loaded PP matrix composites. The neat PP, AO-PP and alumina-G loaded PP composites Tan δ dramatically increased between 40 to 90°C after the 90°C this increment slowed down for neat PP but the other composites Tan δ went on to even higher values. Polymer chain deformation was higher below 90°C and G plaques inhibited amorphous polymer phases into the matrix. G plaques led to ordered polymer chains in the matrix. The crystallinity of PP matrix decreased above 90°C. According to Tan δ values of neat PP and composites T_g values were given in Table 3.3. AO-PP, AOG1-PP, and AOG7-PP composite T_g values were almost the same and at 87.5°C that was 7°C higher than neat PP. AOG3-PP and AOG5-PP T_g values were higher than the other composites and neat PP. G plaque addition to PP matrix did not increase T_g values linearly or mixing facilities could be affected by this increment.

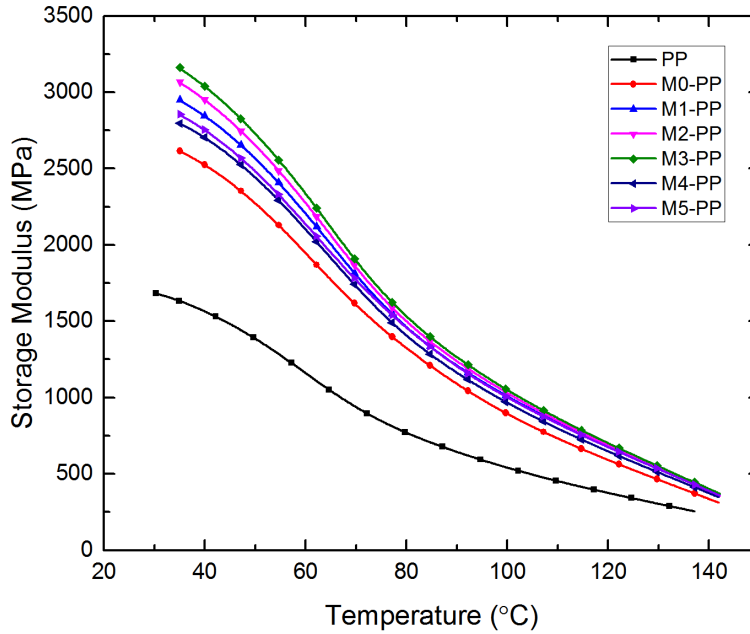


Figure 3.49: Storage Modulus of neat PP, M0-PP, M1-PP, M2-PP, M3-PP, M4-PP and M5-PP

According to Figure 3.49, the neat PP had a low E' value than the other composites. 50% alumina and silan-modified alumina content increment into the PP matrix was increased to E' of composites. M0-PP, M1-PP, M2-PP, M3-PP, M4-PP, and M5-PP composites had nearly same E' values. However, modified alumina loaded PP matrix composites E' values were 10% higher than the unmodified alumina loaded PP matrix composites [153]. E' values decreased with different rate before nearly 70°C and after 70°C. E' values decreased rapidly than before 70°C. The strength of the polymer matrix changed between the ambitions temperatures to 140°C. All composites and neat PP T_g values calculated from bending side of E' graphs and observed that T_g values increased almost 7°C than the neat PP. T_g of the silan-modified alumina loaded PP matrix composite were the same as unmodified alumina loaded PP matrix composites.

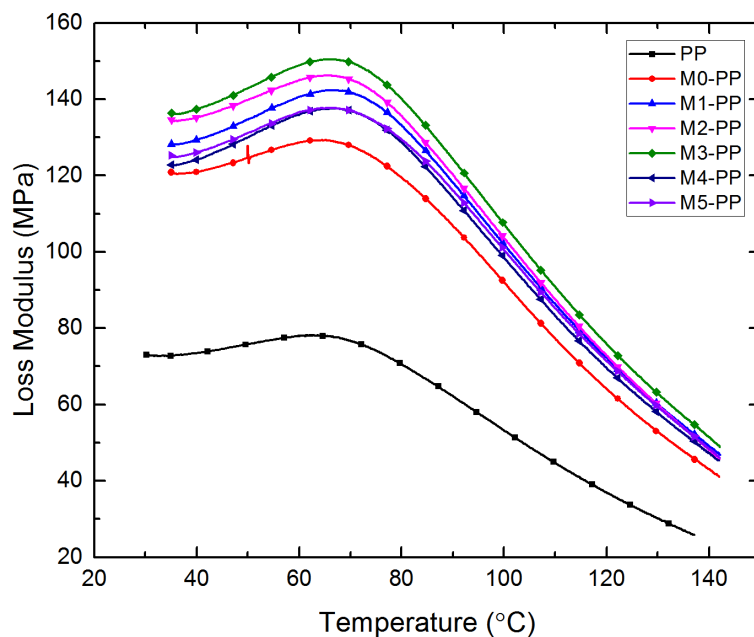


Figure 3.50: Loss Modulus of neat PP, M0-PP, M1-PP, M2-PP, M3-PP, M4-PP and M5-PP

The unmodified alumina and silan-modified alumina particles loaded PP matrix composites and neat PP's E'' values were given in Figure 3.50. E'' values of composites higher than the neat PP. The stiffness of PP matrix increased nearly 60°C but upper 70°C temperature, deformation of matrix started to decrease. Polymer chains orientation increased and macro molecular order of matrix decreased at the top of the E'' values [161]. Amorphous phase of polymer increased and crystalline phase disappear over the 60°C. M5-PP and M4-PP composites E'' values were almost same and higher than M0-PP. M3-PP composite E'' value was the highest value of the other composites and the neat PP. The surface modification of alumina particles increased to almost 10% E'' . If, the upper value of E'' accepted T_g , unmodified alumina particles addition was unchanged T_g values of PP matrix. However, modification of alumina particles increased T_g values of modified alumina loaded PP matrix [162]. M2-PP and M3-PP composites had the highest T_g values than the other modified alumina particles loaded PP matrix composites.

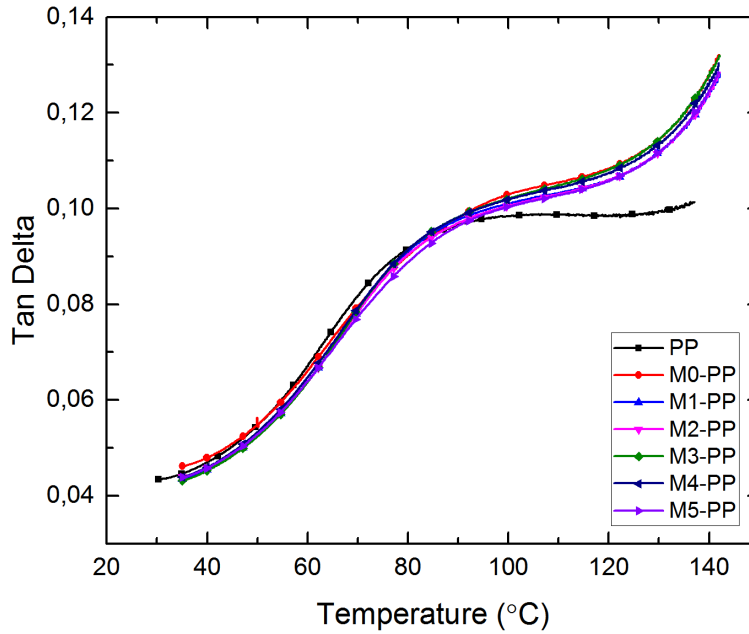


Figure 3.51: Tan δ of neat PP, M0-PP, M1-PP, M2-PP, M3-PP, M4-PP and M5-PP

Tan δ values of, 50% unmodified alumina loaded PP matrix, 50% silan-modified alumina loaded PP matrix and neat PP were given in Figure 3.51. The neat PP Tan δ value was nearly the same as unmodified alumina and modified alumina loaded PP matrix composites. Tan δ values of unmodified and modified alumina particle loaded PP matrix composites higher than the neat PP over 80°C, this difference could be explained with the composites filler side took the loaded forces from the matrix and increased the loading force capacity of the material. The polymer chains deformation was higher below at 80°C that could be referred the high crystalline phase of composites. The crystallinity of PP matrix decreased over the 80°C. According to Tan δ values of neat PP, unmodified and modified alumina particles loaded PP matrix composites T_g values were given at Table 3.3. M-PP composite T_g value was higher than the neat PP, unmodified and modified alumina loaded PP matrix the other composites. However unmodified alumina loaded PP matrix composites T_g value were as same as the neat PP. Modified alumina particle decreased PP matrix T_g value. However, unmodified alumina particle did not change the T_g value of PP matrix.

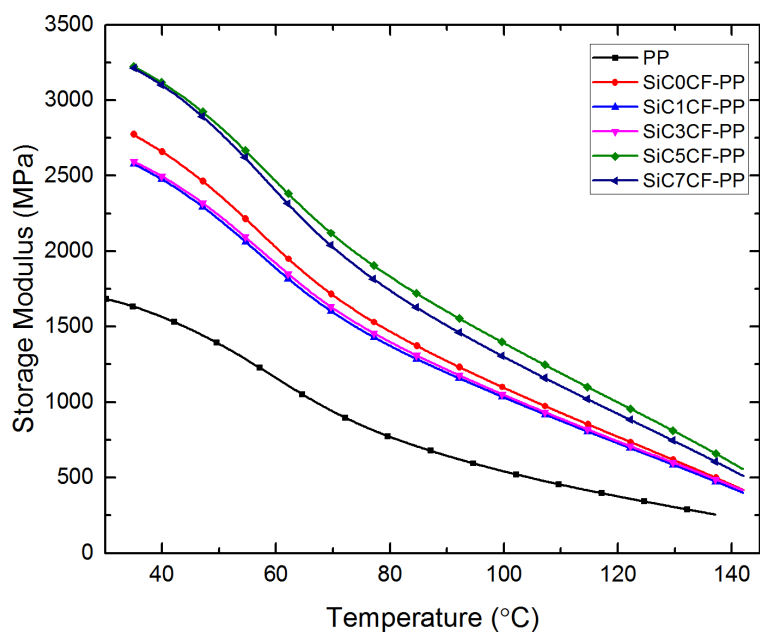


Figure 3.52: Storage Modulus of neat PP, SiC0CF-PP, SiC1CF-PP, SiC3CF-PP, SiC5CF-PP and SiC7CF-PP

According to Figure 3.52, the neat PP had a low E' value than the other composites. 50% SiC and SiC-CF addition into the PP matrix was increased to E' of composites [145]. SiC0CF-PP's E' value was higher than SiC1CF-PP and SiC3CF-PP but lower than SiC5CF-PP and SiC7CF-PP. CF addition and SiC extraction from the PP matrix decreased E' value of composites almost 10% until 3% CF and 47% SiC ratio, according to SiC0CF-PP. However, CF increment started to pass 5% into the PP matrix, E' value of composites increased 18% than SiC0CF-PP. E' values decreased with different rate before nearly 70°C and after 70°C. E' values decreased rapidly than before 70°C. All composites and neat PP T_g values calculated from bending side of E' graphs and observed that T_g values did not changed significantly than the neat PP. T_g of the SiC and SiC-CF loaded PP matrix composites were the same as neat PP.

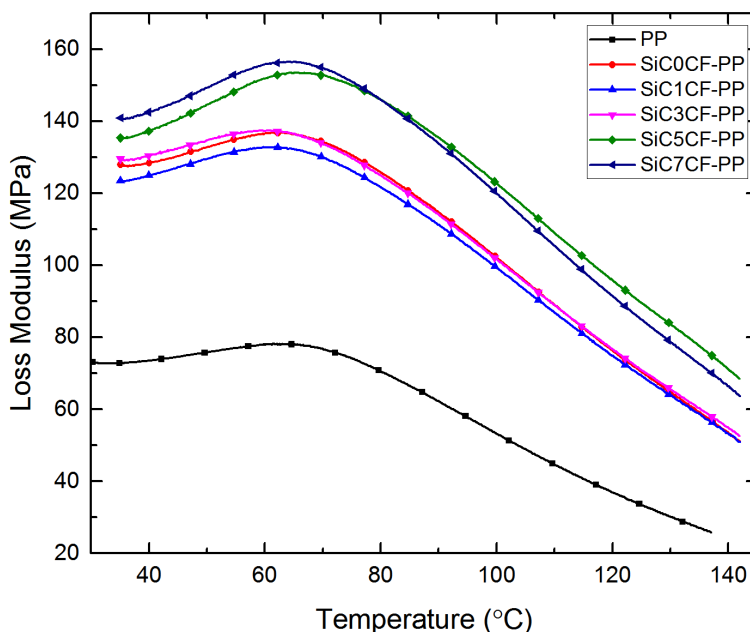


Figure 3.53: Loss Modulus of neat PP, SiC0CF-PP, SiC1CF-PP, SiC3CF-PP, SiC5CF-PP and SiC7CF-PP

50% SiC and SiC-CF loaded PP matrix composites and neat PP's E'' values were given in Figure 3.53. E'' values of composites higher than the neat PP. The stiffness of PP matrix increased nearly 65°C but up to 75°C temperature, deformation of matrix started to decrease. Polymer chains relaxation increased and macro molecular order of matrix decreased at the top of the E'' values. Amorphous phase of polymer increased and crystalline phase disappear over the 65°C. SiC0CF-PP and SiC30CF-PP composites E'' values were almost same and higher than SiC1CF-PP. SiC7CF-PP composite E'' value was the highest value of the other composites and neat PP [163]. The 5% CF addition to SiC particles increased to almost 8% E'' . If, the upper value of E'' accepted T_g , SiC particles addition was decreased 1°C T_g value of PP matrix. 1, 3, and 5% CF addition to PP matrix instead of SiC was decreased 2°C T_g . However, 7% CF addition to PP matrix instead of SiC increased T_g for 2°C.

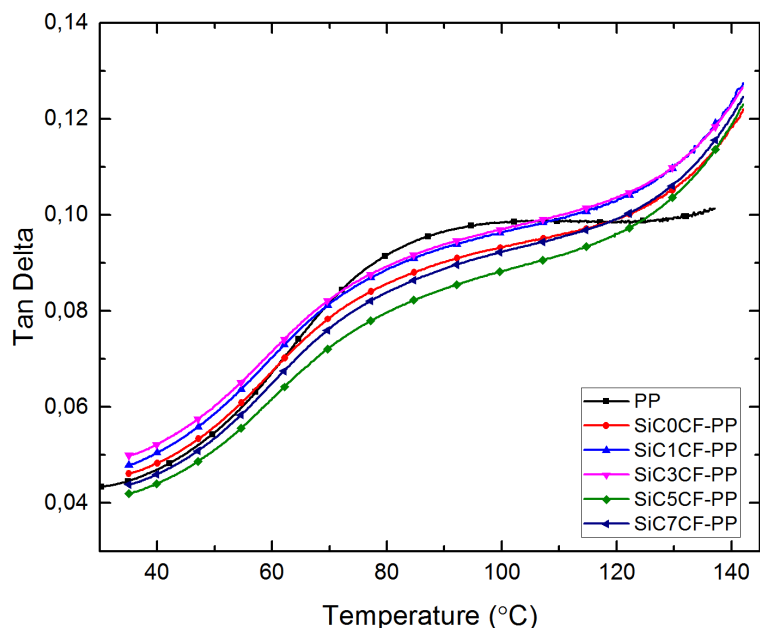


Figure 3.54: Tan δ of neat PP, SiC0CF-PP, SiC1CF-PP, SiC3CF-PP, SiC5CF-PP and SiC7CF-PP

Tan δ values of, 50% SiC, with different ratios 50% SiC-CF loaded PP matrix, and neat PP were given in Figure 3.54. The neat PP Tan δ value was nearly same as SiC and SiC-CF loaded PP matrix composites. Tan δ values of SiC1CF-PP and SiC3CF-PP composites higher than the neat PP below the 70°C, this difference could be explained with composites filler side repealed the loaded forces on to the composites from the matrix and increased the loading force capacity of the composites. However, SiC5CF-PP and SiC7CF-PP had lower Tan δ values than the SiC1CF-PP, SiC3CF-PP, and the neat PP. Polymer chains deformation was higher below at 70°C that could be referred the level of crystalline phase of composites. The crystallinity of PP matrix decreased over the 70°C. According to Tan δ values of neat PP, SiC and SiC-CF loaded PP matrix composites T_g values were given at Table 3.3. All composites T_g values were lower almost 11°C than the neat PP. In spied of that SiC loaded PP matrix composites T_g value were increased 2°C than the neat PP by over 5% CF addition.

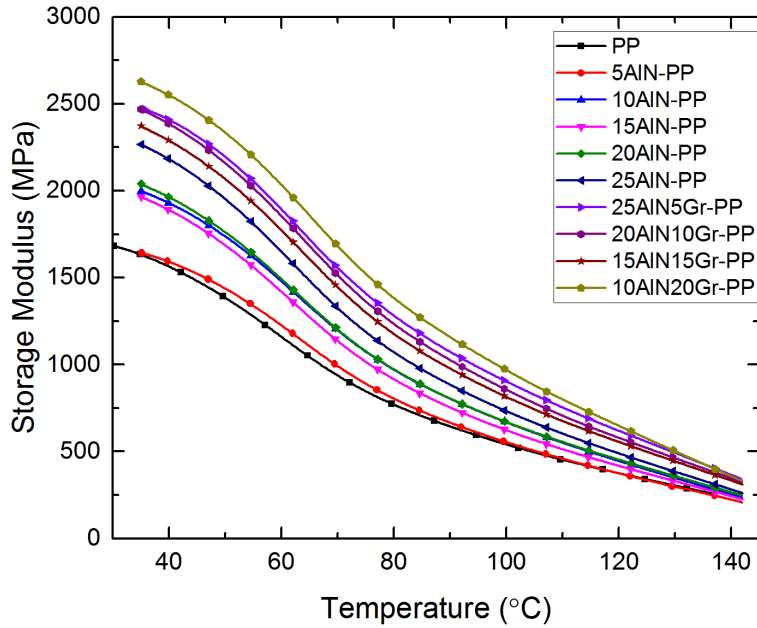


Figure 3.55: Storage Modulus of neat PP, 5AlN-PP, 10AlN-PP, 15AlN-PP, 20AlN-PP, 25AlN-PP, 25AlN5Gr-PP, 20AlN10Gr-PP, 15AlN15Gr-PP, and 10AlN20Gr-PP

According to Figure 3.55, the neat PP had a low E' value than the other composites. AlN and AlN-Gr addition into the PP matrix was increased to E' of composites. The E' values of the composites increased with increment of AlN content into the PP matrix. Gr addition to PP matrix and decreasing AlN partition in to the PP matrix increased E' values of the composites. 25% AlN addition to PP matrix was increased E' value of composite, 30% than the neat PP. 5% Gr addition on to 25% AlN increased E' value of composite, 11% than the 25AlN-PP. The decreasing AlN ratio into the PP matrix and increment of Gr ratio was increased 15% than the 25AlN-PP E' value of composite. E' values decreased with different rates before nearly 70°C and after 70°C. E' values decreased rapidly than below the 70°C. All composites and neat PP T_g values calculated from bending side of E' graphs and observed that T_g values changed significantly with the addition of 5% AlN addition to PP matrix. T_g of the neat PP elevated 5°C but, with increasing AlN content in to PP matrix started to decrease almost same T_g value of neat PP. Gr addition to PP matrix was dramatically increased T_g values of composites than neat PP and over 10% AlN added the PP matrix composites.

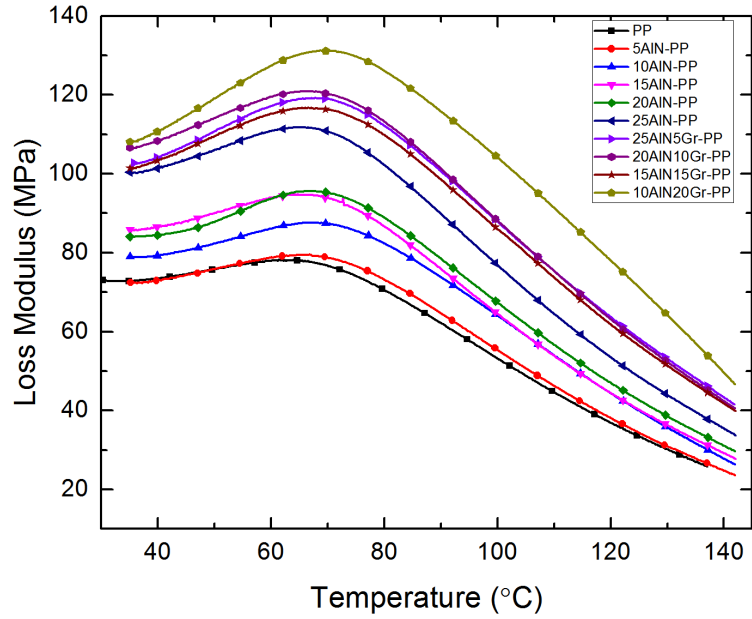


Figure 3.56: Loss Modulus of neat PP, 5AlN-PP, 10AlN-PP, 15AlN-PP, 20AlN-PP, 25AlN-PP, 25AlN5Gr-PP, 20AlN10Gr-PP, 15AlN15Gr-PP, and 10AlN20Gr-PP

The AlN and AlN-Gr loaded PP matrix composites and neat PP's E'' values were given in Figure 3.56. E'' values of composites higher than the neat PP. The stiffness of PP matrix increased nearly 70°C but up to 75°C temperature, deformation of matrix started to decrease. Polymer chains relaxation increased and macro molecular order of matrix decreased at the top of the E'' values. The amorphous phase of polymer increased and crystalline phase disappear over the 75°C. AlN loaded PP matrix composites E'' values were increased with increment of AlN content. 25% AlN addition to PP matrix E'' value increased 25% than the neat PP. Gr addition to PP matrix increased E'' values of composites. 10AlN20Gr-PP composite E'' value was higher than the other composites and neat PP. 15AlN15Gr-PP, 20AlN10Gr-PP, and 25AlN5Gr-PP composites E'' values were nearly the same. If, the upper value of E'' accepted T_g of the composites, 5% AlN particles addition to PP matrix was increased 5°C to T_g value of the PP matrix. Over loading of AlN in to the PP matrix did not change T_g values of composites. Gr addition did not change T_g values of composites meaningfully.

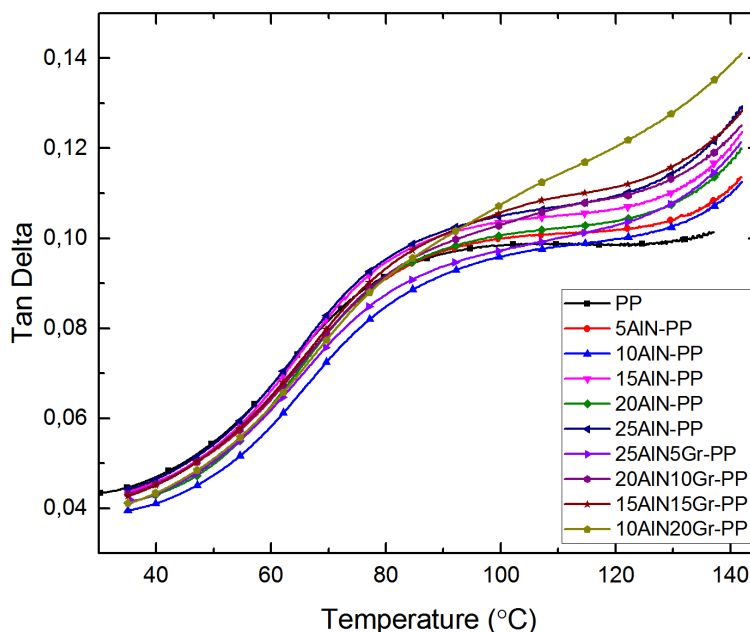


Figure 3.57: Tan δ of neat PP, 5AIN-PP, 10AIN-PP, 15AIN-PP, 20AIN-PP, 25AIN-PP, 25AIN5Gr-PP, 20AIN10Gr-PP, 15AIN15Gr-PP, and 10AIN20Gr-PP

The AIN and AIN-Gr loaded PP matrix composites and neat PP's Tan δ values were given in Figure 3.57. The neat PP Tan δ value was nearly same as AIN and AIN-Gr loaded PP matrix composites. Tan δ values of 25AIN5Gr-PP, 10AIN-PP, and 10AIN20Gr-PP composites lower than the neat PP below the 100°C, this difference could be explained with composites filler side repealed the loaded forces on to the composites from the matrix and increased the loading force capacity of the material. However, at the beginning of the test all of the composites Tan δ values were lower than the neat PP. According to Tan δ values of AIN loaded PP, AIN-Gr loaded PP and the neat PP T_g values were given at Table 3.3. All composites T_g values were lower almost 7°C than the neat PP.

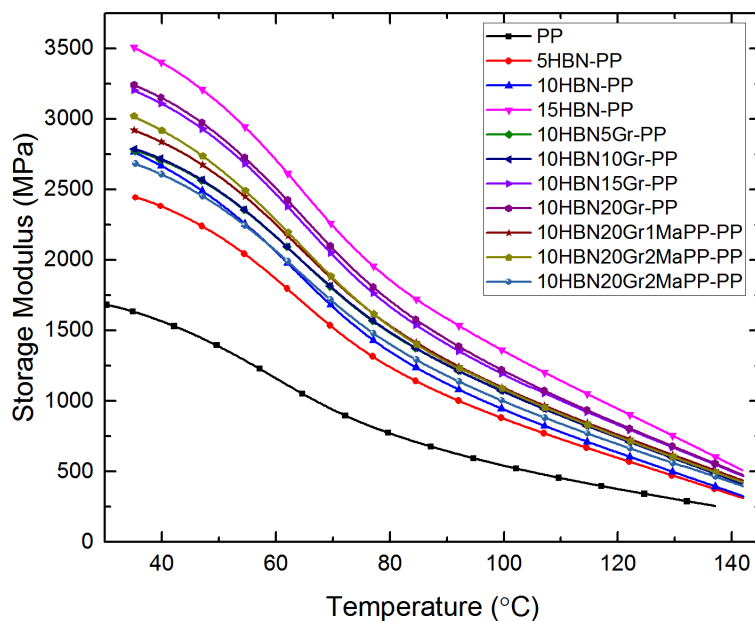


Figure 3.58: Storage Modulus of neat PP, 5HBN-PP, 10HBN-PP, 15HBN-PP, 10HBN5Gr-PP, 10HBN10Gr-PP, 10HBN15Gr-PP, 10HBN20Gr-PP, 10HBN20Gr1MaPP-PP, 10HBN20Gr2MaPP-PP, and 10HBN20Gr3MaPP-PP

According to Figure 3.58, the neat PP had a low E' value than the other composites. HBN, HBN-Gr and HBN-Gr-MaPP addition into the PP matrix was increased to E' of composites. The E' values of the composites increased with increment of HBN content into the PP matrix. Gr addition to PP matrix and decreasing HBN ratios in to the PP matrix decreased E' values of the composites. 15% HBN addition to PP matrix was increased E' value of composite, 115% than the neat PP. 20% Gr addition on to 10% HBN loaded PP composites E' value was lower than the 15% HBN added to PP matrix composite. The decreasing HBN ratio into the PP matrix and increment Gr ratio was decreased 10% than the 15HBN-PP E' value of composite. MaPP addition to 10% HBN and 20% Gr loaded PP composite E' value decreased. E' values decreased with different rate before nearly 70°C and over the 70°C. E' values decreased rapidly than below the 70°C. All composites and neat PP T_g values calculated from bending side of E' graphs and observed that T_g values changed significantly with the addition of HBN, HBN-Gr, and HBN-Gr-MaPP to PP matrix. T_g of the neat PP raised almost 5°C.

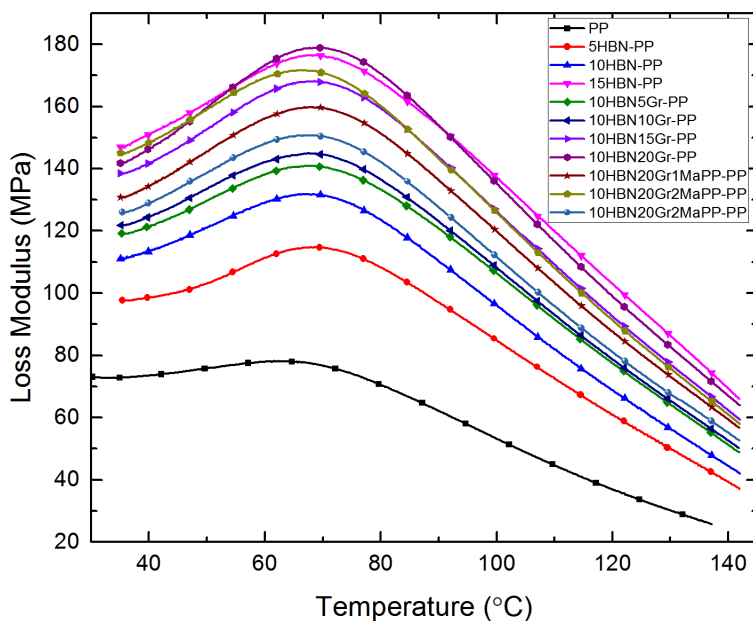


Figure 3.59: Loss Modulus of neat PP, 5HBN-PP, 10HBN-PP, 15HBN-PP, 10HBN5Gr-PP, 10HBN10Gr-PP, 10HBN15Gr-PP, 10HBN20Gr-PP, 10HBN20Gr1MaPP-PP, 10HBN20Gr2MaPP-PP, and 10HBN20Gr3MaPP-PP

The HBN, HBN-Gr and HBN-Gr-MaPP loaded PP matrix composites and neat PP's E'' values were given in Figure 3.59. E'' values of composites higher than the neat PP. The stiffness of PP matrix increased nearly 70°C but up to 75°C temperature, deformation of matrix started to decrease. Polymer chains relaxation increased and macro molecular order of matrix decreased at the top of the E'' values. The amorphous phase of polymer increased and crystalline phase disappear over the 70°C. HBN loaded PP matrix composites E'' values were increased with increment of HBN content in to the PP matrix. 15% HBN addition to PP matrix and 10HBN20Gr-PP composite E'' values increased 125% than the neat PP. Gr addition to PP matrix increased E'' values of composites. 10HBN20Gr-PP composite E'' value was higher than the other Gr included composites. MaPP addition to PP matrix decreased E'' value. If, the upper value of E'' accepted T_g , HBN, HBN-Gr and HBN-GR-MaPP loaded PP matrix composites was increased 3°C to T_g value of the PP matrix.

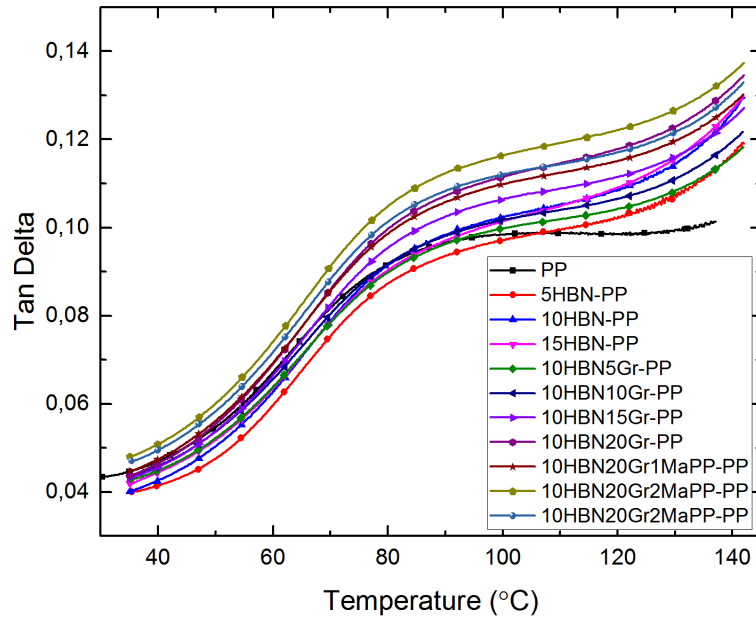


Figure 3.60: $\text{Tan}\delta$ of neat PP, 5HBN-PP, 10HBN-PP, 15HBN-PP, 10HBN5Gr-PP, 10HBN10Gr-PP, 10HBN15Gr-PP, 10HBN20Gr-PP, 10HBN20Gr1MaPP-PP, 10HBN20Gr2MaPP-PP, and 10HBN20Gr3MaPP-PP

The HBN, HBN-Gr and HBN-Gr-MaPP loaded PP matrix composites and the neat PP's $\text{Tan}\delta$ values were given in Figure 3.60. $\text{Tan}\delta$ values of 5HBN-PP, 10HBN-PP, and 15HBN-PP composites below the 100°C lower than the neat PP, this difference could be explained with composites filler side repealed the loaded forces on to the composites from the matrix and increased the loading force capacity of the material. 10HBN20GR2MaPP $\text{tan}\delta$ value of the composites was higher than the all of the composites and the neat PP. According to $\text{Tan}\delta$ values of HBN loaded PP, HBN-Gr loaded PP and the neat PP T_g values were given at Table 3.3. All composites T_g values were lower almost 5 to 7 °C than the neat PP. MaPP added recipes $\text{Tan}\delta$ values were higher than the other composites. MaPP should be increased matrix-filler connection.

3.6 Thermal Conductivity Analysis

Through plane and in plane thermal conductivity measurements have many differences between each other. Through plane measurement method is applied directly smooth surface of the material and heat sensors measures the heat differences of the material surface. However, in plane measurement technique evaluates the motion of heat one side of the material to another side. Two-measurement system philosophies are different to each other. Thermal effusivity was another important parameter to understanding of thermal conductivity of materials. Through plane thermal conductivity measurement steady state equation is generally given as;

$$\alpha = \frac{k}{\rho \cdot c_p}$$

Equation 3.2. Thermal effusivity formula of steady state of matter

α is considered as thermal effusivity values of matter, k is thermal conductivity of matter, ρ is density of matter and c_p is heat capacity of matter. Through plane thermal conductivity measurement supposes that it is a steady state of matter.

The system measures thermal conductivity of matter with two approach. The first one is directly measuring thermal conductivity of the matter from calibrated sample values. The calibration sample material is Plexiglas because of smooth surface and bulk properties. System measure thermal conductivity of Plexiglas almost 1.25 W/m.K and system calibrates itself on to this data. The second measurement technique is indirect measurement technique that needs ρ and c_p values from outside of the system.

Thermal conductivity measurement of all samples was analyzed by through plane measurement method with direct measurement technique. Thermal conductivity and thermal effusivity values were given at the same figures for all composites.

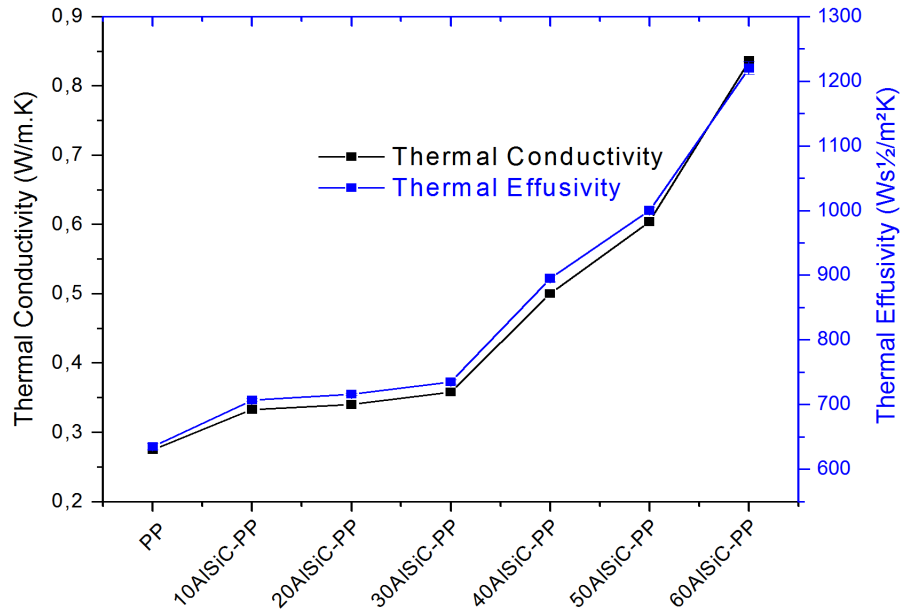


Figure 3.61 Thermal conductivity and thermal effusivity values of neat PP, 10AlSiC-PP, 20AlSiC-PP, 30AlSiC-PP, 40AlSiC-PP, 50AlSiC-PP and 60AlSiC-PP

According to Figure 3.61, thermal conductivity of AlSiC loaded PP matrix composite increased with the increment of AlSiC particles weight percentage into PP matrix. Up to 30% AlSiC addition to PP matrix increased dramatically thermal conductivity of the composite. 10% AlSiC addition to PP matrix increased thermal conductivity of the neat PP 21%. 40% AlSiC addition to PP matrix increased thermal conductivity of neat PP 82%. Thermal effusivity values of composites were parallel to thermal conductivity behaviors of composites. Lee et al. studied hybrid ceramic fillers for improving thermal conductivity of electronic packing polymer matrixes but metal-ceramic hybrid studies have not been done in the literature yet [36]. While discussing the results of thermal conductivity, this reason might be considered carefully. Heat capacity of composites was given at Table 3.2 theoretical density of composites evaluated for seeing differences the between indirect and direct thermal conductivity values of composites. Two techniques showed up nearly same thermal conductivity values for all composites.

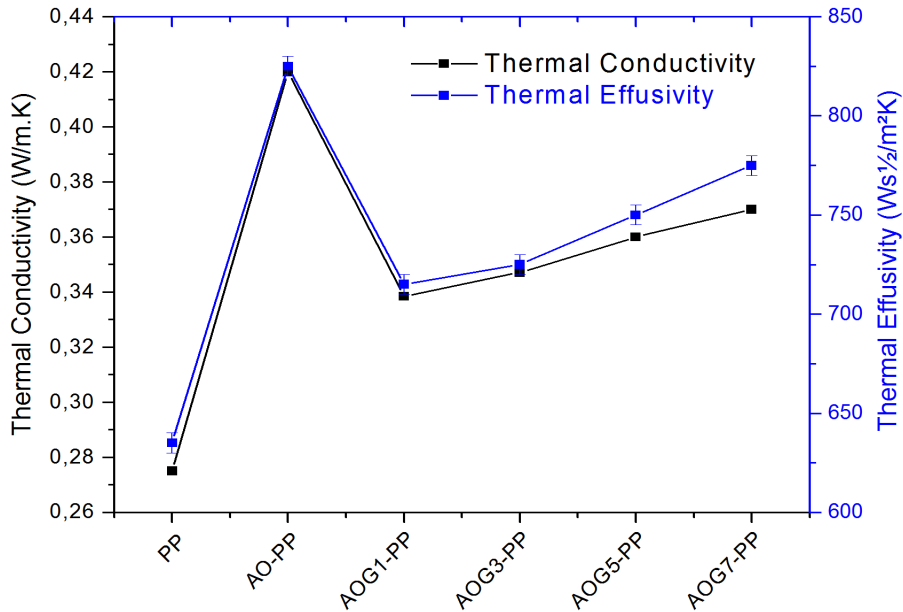


Figure 3.62: Thermal conductivity and thermal effusivity values of neat PP, AO-PP, AOG1-PP, AOG3-PP, AOG5-PP, and AOG7-PP

Figure 3.62 showed that through plane thermal conductivity of composite decreased with the addition of G plaques but thermal conductivity started to rise with the increase of graphene ratio in the filler. The effect of 2D G plaques on the through plane thermal conductivity was negative for the enhancement of thermal conductivity of composites. At the same time, 3D alumina particles at through plane thermal conductivity decreased dramatically with the addition of G plaques into filler. G plaques orientation into polymer matrix was parallel to through plane direction. G plaques could be isolated alumina particles from each other. The G plaques added composites thermal conductivity may decrease with this mechanism.

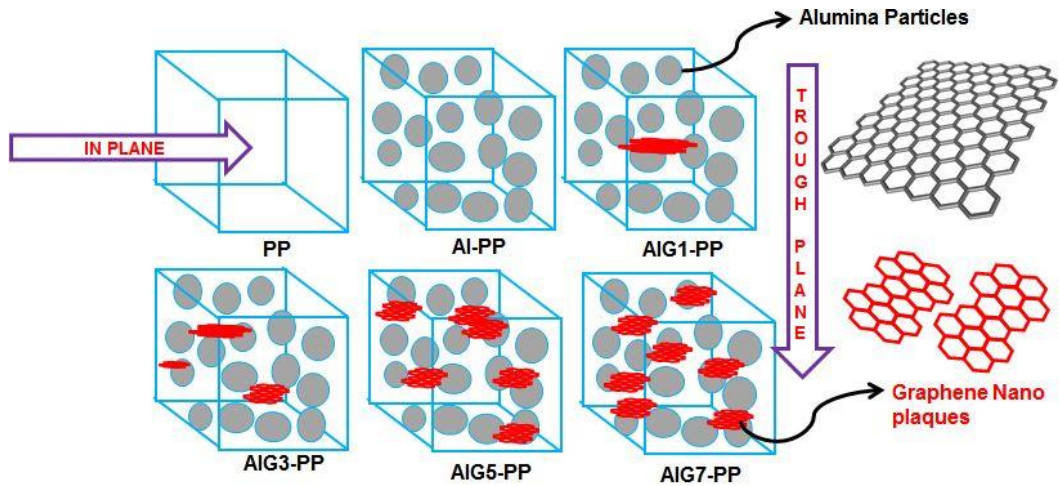


Figure 3.63: Theoretical representation of alumina-G plaques orientation in to PP matrix and effects on the thermal conductivity measurement

Figure 3.63 represent to theoretical orientation of alumina-G plaques into PP matrix. According to this assumption, thermal conductivity measurement way was important for understanding real effects of 2D particles into the matrix. Because G plaques in plane heat transfer was 100 times higher than through plane direction. At the result of through plane thermal conductivity could not be proper technique for measurement thermal conductivity. Seki et al. have studied modified graphene particle loaded PP matrix composite thermal and mechanical properties with increasing modified graphene particle ratio in to the PP matrix. According to thermal conductivity results through plane thermal conductivity of composites were lower than in plane thermal conductivity measurement results. If, thermal conductivity of alumina particles and G plaques added PP composites has been measured by in plane thermal conductivity measurement system, the thermal conductivity of composites would have been higher than the through plane measurement values [164].

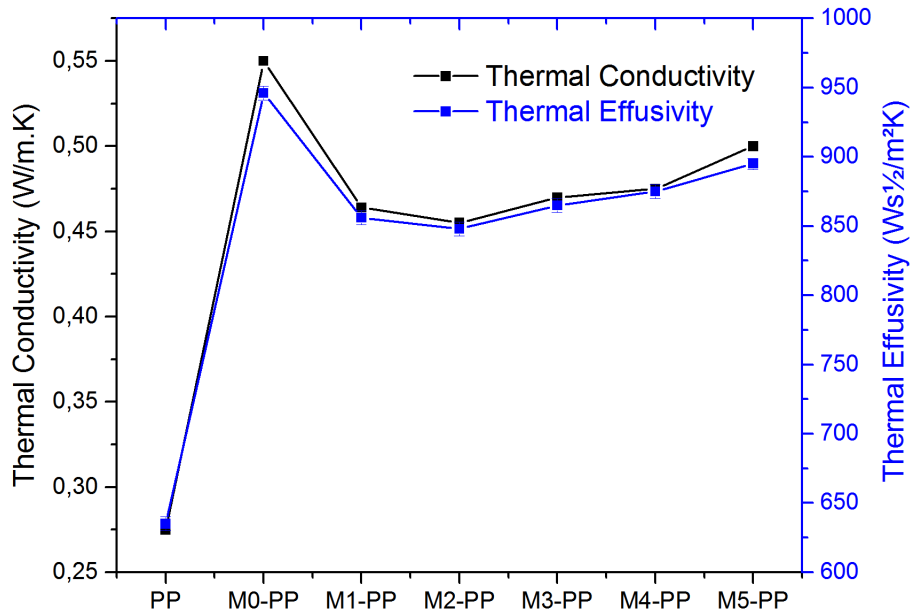


Figure 3.64: Thermal conductivity and thermal effusivity values of neat PP, M0-PP, M1-PP, M2-PP, M3-PP, M4-PP, and M5-PP

According to Figure 3.64, thermal conductivity of unmodified particles loaded PP matrix composites were higher than the modified alumina particles loaded PP matrix composites. The modified alumina particles loaded PP matrix composite decreased thermal conductivity of PP matrix composites Das et al. studied styrene butadiene elastomers thermal conductivity change with the addition of unmodified and modified CNTs and they observed that thermal conductivity of composites decreased by the modification [165]. M5-PP composite thermal conductivity was better than the other modified alumina particle loaded PP matrix composites.

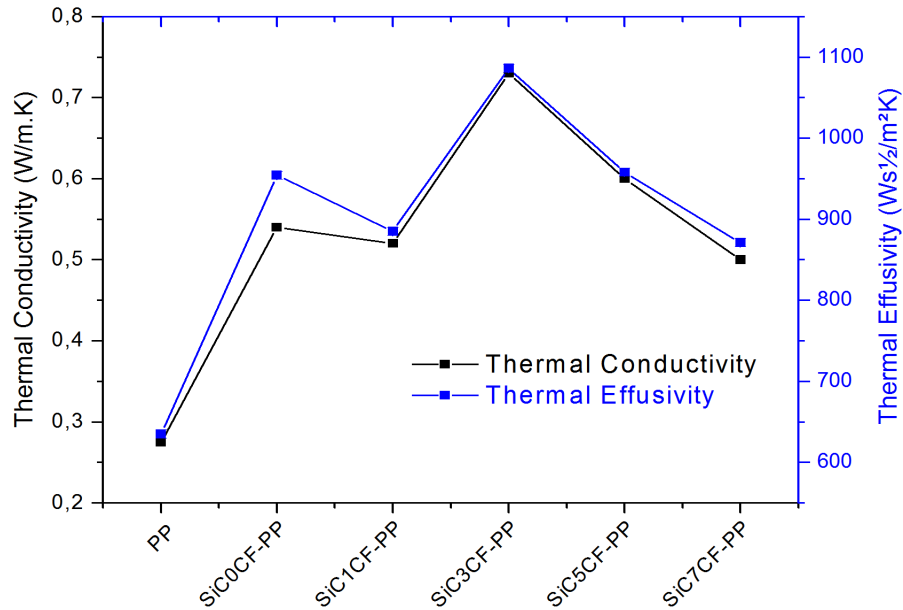


Figure 3.65: Thermal conductivity and thermal effusivity values of neat PP, SiC0CF-PP, SiC1CF-PP, SiC3CF-PP, SiC5CF-PP, and SiC7CF-PP

Figure 3.65 showed that through plane thermal conductivity of composites. SiC0CF-PP thermal conductivity was higher than SiC1CF-PP, SiC7CF-PP and neat PP but lower than SiC3CF-PP and SiC7CF-PP. CF addition to PP matrix affected thermal conductivity over 3% but with addition 5% into the PP matrix, it reduced thermal conductivity and thermal diffusivity. 50% SiC addition to PP matrix increased over 90% thermal conductivity of the neat PP. 3% CF addition into the PP matrix increased to thermal conductivity over the 40% according to %50 SiC loaded PP matrix composite. 47:3 ratio ceramic-carbon hybrid filler mixture increased thermal conductivity of PP almost two times better than the neat PP. CF orientation in to matrix might be increased heat transfer between SiC particles and connected terminal points into the 3D directions [166]. Terminal points number might be started to reduce with over loading of CF into matrix and thermal conductivity of composite started to decrease rapidly.

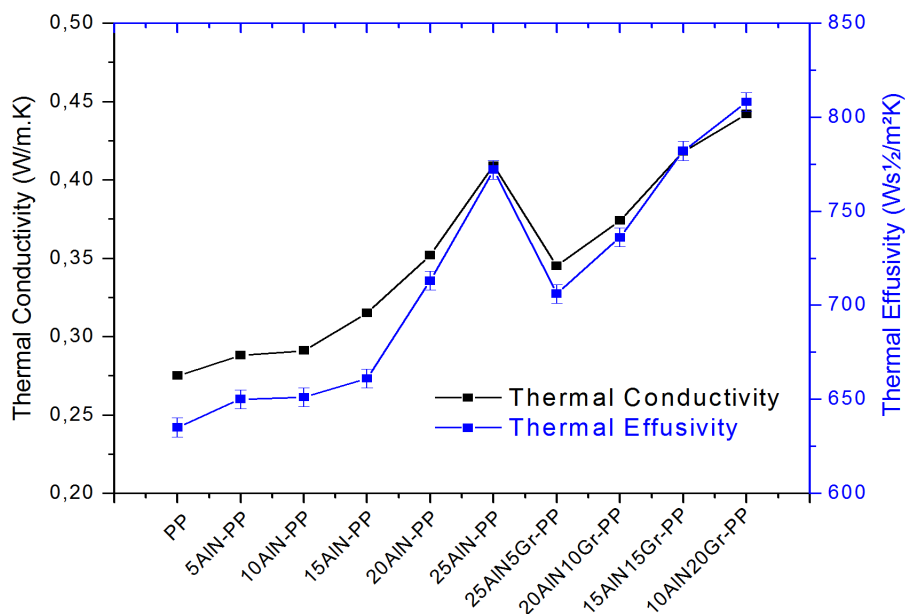


Figure 3.66: Thermal conductivity and thermal effusivity values of neat PP, 5AlN-PP, 10AlN-PP, 15AlN-PP, 20AlN-PP, 25AlN-PP, 25AlN5Gr-PP, 20AlN10Gr-PP, 15AlN15Gr-PP, and 10AlN20Gr-PP

AlN and Gr hybrid filler loaded PP matrix composites thermal conductivity were given at Figure 3.66. AlN addition to PP matrix increased thermal conductivity of composites. However, this change could be seen after the 15% AlN addition to PP matrix. 25% AlN addition to PP matrix increased thermal conductivity of the neat PP 74%. Gr addition to AlN loaded PP matrix firstly decreased thermal conductivity of the composites. However, thermal conductivity started to rise properly with the increasing of Gr content in to the PP matrix. 10AlN20Gr-PP thermal conductivity was higher than almost 7% than 25AlN-PP [84]. With the Gr addition to AlN loaded PP matrix, the PP matrix heat transfer of junction points orientation could be changed and thermal conductivity decreased. The other explanation of this decreasing might be, Gr pull all of the heat inside of the PP matrix and could not transfer excess heat to AlN particles.

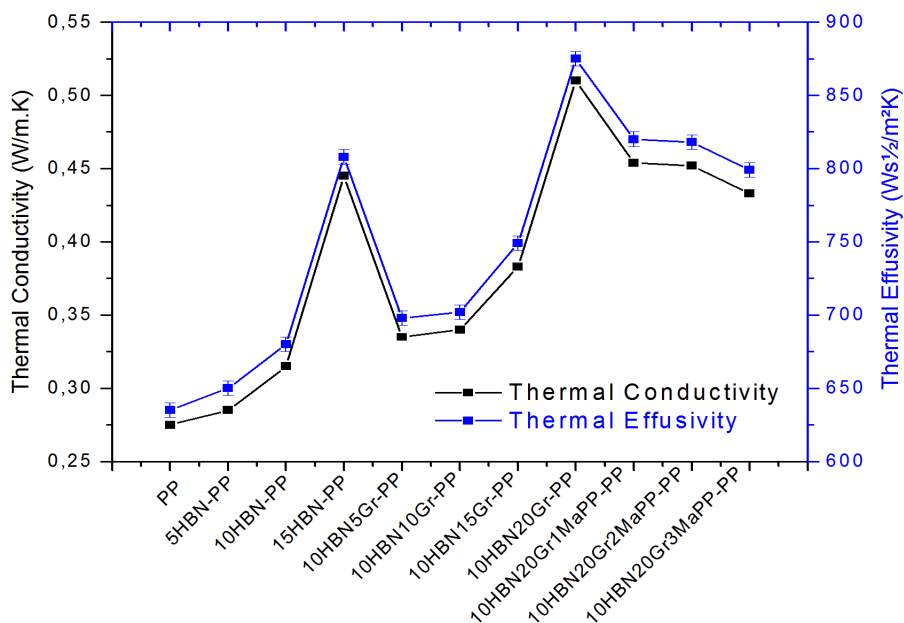


Figure 3.67: Thermal conductivity and thermal effusivity values of neat PP, 5HBN-PP, 10HBN-PP, 15HBN-PP, 10HBN5Gr-PP, 10HBN10Gr-PP, 10HBN15Gr-PP, 10HBN20Gr-PP, 10HBN20Gr1MaPP-PP, 10HBN20Gr2MaPP-PP, and 10HBN20Gr3MaPP-PP

HBN and Gr hybrid filler loaded PP matrix composites thermal conductivity were given at Figure 3.67. HBN addition to PP matrix dramatically increased thermal conductivity of composites in low partition. This change could be seen immediately with the HBN addition to PP matrix. 15% HBN addition to PP matrix increased thermal conductivity of the neat PP 80%. Gr addition into the 10% HBN added PP matrix properly increased thermal conductivity of the ceramic-carbon based filler loaded PP matrix composites. However, thermal conductivity started to rise sharply with the increasing of the Gr content in to the 10%HBN loaded PP matrix composites. 10HBN20Gr-PP thermal conductivity was higher than almost 10% than 15HBN-PP. MaPP addition to 10HBN20Gr-PP composite started to decrease thermal conductivity with increasing ratio of MaPP. MaPP surface modification agent did not proper to use for improving thermal conductivity of the PP matrix.

3.7 Electrical Resistivity

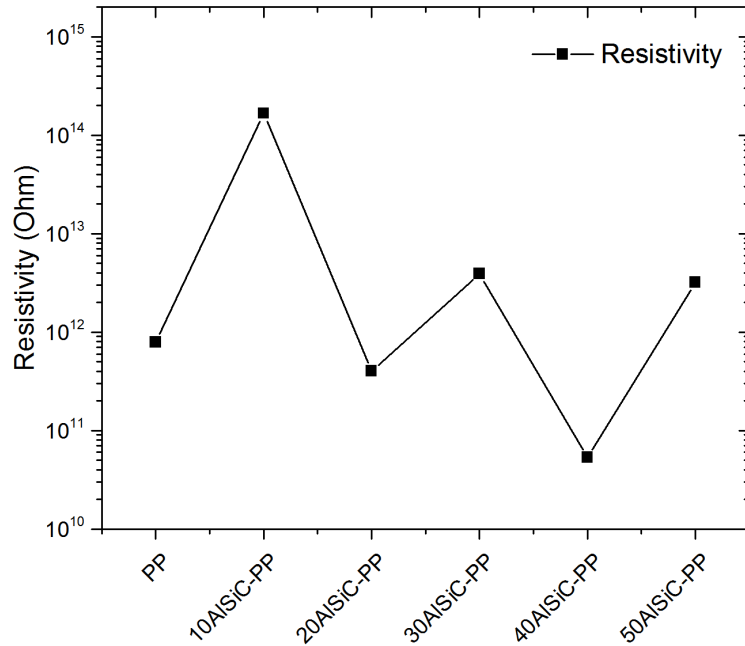


Figure 3.68: Surface electrical resistivity values of neat PP, 10AlSiC-PP, 20AlSiC-PP, 30AlSiC-PP, 40AlSiC-PP, and 50AlSiC-PP

AlSiC particles loaded PP matrix and neat PP surface electrical resistivity values were given Figure 3.68. Surface electrical resistivity of composite increased with 10% AlSiC particle addition to PP matrix. After this ratio, 20% AlSiC addition to PP matrix decreased surface resistivity. However, 30% AlSiC addition to PP matrix increased surface electrical resistivity than neat PP and 20AlSiC-PP. 40% AlSiC addition to PP matrix again decreased surface electrical resistivity of composite but the surface electrical resistivity started to increase with addition 50% AlSiC into the PP matrix. 60% AlSiC laded PP matrix surface electrical resistivity values could not measure. Because, 60AlSiC-PP surface started to conduct electric current and resistivity signal lost [167]. According to these results, AlSiC particle loaded PP matrix surface became electrically conductive over 60% AlSiC particle addition to PP matrix.

Aluminum metal is a good electrical conductive material but surface of aluminum is very reactive to oxygen and generate aluminum oxide film on to the surface of the metal. This reaction is very rapid and it occurs with everywhere under open atmosphere. AlSiC production was under the nitrogen atmosphere but storing

facilities could not be enough for inhibition of oxidation reaction. If, the surface of the AlSiC particles oxidized, this condition would reduce of electrical conductivity of composites.

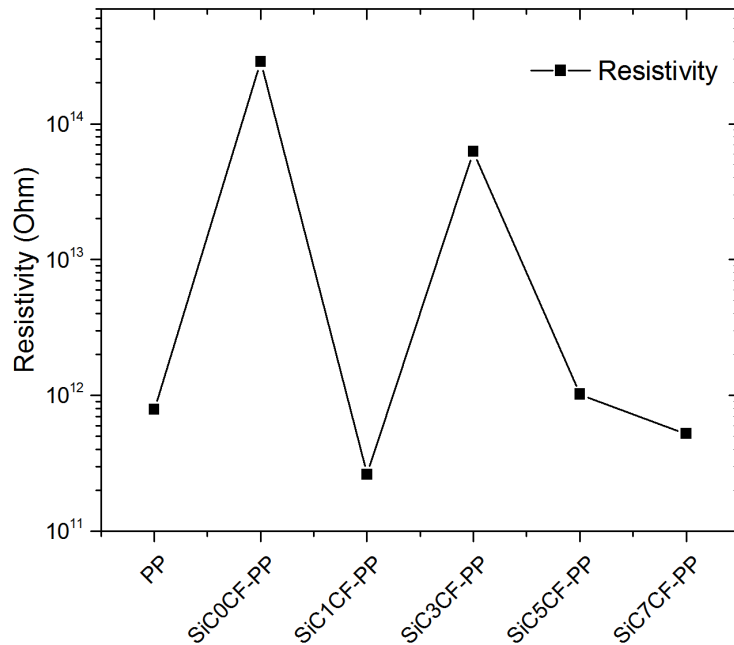


Figure 3.69: Surface electrical resistivity values of neat PP, SiC0CF-PP, SiC1CF-PP, SiC3CF-PP, SiC5CF-PP, and SiC7CF-PP

Surface electrical resistivity of neat PP and SiC-CF loaded PP matrix composites were given in Figure 3.69. The surface electrical resistivity increased with 50% SiC addition to PP matrix. 1% CF addition to PP matrix with decreasing 1% SiC amount into the PP decreased surface electrical resistivity of composite. However, 3% CF addition to PP matrix with decreasing 3% amount of SiC increased surface electrical resistivity almost 100 times than 1% CF loaded PP matrix. 5% CF addition to PP matrix with decreasing 5% SiC amount into the PP matrix decreased surface electrical resistivity of composite. % CF addition to PP matrix with decreasing 7% amount of SiC decreased electrical resistivity of the composite surfaces. According to these results, CF addition to PP matrix decreased surface electrical resistivity of composites and increase surface conductivity but this increment did not linear or meaningfully [168].

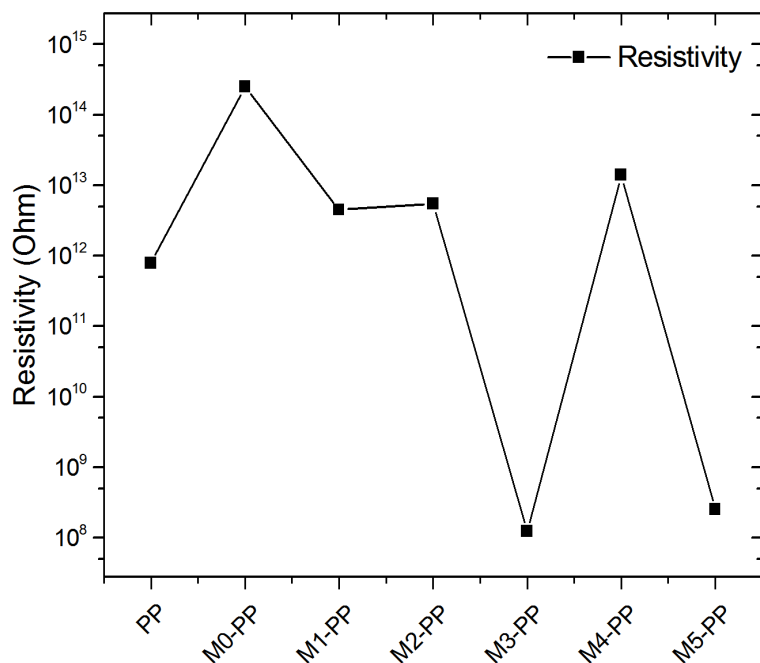


Figure 3.70: Surface electrical resistivity values of neat PP, M0-PP, M1-PP, M2-PP, M3-PP, M4-PP and M5-PP

Surface electrical resistivity of neat PP and unmodified-modified alumina particles loaded PP matrix composites were given in Figure 3.70. Surface electrical resistivity of 50% unmodified alumina particles addition to PP matrix increased. However, surface electrical resistivity of composites decreased with the silan-modification of alumina particles. M1-PP, M2-PP and M4-PP surface electrical resistivity were nearly same but M3-PP and M5-PP surface electrical resistivity lower than the other composites. (3-Glycidioxypropyl) trimethoxysilane modification of alumina particles might be increased charge transfer in to the PP matrix and decreased surface electrical resistivity. Vinyltrimethoxysilane modification of alumina particles matrix connection could be accelerated charge transfer into the composite and surface resistivity of the PP matrix decreased. Generally, modified alumina particle loaded PP matrix electrical resistivity decreased [169; 170].

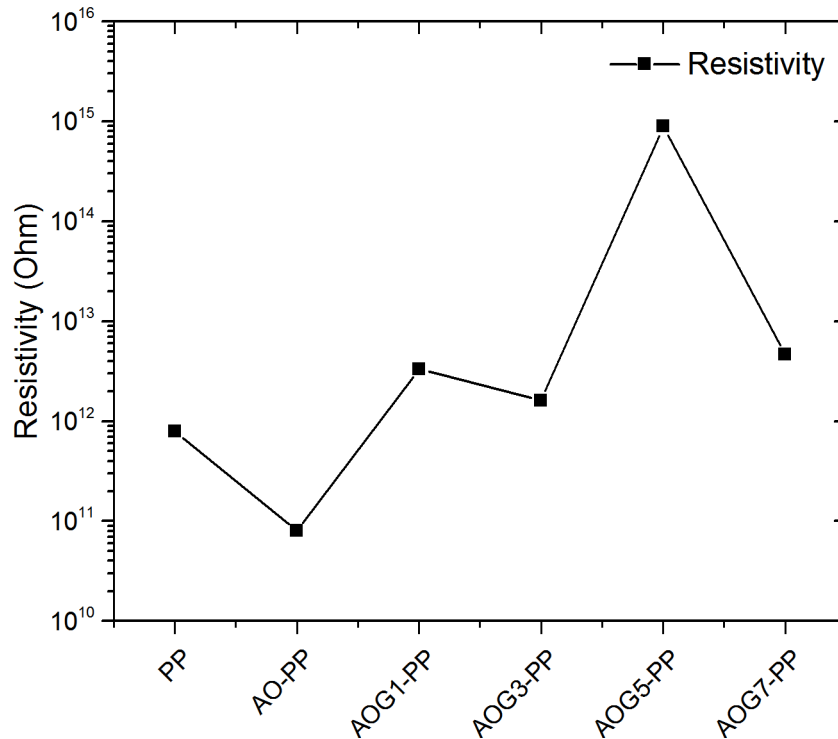


Figure 3.71: Surface electrical resistivity values of neat PP, AO-PP, AOG1-PP, AOG3-PP, AOG5-PP, and AOG7-PP

Surface electrical resistivity of neat PP and alumina-G plaques loaded PP matrix composites were given in Figure 3.71. %40 alumina particles addition to PP matrix decreased surface electrical resistivity of composites. However, G plaques addition to PP matrix with alumina started to increase surface electrical resistivity of composites. 5% G plaques addition to filler content of composite had higher resistivity value than neat PP and alumina-G plaques loaded PP matrix composites. 7% G plaques addition to filler content of composite started to decrease surface electrical resistivity of alumina-G plaques loaded PP matrix composites. However this value was lower than the neat PP and AO-PP. G plaques total amount were lower than 2.8% in to the PP matrix for AOG7-PP and it means that this value did not enough for seeing electrical effect of G plaques in to PP matrix composites [171].

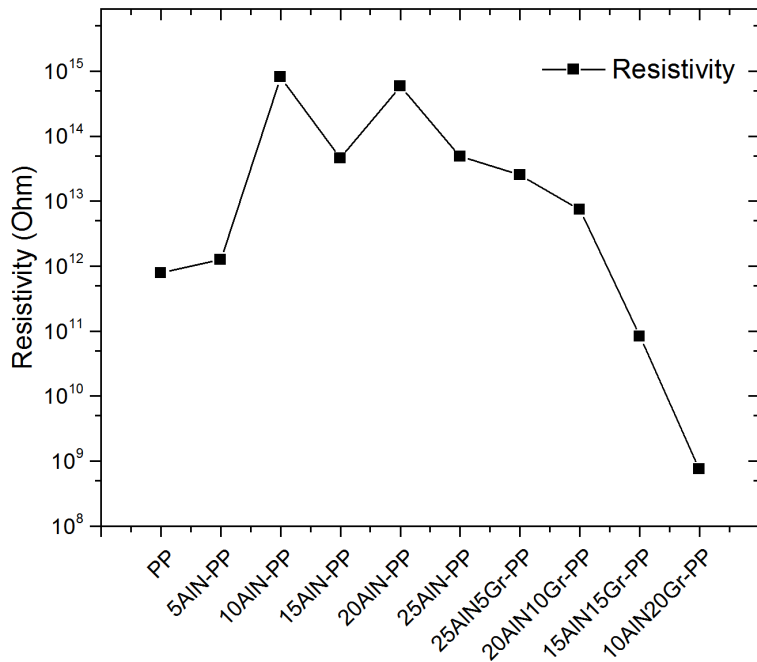


Figure 3.72: Surface electrical resistivity values of neat PP, 5AlN-PP, 10AlN-PP, 15AlN-PP, 20AlN-PP, 25AlN-PP, 25AlN5Gr-PP, 20AlN10Gr-PP, 15AlN15Gr-PP, and 10AlN20Gr-PP

Surface electrical resistivity of neat PP and AlN-Gr loaded PP matrix composites were given in Figure 3.72. Surface electrical resistivity of AlN loaded PP matrix composites increased with the addition of AlN. 10% AlN addition to PP matrix increased more than the other AlN and AlN-Gr filler combinations. Gr addition to PP matrix decreased surface electrical resistivity of composites. 20%Gr addition to PP matrix had lower surface electrical resistivity. Over the 20% Gr addition to PP matrix could be made composite surface electrically conductive. Percolation value of composites could be a little bit higher than 20%Gr which is the limit values of electrical surface diffusion [136].

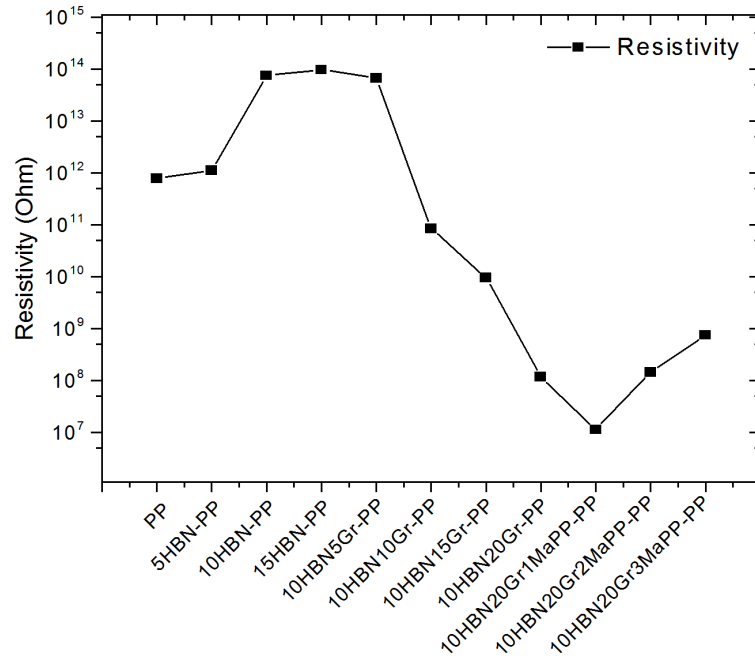


Figure 3.73: Surface electrical resistivity values of neat PP, 5HBN-PP, 10HBN-PP, 15HBN-PP, 10HBN5Gr-PP, 10HBN10Gr-PP, 10HBN15Gr-PP, 10HBN20Gr-PP, 10HBN20Gr1MaPP-PP, 10HBN20Gr2MaPP-PP, and 10HBN20Gr3MaPP-PP

HBN addition to PP matrix was decreased surface electrical resistivity (Figure 3.73). However, Gr addition to PP matrix started to decrease surface resistivity of composites. 20% Gr addition to PP matrix had lower surface electrical resistivity. MaPP addition to PP matrix increased surface electrical resistivity than 10HBN20Gr-PP. Gr particles electrical charge transfer could affect by MaPP modification and decreased electrical conductivity.

Electronic industry of Turkey is growing up rapidly but some parts of products supplying from outside of country. Thermal conductive polymeric composite materials are not produced in Turkey yet. These products are imported from the other countries for electronic industry. We tried to get the innovative knowledge to compounding sectors in Turkey with this thesis about thermal conductive polymer matrix composite manufacturing.

The outcome of the study brings out new perspective of filler system combinations effects into the polymer matrix. We believe that, hybrid filler systems will be designed and applied into the compounding engineering near future.

In this thesis, our major limitation was twin-screw extruder manufacturing for understanding mixing facilities of compounds better. The other limitation can be the filler prices that were high and they did not produce in Turkey. We supplied all fillers from outside of the country.

4. CONCLUSION

This thesis aimed to investigate hybrid filler loaded PP matrix's thermal, mechanical and electrical properties for electronic packaging industry. To our knowledge, this is the first study that used ceramic and carbon-based filler together into the PP matrix. In the study, mechanical properties, SEM, SDT, DSC, DMA analyses, thermal and electrical conductivity characteristics were assessed with different composites.

According to mechanical analyses of composites, increasing of filler content into PP matrix decreased the tensile strength and flexural strength. However, tensile and flexural modulus of the composites increased. Ceramic-based fillers dramatically decreased mechanical properties while, carbon-based material addition to ceramic fillers and PP matrix increased mechanical properties. G plaques addition to PP matrix and decreasing the ceramic content into the filler increased the nucleation sites into the PP matrix and it improved the mechanical properties of the pp matrix composites.

SEM results showed that ceramic particles distribution into PP matrix was homogeneous. AlSiC particles were amorphous and spherical form. Filler and matrix interaction was weak and generally, ceramic particles PP matrix interactions were poor. The ceramic particles surface chemical bond structures were not similar for making a good interaction with the PP matrix. The silan modification of ceramic surface of particles improved interaction between polymer and ceramic interface, especially the modifications of ethyltrimethoxysilane (M1), (3-Aminopropyl) tetraethoxysilane (M4), and Vinyltrimethoxysilane (M5). MaPP addition to the composite recipes improved ceramic and carbon-based filler interface between PP matrix. Furthermore, Gr addition to PP matrix, the filler an matrix interaction and particles distribution into the PP matrix became better.

According to SDT analysis, the addition of metal ceramic-based filler into the PP matrix increased the thermal degradation temperature of composites. Ceramic filler

addition to PP matrix increased thermal degradation of composites too. Thermal degradation onset temperature increased dramatically with the carbon-based material addition to the ceramic particles loaded PP matrix. However, degradation offset temperature of composites did not change meaningfully.

The DTG thermogram of composites was given the thermal degradation rate of composites properly. The thermal degradation rate of composites increased with the addition of carbon-based materials into the PP matrix. The silane modification of ceramic surface increased thermal degradation onset temperature of PP matrix composites but 3-(Trimethoxysilyl) propyl methacrylate modification decreased thermal degradation onset and offset temperature of PP matrix. CF addition to ceramic particles loaded PP matrix composites acted as ceramic filler and did not change meaningfully thermal degradation temperature of composites. Gr addition to addition of ceramic loaded PP matrix increased thermal degradation temperature of the composites. MaPP addition increased thermal stability and the degradation temperature of ceramic and carbon-based material loaded PP matrix.

DTA thermogram of composites showed that two different stage of the physical and chemical reaction. The first reaction was the melting process of composites and the second one was the decomposition of PP matrix. Melting temperature of composites observed between 160 to 180°C. Decomposition of the PP matrix was observed between 400 to 500°C. DTA signals identified some different reactions pathways during the thermal degradation process of the composites.

According to DSC analysis, T_m values of composite decreased and T_c values of composites increased with the addition of a metal-ceramic based composite to the PP matrix addition to PP matrix than the ratio of the metal-ceramic based composite. The c_p of metal-ceramic composite loaded PP matrix decreased with the addition of the metal-ceramic composite amount into the PP matrix and increased crystallinity of composites.

Modified ceramic particles addition to the PP matrix did not change the T_m values of composite however increased T_c values of composites. The c_p value of composites decreased and the crystallinity percentage increased. G plaques matrix effect was identified by ceramic particle loaded PP matrix easily. T_m values of composite

increased and T_c values of composites increased dramatically with the addition of G plaques into the PP matrix. G plaques showed nucleation effect into the PP matrix. However over loading of G plaques did not change this increment. 1% G plaques usage in to the PP matrix could improve the thermal properties of composites. The c_p values of composite did not change meaningfully which was necessary for the thermal conductivity properties of materials. CF addition to ceramic filler loaded PP matrix increased T_m and T_c values of composites. Crystallinity of composites were increased with the addition of CF. Furthermore CF addition to ceramic filler loaded PP matrix decreased c_p values of composites. Gr addition to ceramic particle loaded PP matrix increased T_m and T_c values of composites and increased percentage of crystallinity of composites. Gr and ceramic loaded PP matrix composites c_p values decreased. However, Gr addition of 10% HBN loaded PP matrix composites did not change the T_m and T_c values of composites. HBN ceramic particles were dominate than carbon-based particles especially the other ceramic particles those were used in this thesis. MaPP modification did not affect T_m and T_c values of composites.

Viscoelastic properties of PP matrix composites showed that E' and E'' values increased with the addition of metal-ceramic composite into the PP matrix. The addition of metal-ceramic composite into the PP matrix increased T_g values of composites. $\tan\delta$ values of composites decreased with the addition of metal-ceramic composite into the PP matrix. E' and E'' values of composites increased with the addition of G plaques and ceramic particles into the PP matrix. G plaques improved viscoelastic properties of PP matrix than ceramic filler. T_g value of PP matrix composites increased with the G plaques addition to ceramic filler content of composite. Silane Modification of ceramic particle increased E' and E'' values of composites. T_g value of PP matrix composites increased with the silane modified ceramic particle usage in to the PP matrix. Silane modified side of ceramic particles enhanced polymer crystal growing into the PP matrix. CF addition to ceramic particles loaded PP matrix composites increased E' , E'' and percentage of crystallinity of composites. However, this increment rate was lower than G plaques added ceramic particles loaded PP matrix. T_g value of PP matrix composites increased with the CF addition to ceramic filler content of composite. Gr addition to PP matrix composite increased E' and E'' values. HBN addition to PP matrix changed

viscoelastic properties of the composites more effective than Gr. 15% HBN addition to PP matrix increased E' and E'' value than Gr added and 30% particle loaded PP matrix composites. HBN plaque structure changed motion pathway into the PP matrix and increase stiffness of composite. However, HBN loaded PP matrix composites T_g values were lower than the neat PP.

Main aim of the study was improved the thermal conductivity of PP matrix by hybrid filler applications. PP through plane thermal conductivity was 0,245 W/m.K and this value was generated to 0,840 W/m.K by 60% AlSiC metal matrix composite addition to PP matrix. However 60AlSiC-PP composite conducted to electrical energy. With increasing over 30% filler content into the PP matrix through plane thermal conductivity of composite started to increase sharply. 15% HBN addition to PP matrix through plane thermal conductivity was most efficient than the other all composite, because the highest through plane thermal conductivity was obtained with the lower filler addition ratio. Gr addition to 10%HBN loaded PP matrix improved thermal conductivity but to reach the 15HBN-PP composite through plane thermal conductivity should be added over 15% Gr to PP matrix. HBN was most efficient as a thermal conductive filler. Alumina particle was the cheapest thermal conductive filler in this study however; it was showed as same performance as the SiC into the PP matrix.

3% CF addition to PP matrix improved network in to the matrix for conducting thermal energy and increased thermal conductivity of composites. G addition to PP matrix did not improved through plane thermal conductivity of PP matrix but it increased mechanical and thermal stability properties of PP matrix. Chemical surface modification agents and additive usage in to PP matrix decreased thermal conductivity of polymer. These agents were improved mechanical properties, thermal stability and viscoelastic behaviors of composites.

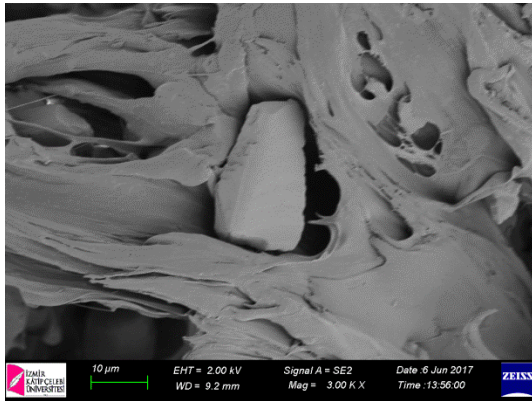
More recipes that are efficient could arrange for usage are according to these results. Although, we can offer three different recipes can produce for good thermal conductive composites manufacturing. The first one is 1% G, 3%CF and 16%HBN loaded PP matrix. The second recipe is 1%G, 3%CF, 10% Gr, 26%AlN loaded PP

matrix. The last one can be 1%G, 3%CF, 40%AlSiC loaded PP matrix. All recipes could be tried by different matrix.

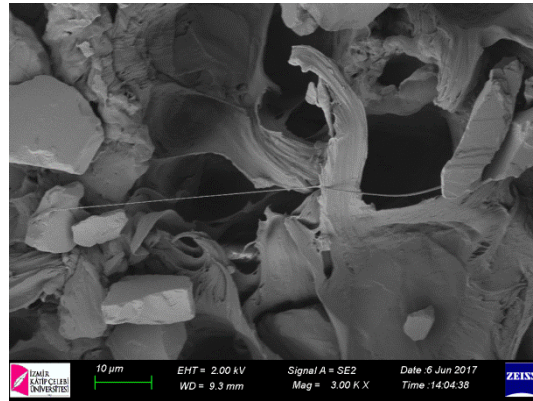
In the further study, computational modellings of the composites will evaluate under simulation programs and will try to get best thermal conductivity results before manufacturing of composites.

5. APPENDIX

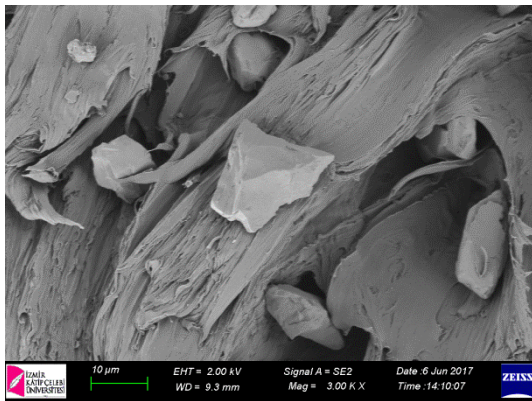
3000X SEM images of alumina-G filled PP matrix composites.



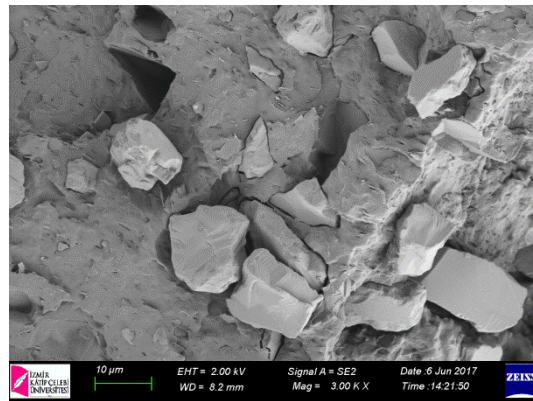
AO-PP



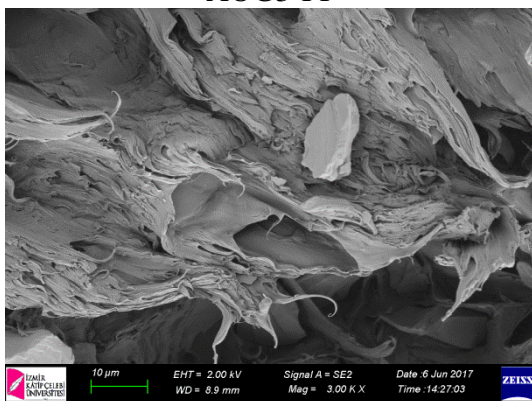
AOG1-PP



AOG3-PP

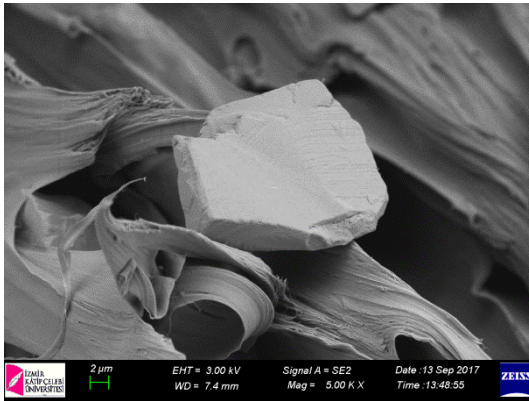


AOG5-PP

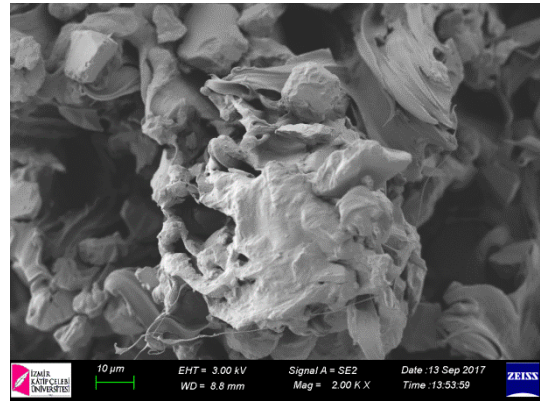


AOG7-PP

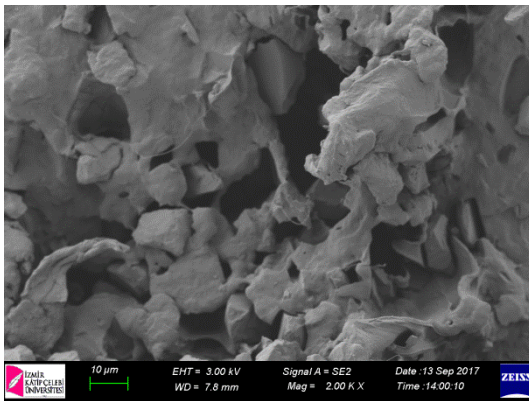
2000X SEM images of un modified and silane modified alumina particles loaded PP matrix composites.



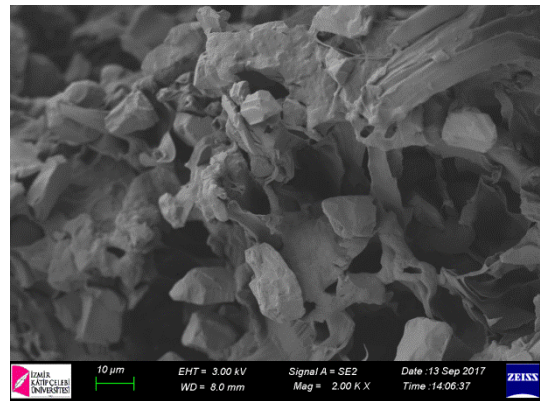
M0-PP



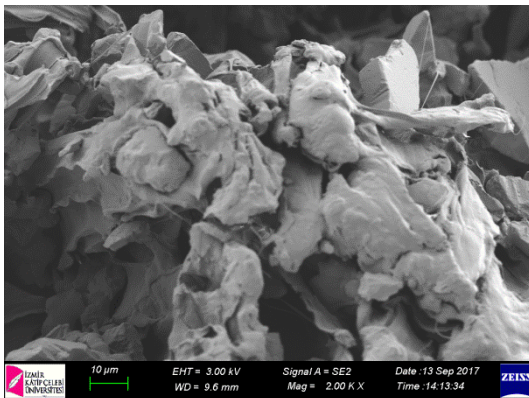
M1-PP



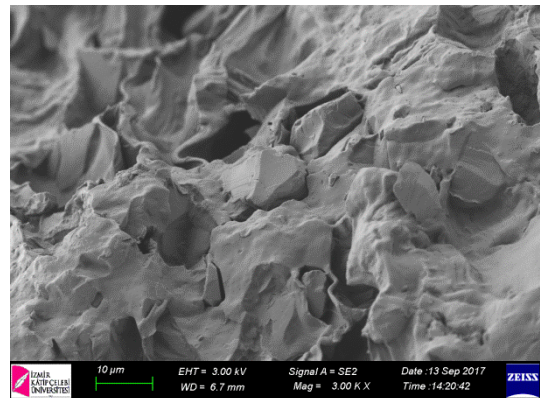
M2-PP



M3-PP



M4-PP



M5-PP

6. REFERENCES

- [1] Ram, A. (1997). *Fundamentals of POLYMER ENGINEERING* (R. Solomon Ed.). United States of America: PLENUM PRESS.
- [2] *Advances in Polymer Processing*. (2009). (S. T. a. Y. Weimin Ed.). New York: CRC Press.
- [3] Sperling, L. H. (2006). Introduction to Polymer Science, *Introduction to Physical Polymer Science*, (pp. 28): John Wiley & Sons, Inc.
- [4] Blythe, A. R., & Bloor, D. (2005). *Electrical properties of polymers*: Cambridge University Press.
- [5] Riande, E., & Díaz-Calleja, R. (2004). *Electrical properties of polymers*: Wiley Online Library.
- [6] Seanor, D. A. (2013). *Electrical properties of polymers*: Elsevier.
- [7] Kuilla, T., Bhadra, S., Yao, D., Kim, N. H., Bose, S., & Lee, J. H. (2010). Recent advances in graphene based polymer composites. *Progress in polymer science*, 35(11), 1350-1375. doi: <https://doi.org/10.1016/j.progpolymsci.2010.07.005>
- [8] Yu, Y.-H., Lin, Y.-Y., Lin, C.-H., Chan, C.-C., & Huang, Y.-C. (2014). High-performance polystyrene/graphene-based nanocomposites with excellent anti-corrosion properties. *Polymer Chemistry*, 5(2), 535-550.
- [9] Yang, Z., Zhou, L., Luo, W., Wan, J., Dai, J., Han, X., . . . Hu, L. (2016). Thermally conductive, dielectric PCM-boron nitride nanosheet composites for efficient electronic system thermal management. *Nanoscale*, 8(46), 19326-19333. doi: 10.1039/c6nr07357c
- [10] Ye, Y., Chen, H., Wu, J., & Ye, L. (2007). High impact strength epoxy nanocomposites with natural nanotubes. *Polymer*, 48(21), 6426-6433.
- [11] Woo, G., Mittelman, M., & Santerre, J. (2000). Synthesis and characterization of a novel biodegradable antimicrobial polymer. *Biomaterials*, 21(12), 1235-1246.
- [12] Houssa, M. (2003). *High k Gate Dielectrics*: CRC Press.
- [13] Chau, R., Doyle, B., Datta, S., Kavalieros, J., & Zhang, K. (2007). Integrated nanoelectronics for the future. *Nature materials*, 6(11), 810.
- [14] Incropera, F. (1988). Convection heat transfer in electronic equipment cooling. *Journal of heat transfer*, 110(4b), 1097-1111.
- [15] Lima, D. J. (2011). Thermal management of electronic devices: Google Patents.
- [16] Tan, F., & Tso, C. (2004). Cooling of mobile electronic devices using phase change materials. *Applied thermal engineering*, 24(2-3), 159-169.
- [17] Grujicic, M., Zhao, C., & Dusel, E. (2005). The effect of thermal contact resistance on heat management in the electronic packaging. *Applied Surface Science*, 246(1-3), 290-302.

- [18] Ohring, M. (1998). *Reliability and failure of electronic materials and devices*: Elsevier.
- [19] Talbot, C. D., Moberg, S. B., Causey III, J. D., & Yonemoto, J. A. (2004). Selective potting for controlled failure and electronic devices employing the same: Google Patents.
- [20] Cengel, A. (2003). HEHT TRANSFER.
- [21] Fedorov, A. G., & Viskanta, R. (2000). Three-dimensional conjugate heat transfer in the microchannel heat sink for electronic packaging. *International Journal of Heat and Mass Transfer*, 43(3), 399-415.
- [22] Qi, X., Dho, J., Tomov, R., Blamire, M. G., & MacManus-Driscoll, J. L. (2005). Greatly reduced leakage current and conduction mechanism in aliovalent-ion-doped BiFeO₃. *Applied Physics Letters*, 86(6), 062903.
- [23] Roy, K., Mukhopadhyay, S., & Mahmoodi-Meimand, H. (2003). Leakage current mechanisms and leakage reduction techniques in deep-submicrometer CMOS circuits. *Proceedings of the IEEE*, 91(2), 305-327.
- [24] Reddy, G. P., & Gupta, N. (2010). Material selection for microelectronic heat sinks: an application of the Ashby approach. *Materials & Design*, 31(1), 113-117.
- [25] Lee, S. (1995). *Optimum design and selection of heat sinks*. Paper presented at the Semiconductor Thermal Measurement and Management Symposium, 1995. SEMI-THERM XI., Eleventh Annual IEEE.
- [26] Werner, M. R., & Fahrner, W. R. (2001). Review on materials, microsensors, systems and devices for high-temperature and harsh-environment applications. *IEEE Transactions on Industrial Electronics*, 48(2), 249-257.
- [27] Krishnan, S., Garimella, S. V., & Kang, S. S. (2005). A novel hybrid heat sink using phase change materials for transient thermal management of electronics. *IEEE Transactions on Components and Packaging Technologies*, 28(2), 281-289.
- [28] Li, Y., & Wong, C. (2006). Recent advances of conductive adhesives as a lead-free alternative in electronic packaging: Materials, processing, reliability and applications. *Materials Science and Engineering: R: Reports*, 51(1-3), 1-35.
- [29] Sekar, D., King, C., Dang, B., Spencer, T., Thacker, H., Joseph, P., . . . Meindl, J. (2008). *A 3D-IC technology with integrated microchannel cooling*. Paper presented at the Interconnect Technology Conference, 2008. IITC 2008. International.
- [30] Cong, J., Wei, J., & Zhang, Y. (2004). *A thermal-driven floorplanning algorithm for 3D ICs*. Paper presented at the Proceedings of the 2004 IEEE/ACM International conference on Computer-aided design.
- [31] Shenogin, S., Xue, L., Ozisik, R., Keblinski, P., & Cahill, D. G. (2004). Role of thermal boundary resistance on the heat flow in carbon-nanotube composites. *Journal of applied physics*, 95(12), 8136-8144.
- [32] Cote, L. J., Cruz-Silva, R., & Huang, J. (2009). Flash reduction and patterning of graphite oxide and its polymer composite. *J Am Chem Soc*, 131(31), 11027-11032.
- [33] Sim, L. C., Ramanan, S., Ismail, H., Seetharamu, K., & Goh, T. (2005). Thermal characterization of Al₂O₃ and ZnO reinforced silicone rubber as

- thermal pads for heat dissipation purposes. *Thermochimica acta*, 430(1-2), 155-165.
- [34] T'Joen, C., Park, Y., Wang, Q., Sommers, A., Han, X., & Jacobi, A. (2009). A review on polymer heat exchangers for HVAC&R applications. *International Journal of Refrigeration*, 32(5), 763-779.
- [35] Xu, Y., Ray, G., & Abdel-Magid, B. (2006). Thermal behavior of single-walled carbon nanotube polymer–matrix composites. *Composites Part A: Applied Science and Manufacturing*, 37(1), 114-121.
- [36] Lee, G.-W., Park, M., Kim, J., Lee, J. I., & Yoon, H. G. (2006). Enhanced thermal conductivity of polymer composites filled with hybrid filler. *Composites Part A: Applied Science and Manufacturing*, 37(5), 727-734.
- [37] Chu, K., Wu, Q., Jia, C., Liang, X., Nie, J., Tian, W., . . . Guo, H. (2010). Fabrication and effective thermal conductivity of multi-walled carbon nanotubes reinforced Cu matrix composites for heat sink applications. *Composites Science and Technology*, 70(2), 298-304.
- [38] Han, X.-H., Wang, Q., Park, Y.-G., T'Joen, C., Sommers, A., & Jacobi, A. (2012). A review of metal foam and metal matrix composites for heat exchangers and heat sinks. *Heat Transfer Engineering*, 33(12), 991-1009.
- [39] Zhou, M., Lin, T., Huang, F., Zhong, Y., Wang, Z., Tang, Y., . . . Lin, J. (2013). Highly conductive porous graphene/ceramic composites for heat transfer and thermal energy storage. *Advanced Functional Materials*, 23(18), 2263-2269.
- [40] Hammel, E., Tang, X., Trampert, M., Schmitt, T., Mauthner, K., Eder, A., & Pötschke, P. (2004). Carbon nanofibers for composite applications. *Carbon*, 42(5-6), 1153-1158.
- [41] Windhorst, T., & Blount, G. (1997). Carbon-carbon composites: a summary of recent developments and applications. *Materials & Design*, 18(1), 11-15.
- [42] Harris, P. J. (2004). Carbon nanotube composites. *International Materials Reviews*, 49(1), 31-43.
- [43] Sommers, A., Wang, Q., Han, X., T'Joen, C., Park, Y., & Jacobi, A. (2010). Ceramics and ceramic matrix composites for heat exchangers in advanced thermal systems—a review. *Applied thermal engineering*, 30(11-12), 1277-1291.
- [44] Arik, M., & Weaver, S. (2004). *Chip-scale thermal management of high-brightness LED packages*. Paper presented at the Fourth International Conference on Solid State Lighting.
- [45] Fuchs, E. R., Field, F. R., Roth, R., & Kirchain, R. E. (2008). Strategic materials selection in the automobile body: Economic opportunities for polymer composite design. *Composites Science and Technology*, 68(9), 1989-2002.
- [46] Parker, W., Jenkins, R., Butler, C., & Abbott, G. (1961). Flash method of determining thermal diffusivity, heat capacity, and thermal conductivity. *Journal of applied physics*, 32(9), 1679-1684.
- [47] Hsu, S.-P., & Wong, L.-Y. (2006). Heat sink structure with embedded electronic components for semiconductor package: Google Patents.
- [48] Culnane, T. M., Gaynes, M. A., Seto, P. K., & Shaukatullah, H. (1998). Chip carrier modules with heat sinks attached by flexible-epoxy: Google Patents.

- [49] Culnane, T. M., Gaynes, M. A., Seto, P. K., & Shaukatullah, H. (1997). Method for attaching heat sinks directly to chip carrier modules using flexible-epoxy: Google Patents.
- [50] Huang, W., & Askin, R. G. (2003). Reliability analysis of electronic devices with multiple competing failure modes involving performance aging degradation. *Quality and Reliability Engineering International*, 19(3), 241-254.
- [51] Carcia, P. F., & McLean, R. S. (2004). Flexible organic electronic device with improved resistance to oxygen and moisture degradation: Google Patents.
- [52] Barontini, F., & Cozzani, V. (2006). Formation of hydrogen bromide and organobrominated compounds in the thermal degradation of electronic boards. *Journal of Analytical and Applied Pyrolysis*, 77(1), 41-55.
- [53] Zweben, C. (1992). Metal-matrix composites for electronic packaging. *Jom*, 44(7), 15-23.
- [54] Zweben, C. H., Mogle, R. A., Rodini Jr, B. T., & Thaw, C. L. (1989). Low-thermal-expansion, heat conducting laminates having layers of metal and reinforced polymer matrix composite: Google Patents.
- [55] Chung, D. (2001). Materials for thermal conduction. *Applied thermal engineering*, 21(16), 1593-1605.
- [56] Surappa, M. (2003). Aluminium matrix composites: Challenges and opportunities. *Sadhana*, 28(1-2), 319-334.
- [57] Nafisi, S., Emadi, D., Shehata, M., & Ghomashchi, R. (2006). Effects of electromagnetic stirring and superheat on the microstructural characteristics of Al–Si–Fe alloy. *Materials Science and Engineering: A*, 432(1-2), 71-83.
- [58] Schubert, T., Zieliński, W., Michalski, A., Weißgärber, T., & Kieback, B. (2008). Interfacial characterization of Cu/diamond composites prepared by powder metallurgy for heat sink applications. *Scripta Materialia*, 58(4), 263-266.
- [59] Ruch, P., Beffort, O., Kleiner, S., Weber, L., & Uggowitzer, P. J. (2006). Selective interfacial bonding in Al (Si)–diamond composites and its effect on thermal conductivity. *Composites Science and Technology*, 66(15), 2677-2685.
- [60] Do Kim, Y., Oh, N. L., Oh, S.-T., & Moon, I.-H. (2001). Thermal conductivity of W–Cu composites at various temperatures. *Materials Letters*, 51(5), 420-424.
- [61] Cheng, Q. (2007). *Thermal management of high-power white LED package*. Paper presented at the Electronic Packaging Technology, 2007. ICEPT 2007. 8th International Conference on.
- [62] Chung, D. (2001). Thermal interface materials. *Journal of Materials Engineering and Performance*, 10(1), 56-59.
- [63] Nguyen, M. N. (2002). Thermal interface materials: Google Patents.
- [64] Thermal interface materials. (2004): Google Patents.
- [65] Le, K.-C. (2004). Thermal interface materials: Google Patents.
- [66] Yu, A., Ramesh, P., Itkis, M. E., Bekyarova, E., & Haddon, R. C. (2007). Graphite nanoplatelet– epoxy composite thermal interface materials. *The Journal of Physical Chemistry C*, 111(21), 7565-7569.

- [67] Mu, Q., Feng, S., & Diao, G. (2007). Thermal conductivity of silicone rubber filled with ZnO. *Polymer composites*, 28(2), 125-130.
- [68] Kuzmin, G. F., & Clemens, D. L. (1999). Heat sink mounting assembly for surface mount electronic device packages: Google Patents.
- [69] Gwinn, J. P., & Webb, R. (2003). Performance and testing of thermal interface materials. *Microelectronics Journal*, 34(3), 215-222.
- [70] Huang, X., Jiang, P., & Tanaka, T. (2011). A review of dielectric polymer composites with high thermal conductivity. *IEEE Electrical Insulation Magazine*, 27(4).
- [71] Xu, Y., Chung, D., & Mroz, C. (2001). Thermally conducting aluminum nitride polymer-matrix composites. *Composites Part A: Applied Science and Manufacturing*, 32(12), 1749-1757.
- [72] Wong, C., & Bollampally, R. S. (1999). Thermal conductivity, elastic modulus, and coefficient of thermal expansion of polymer composites filled with ceramic particles for electronic packaging. *Journal of Applied Polymer Science*, 74(14), 3396-3403.
- [73] Martienssen, W., & Warlimont, H. (2006). *Springer handbook of condensed matter and materials data*: Springer Science & Business Media.
- [74] Vel, L., Demazeau, G., & Etourneau, J. (1991). Cubic boron nitride: synthesis, physicochemical properties and applications. *Materials Science and Engineering: B*, 10(2), 149-164.
- [75] Kingon, A. I., Maria, J.-P., & Streiffer, S. (2000). Alternative dielectrics to silicon dioxide for memory and logic devices. *nature*, 406(6799), 1032.
- [76] Auerkari, P. (1996). *Mechanical and physical properties of engineering alumina ceramics*: Technical Research Centre of Finland Espoo.
- [77] Boch, P., Glandus, J., Jarrige, J., Lecompte, J., & Mexmain, J. (1982). Sintering, oxidation and mechanical properties of hot pressed aluminium nitride. *Ceramics International*, 8(1), 34-40.
- [78] Callister, W. D., & Rethwisch, D. G. (2011). *Materials science and engineering* (Vol. 5): John Wiley & Sons NY.
- [79] Matović, B., & Yano, T. (2013). Chapter 3.1 - Silicon Carbide and Other Carbides: From Stars to the Advanced Ceramics. In S. Somiya (Ed.), *Handbook of Advanced Ceramics (Second Edition)* (pp. 225-244). Oxford: Academic Press.
- [80] Gracia-Espino, E., López-Urías, F., Kim, Y. A., Hayashi, T., Muramatsu, H., Endo, M., . . . Dresselhaus, M. S. (2013). Chapter 2.2 - Novel Carbon-Based Nanomaterials: Graphene and Graphitic Nanoribbons. In S. Somiya (Ed.), *Handbook of Advanced Ceramics (Second Edition)* (pp. 61-87). Oxford: Academic Press.
- [81] Jeon, Y.-P., Alway-Cooper, R., Morales, M., & Ogale, A. A. (2013). Chapter 2.8 - Carbon Fibers. In S. Somiya (Ed.), *Handbook of Advanced Ceramics (Second Edition)* (pp. 143-154). Oxford: Academic Press.
- [82] Zhou, W., Wang, C., Ai, T., Wu, K., Zhao, F., & Gu, H. (2009). A novel fiber-reinforced polyethylene composite with added silicon nitride particles for enhanced thermal conductivity. *Composites Part A: Applied Science and Manufacturing*, 40(6-7), 830-836.

- [83] Kemaloglu, S., Ozkoc, G., & Aytac, A. (2010). Properties of thermally conductive micro and nano size boron nitride reinforced silicon rubber composites. *Thermochimica acta*, 499(1-2), 40-47.
- [84] Yu, S., Hing, P., & Hu, X. (2002). Thermal conductivity of polystyrene–aluminum nitride composite. *Composites Part A: Applied Science and Manufacturing*, 33(2), 289-292.
- [85] Hong, J.-P., Yoon, S.-W., Hwang, T., Oh, J.-S., Hong, S.-C., Lee, Y., & Nam, J.-D. (2012). High thermal conductivity epoxy composites with bimodal distribution of aluminum nitride and boron nitride fillers. *Thermochimica acta*, 537, 70-75.
- [86] Cho, W.-S., Cho, M.-W., Lee, J.-H., & Munir, Z. A. (2006). Effects of h-BN additive on the microstructure and mechanical properties of AlN-based machinable ceramics. *Materials Science and Engineering: A*, 418(1-2), 61-67.
- [87] Zhou, W., Qi, S., An, Q., Zhao, H., & Liu, N. (2007). Thermal conductivity of boron nitride reinforced polyethylene composites. *Materials Research Bulletin*, 42(10), 1863-1873.
- [88] Li, S., Qi, S., Liu, N., & Cao, P. (2011). Study on thermal conductive BN/novolac resin composites. *Thermochimica acta*, 523(1-2), 111-115.
- [89] Ishida, H., & Rimdusit, S. (1998). Very high thermal conductivity obtained by boron nitride-filled polybenzoxazine. *Thermochimica acta*, 320(1-2), 177-186.
- [90] Zhou, W., Qi, S., Li, H., & Shao, S. (2007). Study on insulating thermal conductive BN/HDPE composites. *Thermochimica acta*, 452(1), 36-42.
- [91] Zhou, W. Y., Qi, S. H., Zhao, H. Z., & Liu, N. L. (2007). Thermally conductive silicone rubber reinforced with boron nitride particle. *Polymer composites*, 28(1), 23-28.
- [92] Xie, S.-H., Zhu, B.-K., Li, J.-B., Wei, X.-Z., & Xu, Z.-K. (2004). Preparation and properties of polyimide/aluminum nitride composites. *Polymer testing*, 23(7), 797-801.
- [93] Chen, X., Gonsalves, K. E., Chow, G. M., & Xiao, T. D. (1994). Homogeneous dispersion of nanostructured aluminum nitride in a polyimide matrix. *Advanced Materials*, 6(6), 481-484.
- [94] Chen, X., & Gonsalves, K. E. (1997). Synthesis and properties of an aluminum nitride/polyimide nanocomposite prepared by a nonaqueous suspension process. *Journal of materials research*, 12(5), 1274-1286.
- [95] Gonsalves, K. E., & Chen, X. (1996). Studies on the Structure and Properties of Ceramic/Polymernanocomposites. *MRS Online Proceedings Library Archive*, 435.
- [96] Ku, C. C., & Liepins, R. (1987). *Electrical properties of polymers*: Hanser Publishers New York.
- [97] Dissado, L. A., & Fothergill, J. C. (1992). *Electrical degradation and breakdown in polymers* (Vol. 9): IET.
- [98] Hong, C.-C., & Chen, J.-C. (2011). Pre-programmable polymer transformers as on-chip microfluidic vacuum generators. *Microfluidics and nanofluidics*, 11(4), 385-393.

- [99] Angelopoulos, M., Huang, W.-S., Park, J. M., & White, J. R. (1994). Fabrication of printed circuit boards using conducting polymer: Google Patents.
- [100] Chu, B., Zhou, X., Ren, K., Neese, B., Lin, M., Wang, Q., . . . Zhang, Q. (2006). A dielectric polymer with high electric energy density and fast discharge speed. *Science*, 313(5785), 334-336.
- [101] Mallick, P. K. (2007). *Fiber-reinforced composites: materials, manufacturing, and design*: CRC press.
- [102] Liberty, J., & Jones, P. (1993). Thermally conductive interface materials and methods of using the same: Google Patents.
- [103] Vasudevan, A., & Petrovic, J. (1992). A comparative overview of molybdenum disilicide composites. *Materials Science and Engineering: A*, 155(1-2), 1-17.
- [104] Geiger, A. L., & Walker, J. A. (1991). The processing and properties of discontinuously reinforced aluminum composites. *Jom*, 43(8), 8-15.
- [105] Neubauer, E., Kitzmantel, M., Hulman, M., & Angerer, P. (2010). Potential and challenges of metal-matrix-composites reinforced with carbon nanofibers and carbon nanotubes. *Composites Science and Technology*, 70(16), 2228-2236.
- [106] Besmann, T., Sheldon, B., Lowden, R., & Stinton, D. (1991). Vapor-phase fabrication and properties of continuous-filament ceramic composites. *Science*, 253(5024), 1104-1109.
- [107] Han, Z., & Fina, A. (2011). Thermal conductivity of carbon nanotubes and their polymer nanocomposites: a review. *Progress in polymer science*, 36(7), 914-944.
- [108] Jiang, H., Moon, K.-s., Li, Y., & Wong, C. (2006). Surface functionalized silver nanoparticles for ultrahigh conductive polymer composites. *Chemistry of Materials*, 18(13), 2969-2973.
- [109] Yang, K., & Gu, M. (2010). Enhanced thermal conductivity of epoxy nanocomposites filled with hybrid filler system of triethylenetetramine-functionalized multi-walled carbon nanotube/silane-modified nano-sized silicon carbide. *Composites Part A: Applied Science and Manufacturing*, 41(2), 215-221.
- [110] Fornes, T., Yoon, P., Keskkula, H., & Paul, D. (2001). Nylon 6 nanocomposites: the effect of matrix molecular weight. *Polymer*, 42(25), 09929-09940.
- [111] Liang, J., Huang, Y., Zhang, L., Wang, Y., Ma, Y., Guo, T., & Chen, Y. (2009). Molecular-level dispersion of graphene into poly (vinyl alcohol) and effective reinforcement of their nanocomposites. *Advanced Functional Materials*, 19(14), 2297-2302.
- [112] Shi, H., Lan, T., & Pinnavaia, T. J. (1996). Interfacial effects on the reinforcement properties of polymer- organoclay nanocomposites. *Chemistry of Materials*, 8(8), 1584-1587.
- [113] Dang, Z.-M., Yuan, J.-K., Zha, J.-W., Zhou, T., Li, S.-T., & Hu, G.-H. (2012). Fundamentals, processes and applications of high-permittivity polymer-matrix composites. *Progress in Materials Science*, 57(4), 660-723.
- [114] Chujo, Y. (2011). *Conjugated polymer synthesis: methods and reactions*: John Wiley & Sons.

- [115] Burger, C., Hertler, W., Kochs, P., Kreuzer, F.-H., & Mülhaupt, R. (2012). *Silicon in polymer synthesis*: Springer Science & Business Media.
- [116] Inc., G. (2015). *Silane Coupling Agents Connecting Across Boundaries* (3 ed.). 11 East Steel Rd. Morrisville, PA 19067: Gelest.
- [117] Gopakumar, T., & Pagé, D. (2005). Compounding of nanocomposites by thermokinetic mixing. *Journal of Applied Polymer Science*, *96*(5), 1557-1563.
- [118] Seki, Y., Avci, B., Uzun, S., Kaya, N., Atagur, M., Sever, K., & Sarikanat, M. The Using of Graphene Nano-Platelets for a Better through-Plane Thermal Conductivity for Polypropylene. *Polymer composites*.
- [119] Standard, A. (2010). D638-10, 2010. *Standard Test Methods for Tensile Properties of Plastics*. ASTM International, West Conshohocken, PA.
- [120] Testing, A. S. f., & Materials. (2003). *ASTM D790 Standard Test Methods: Flexural properties of unreinforced and reinforced plastics and electrical insulating materials*.
- [121] Kaya, N., Atagur, M., Akyuz, O., Seki, Y., Sarikanat, M., Sutcu, M., . . . Sever, K. (2017). Fabrication and characterization of olive pomace filled PP composites. *Composites Part B: Engineering*. doi: <https://doi.org/10.1016/j.compositesb.2017.08.017>
- [122] I.F.Groves, T. J. L. a. N. A. H. (2008). Dynamic mechanical analysis a versatile technique for the viscoelastic characterization of materials. *International Labmate*, *TA-070*, 5.
- [123] Standard Test Method for Thermal Endurance of Coating Powders Used for Integral Bus Bar Insulation Systems.
- [124] Pak, S. Y., Kim, H. M., Kim, S. Y., & Youn, J. R. (2012). Synergistic improvement of thermal conductivity of thermoplastic composites with mixed boron nitride and multi-walled carbon nanotube fillers. *Carbon*, *50*(13), 4830-4838.
- [125] Shimizu, S., Nomura, I., & Narita, K. (1987). Electrically conductive polyamide resin composition: Google Patents.
- [126] Shumigin, D., Tarasova, E., Krumme, A., & Meier, P. (2011). Rheological and Mechanical Properties of Poly(lactic) Acid/Cellulose and LDPE/Cellulose Composites. *Materials Science-Medziagotyra*, *17*(1), 32-37.
- [127] Fang, M., Wang, K. G., Lu, H. B., Yang, Y. L., & Nutt, S. (2009). Covalent polymer functionalization of graphene nanosheets and mechanical properties of composites. *Journal of Materials Chemistry*, *19*(38), 7098-7105. doi: 10.1039/b908220d
- [128] Bortz, D. R., Heras, E. G., & Martin-Gullon, I. (2012). Impressive Fatigue Life and Fracture Toughness Improvements in Graphene Oxide/Epoxy Composites. *Macromolecules*, *45*(1), 238-245. doi: 10.1021/ma201563k
- [129] Fu, S.-Y., Feng, X.-Q., Lauke, B., & Mai, Y.-W. (2008). Effects of particle size, particle/matrix interface adhesion and particle loading on mechanical properties of particulate-polymer composites. *Composites Part B: Engineering*, *39*(6), 933-961.
- [130] Gu, J., Zhang, Q., Dang, J., Zhang, J., & Chen, S. (2009). Preparation and mechanical properties researches of silane coupling reagent modified β -silicon carbide filled epoxy composites. *Polymer Bulletin*, *62*(5), 689-697. doi: 10.1007/s00289-009-0045-z

- [131] Shokoohi, S., Arefazar, A., & Khosrokhavar, R. (2008). Silane Coupling Agents in Polymer-based Reinforced Composites: A Review. *Journal of Reinforced Plastics and Composites*, 27(5), 473-485. doi: 10.1177/0731684407081391
- [132] Fu, S. Y., Lauke, B., Mäder, E., Yue, C. Y., & Hu, X. (2000). Tensile properties of short-glass-fiber- and short-carbon-fiber-reinforced polypropylene composites. *Composites Part A: Applied Science and Manufacturing*, 31(10), 1117-1125. doi: [https://doi.org/10.1016/S1359-835X\(00\)00068-3](https://doi.org/10.1016/S1359-835X(00)00068-3)
- [133] Fu, S.-Y., & Lauke, B. (1996). Effects of fiber length and fiber orientation distributions on the tensile strength of short-fiber-reinforced polymers. *Composites Science and Technology*, 56(10), 1179-1190. doi: [https://doi.org/10.1016/S0266-3538\(96\)00072-3](https://doi.org/10.1016/S0266-3538(96)00072-3)
- [134] Dong, C., & Davies, I. J. (2012). Optimal design for the flexural behaviour of glass and carbon fibre reinforced polymer hybrid composites. *Materials & Design*, 37, 450-457. doi: <https://doi.org/10.1016/j.matdes.2012.01.021>
- [135] Rezaei, F., Yunus, R., Ibrahim, N. A., & Mahdi, E. S. (2008). Development of Short-Carbon-Fiber-Reinforced Polypropylene Composite for Car Bonnet. *Polymer-Plastics Technology and Engineering*, 47(4), 351-357. doi: 10.1080/03602550801897323
- [136] Sengupta, R., Bhattacharya, M., Bandyopadhyay, S., & Bhowmick, A. K. (2011). A review on the mechanical and electrical properties of graphite and modified graphite reinforced polymer composites. *Progress in polymer science*, 36(5), 638-670.
- [137] Zhou, W., Zuo, J., Zhang, X., & Zhou, A. (2013). Thermal, electrical, and mechanical properties of hexagonal boron nitride-reinforced epoxy composites. *Journal of Composite Materials*, 48(20), 2517-2526. doi: 10.1177/0021998313499953
- [138] Stark, N. M., & Rowlands, R. E. (2003). Effects of wood fiber characteristics on mechanical properties of wood/polypropylene composites. *Wood and Fiber Science*, 35(2), 167-174.
- [139] Bertini, F., Canetti, M., Audisio, G., Costa, G., & Falqui, L. (2006). Characterization and thermal degradation of polypropylene-montmorillonite nanocomposites. *Polymer Degradation and Stability*, 91(3), 600-605.
- [140] Tartaglione, G., Tabuani, D., Camino, G., & Moisio, M. (2008). PP and PBT composites filled with sepiolite: morphology and thermal behaviour. *Composites Science and Technology*, 68(2), 451-460.
- [141] Joseph, P. V., Joseph, K., Thomas, S., Pillai, C. K. S., Prasad, V. S., Groeninckx, G., & Sarkissova, M. (2003). The thermal and crystallisation studies of short sisal fibre reinforced polypropylene composites. *Composites Part A: Applied Science and Manufacturing*, 34(3), 253-266. doi: [https://doi.org/10.1016/S1359-835X\(02\)00185-9](https://doi.org/10.1016/S1359-835X(02)00185-9)
- [142] Nachtigall, S. M., Cerveira, G. S., & Rosa, S. M. (2007). New polymeric-coupling agent for polypropylene/wood-flour composites. *Polymer testing*, 26(5), 619-628.
- [143] Xie, Y., Hill, C. A., Xiao, Z., Miltz, H., & Mai, C. (2010). Silane coupling agents used for natural fiber/polymer composites: A review. *Composites Part A: Applied Science and Manufacturing*, 41(7), 806-819.

- [144] Qin, H., Zhang, S., Zhao, C., Feng, M., Yang, M., Shu, Z., & Yang, S. (2004). Thermal stability and flammability of polypropylene/montmorillonite composites. *Polymer Degradation and Stability*, 85(2), 807-813. doi: <https://doi.org/10.1016/j.polymdegradstab.2004.03.014>
- [145] Rezaei, F., Yunus, R., & Ibrahim, N. (2009). Effect of fiber length on thermomechanical properties of short carbon fiber reinforced polypropylene composites. *Materials & Design*, 30(2), 260-263.
- [146] Othman, N., Ismail, H., & Mariatti, M. (2006). Effect of compatibilisers on mechanical and thermal properties of bentonite filled polypropylene composites. *Polymer Degradation and Stability*, 91(8), 1761-1774.
- [147] Li, J. X., Cheung, W. L., & Jia, D. (1999). A study on the heat of fusion of β -polypropylene. *Polymer*, 40(5), 1219-1222. doi: [https://doi.org/10.1016/S0032-3861\(98\)00345-0](https://doi.org/10.1016/S0032-3861(98)00345-0)
- [148] Zuiderduin, W., Westzaan, C., Huetink, J., & Gaymans, R. (2003). Toughening of polypropylene with calcium carbonate particles. *Polymer*, 44(1), 261-275.
- [149] Rong, M. Z., Zhang, M. Q., Zheng, Y. X., Zeng, H. M., Walter, R., & Friedrich, K. (2001). Structure–property relationships of irradiation grafted nano-inorganic particle filled polypropylene composites. *Polymer*, 42(1), 167-183.
- [150] Sari, A., & Karaipekli, A. (2007). Thermal conductivity and latent heat thermal energy storage characteristics of paraffin/expanded graphite composite as phase change material. *Applied thermal engineering*, 27(8-9), 1271-1277.
- [151] Potts, J. R., Dreyer, D. R., Bielawski, C. W., & Ruoff, R. S. (2011). Graphene-based polymer nanocomposites. *Polymer*, 52(1), 5-25.
- [152] Song, P., Cao, Z., Cai, Y., Zhao, L., Fang, Z., & Fu, S. (2011). Fabrication of exfoliated graphene-based polypropylene nanocomposites with enhanced mechanical and thermal properties. *Polymer*, 52(18), 4001-4010.
- [153] Huda, M., Drzal, L., Mohanty, A., & Misra, M. (2007). The effect of silane treated-and untreated-talc on the mechanical and physico-mechanical properties of poly (lactic acid)/newspaper fibers/talc hybrid composites. *Composites Part B: Engineering*, 38(3), 367-379.
- [154] Huda, M. S., Drzal, L. T., Mohanty, A. K., & Misra, M. (2007). The effect of silane treated- and untreated-talc on the mechanical and physico-mechanical properties of poly(lactic acid)/newspaper fibers/talc hybrid composites. *Composites Part B: Engineering*, 38(3), 367-379. doi: <https://doi.org/10.1016/j.compositesb.2006.06.010>
- [155] Yuan, B., Bao, C., Song, L., Hong, N., Liew, K. M., & Hu, Y. (2014). Preparation of functionalized graphene oxide/polypropylene nanocomposite with significantly improved thermal stability and studies on the crystallization behavior and mechanical properties. *Chemical Engineering Journal*, 237, 411-420.
- [156] Nayak, S. K., & Mohanty, S. (2010). Sisal glass fiber reinforced PP hybrid composites: Effect of MAPP on the dynamic mechanical and thermal properties. *Journal of Reinforced Plastics and Composites*, 29(10), 1551-1568.

- [157] Bleach, N., Nazhat, S., Tanner, K., Kellomäki, M., & Törmälä, P. (2002). Effect of filler content on mechanical and dynamic mechanical properties of particulate biphasic calcium phosphate—polylactide composites. *Biomaterials*, 23(7), 1579-1585.
- [158] Filippone, G., Dintcheva, N. T., La Mantia, F., & Acierno, D. (2010). Using organoclay to promote morphology refinement and co-continuity in high-density polyethylene/polyamide 6 blends—Effect of filler content and polymer matrix composition. *Polymer*, 51(17), 3956-3965.
- [159] Ramanathan, T., Abdala, A., Stankovich, S., Dikin, D., Herrera-Alonso, M., Piner, R., . . . Ruoff, R. (2008). Functionalized graphene sheets for polymer nanocomposites. *Nature nanotechnology*, 3(6), 327.
- [160] Vadukumpully, S., Paul, J., Mahanta, N., & Valiyaveetil, S. (2011). Flexible conductive graphene/poly (vinyl chloride) composite thin films with high mechanical strength and thermal stability. *Carbon*, 49(1), 198-205.
- [161] Kango, S., Kalia, S., Celli, A., Njuguna, J., Habibi, Y., & Kumar, R. (2013). Surface modification of inorganic nanoparticles for development of organic–inorganic nanocomposites—a review. *Progress in polymer science*, 38(8), 1232-1261.
- [162] Robertson, C. G., Lin, C., Rackaitis, M., & Roland, C. (2008). Influence of particle size and polymer– filler coupling on viscoelastic glass transition of particle-reinforced polymers. *Macromolecules*, 41(7), 2727-2731.
- [163] Van Hattum, F., Bernardo, C., Finegan, J., Tibbetts, G., Alig, R., & Lake, M. (1999). A study of the thermomechanical properties of carbon fiber-polypropylene composites. *Polymer composites*, 20(5), 683-688.
- [164] Seki, Y., Avci, B., Uzun, S., Kaya, N., Atagur, M., Sever, K., & Sarikanat, M. The Using of Graphene Nano-Platelets for a Better through-Plane Thermal Conductivity for Polypropylene. *Polymer composites*, 0(0). doi: doi:10.1002/pc.24979
- [165] Das, A., Stöckelhuber, K., Jurk, R., Saphiannikova, M., Fritzsche, J., Lorenz, H., . . . Heinrich, G. (2008). Modified and unmodified multiwalled carbon nanotubes in high performance solution-styrene–butadiene and butadiene rubber blends. *Polymer*, 49(24), 5276-5283.
- [166] Chand, S. (2000). Review carbon fibers for composites. *Journal of Materials Science*, 35(6), 1303-1313.
- [167] Psarras, G. (2006). Hopping conductivity in polymer matrix–metal particles composites. *Composites Part A: Applied Science and Manufacturing*, 37(10), 1545-1553.
- [168] Bekyarova, E., Thostenson, E. T., Yu, A., Kim, H., Gao, J., Tang, J., . . . Haddon, R. C. (2007). Multiscale Carbon Nanotube–Carbon Fiber Reinforcement for Advanced Epoxy Composites. *Langmuir*, 23(7), 3970-3974. doi: 10.1021/la062743p
- [169] Xu, H.-P., Dang, Z.-M., Jiang, M.-J., Yao, S.-H., & Bai, J. (2008). Enhanced dielectric properties and positive temperature coefficient effect in the binary polymer composites with surface modified carbon black. *Journal of Materials Chemistry*, 18(2), 229-234.
- [170] Plueddemann, E. P. (2016). *Interfaces in Polymer Matrix Composites: Composite Materials* (Vol. 6): Elsevier.

- [171] Stankovich, S., Dikin, D. A., Dommett, G. H., Kohlhaas, K. M., Zimney, E. J., Stach, E. A., . . . Ruoff, R. S. (2006). Graphene-based composite materials. *nature*, 442(7100), 282.

7. CURRICULUM VITAE (CV)

1. Adı Soyadı : NUSRET KAYA
2. Doğum Tarihi : 03/02/1980
3. Unvanı : Uzman
4. Öğrenim Durumu : Doktora Öğrencisi

Derece	Alan	Üniversite	Yıl
Doktora	Malzeme Bilimi ve Mühendisliği ABD.(İngilizce)	İzmir Katip Çelebi Üniversitesi	2018
Y. Lisans	Biyomühendislik ABD.	Ege Üniversitesi	2007
Lisans	Kimya (İngilizce)	Hacettepe Üniversitesi	2003

5. Akademik Unvanlar

2016-Bugün	Uzman	Merkezi Araştırma Uygulama Laboratuvarı	İzmir Katip Çelebi Üniversitesi
2011-2015	Uzman	Merkezi Araştırma Uygulama Laboratuvarı Müdürlüğü	Ahi Evran Üniversitesi

6. Yönetilen Yüksek Lisans ve Doktora Tezleri

-

7. Yayınlar

A. SCI

1. **N. Kaya**, Ahmet M. Oztarhan, E.S. Urkac, D. İla, S. Budak, E. Oks, A. Nikolaev, A. Ezdesir, F. Tihminlioglu, Z. Tek "Article title: Polymeric Thermal Analysis of C+H and C+H+Ar Ion Implanted UHMWPE Samples"2007, Beam Interactions with Materials and Atoms, Volume 261, Issues 1-2, August 2007, Pages 711-714
2. E. Sokullu Urkac, A. Oztarhan,F. Tihminlioglu, **N. Kaya**, D. İla, C. Muntele, S. Budak, E. Oks, A.Nikolaev, A. Ezdesir "Thermal characterization of Ag and Ag + N

ion implanted ultrahigh molecular weight polyethylene", Beam Interactions with Materials and Atoms, Volume 261, Issues 1-2, August 2007, Pages 699-703

3. Ahmet Oztarhan, Emel Sokullu Urkac, **Nusret Kaya**, Mesut Yenigul, Funda Tihminlioglu, Ayhan Ezdesir, Robert Zimmerman, SatilmisBudak, C Muntele, Bopha Chhay, Daryush Ila, Efim Oks, Alexey Nikolaev, Zekai Tek, Rengin Eltem - 'Modification of Surface Morphology of UHMWPE for Biomedical Implants", 2007 Spring, 1020-GG05-03, Ion-Beam-Based Nanofabrication MRS Proceedings Vol. 1020
4. E. Sokullu Urkac, A. Oztarhan, F. Tihminlioglu, **N. Kaya**, S. Budak, B. Chay, C. Muntele, E. Oks, A. Nikolaev, D. ILA, "Nanoscale Surface Modification of UltraHigh Molecular Weight Polyethylene (UHMWPE) Samples with the W+C Ion Implantation - 2007 Spring, 1020-GG07-05 Ion-Beam-Based Nanofabrication MRS
5. E. Sokullu Urkac, A. Oztarhan, F. Tihminlioglu, **N. Kaya**, D. Ila, C. Muntele, S. Budak, B. Chay, E. Oks, A. Nikolaev, "Structural and Thermal Characterization of Ti+O Ion Implanted Ultra High Molecular Weight Polyethylene (UHMWPE) AIP Conf. Proc. 1099, 545 (2009); doi: 10.1063/1.3120095
6. **Kaya N.**, Atagur M, Akyuz O, Seki Y, Sarikanat M, Sutcu M, Seydibeyoglu MO, Sever K, Fabrication and characterization of olive pomace filled PP composites, Composites Part B (2017), doi: 10.1016/j.compositesb.2017.08.017.
7. Seki Y, Beliz Avci, Secil Uzun, **Kaya N.**, Atagur M, , Sever K, Sarikanat M, The Using of Graphene Nano-Platelets for a Better through-Plane Thermal Conductivity for Polypropylene, Polymer Composites (2018)

B. Uluslararası sözlü ve poster bildiriler.

1. **Nusret KAYA**, Metehan ATAGÜR, Orhan AKYÜZ, Mehmet SARIKANAT, Yoldaş SEKİ, Kutlay SEVER, Mechanical and Thermal Analysis of Different Ratios of Vermiculite-PP Composites, 16 th International Materials Symposium (IMSP'2016) 12-14 October 2016 – Pamukkale University – Denizli – Turkey
2. Eyyup YALCIN, Duygu Akın Kara, Caner Karakaya, Mustafa Can, **Nusret Kaya** and Seraffetin Demić. "Using Self Assembled Monolayer to Improve Device Performance of Organic Light Emitting Diodes". 4th International Conference on Energy and Environment Research (ICEER 2017). Porto, Portugal, July 17-20, 2017
3. **Nusret KAYA**, Şerafettin DEMİÇ "Effects of nonaromatic oil as a filler on to mechanical and rheological properties of three different tire-tread recipes" IPC 2017 "V.ULUSLARARASI POLİMERİK KOMPOZİTLER SEMPOZYUMU VE ÇALIŞTAYLARI"- 2-4 Kasım 2017 tarihleri arasında, TEPEKULE KONGRE VE SERGİ MERKEZİ Bayraklı-İzmir
4. **Nusret KAYA**, Orhan AKYÜZ, Mustafa CAN, Şerafettin DEMİÇ "Investigation of thermal conductivity and mechanical properties of three different particles sized 50% silicon carbide (SiC) loaded polypropylene (PP) matrix based composites". IPC 2017, "V.ULUSLARARASI POLİMERİK KOMPOZİTLER SEMPOZYUMU VE ÇALIŞTAYLARI" 2-4 Kasım

2017 tarihleri arasında, TEPEKULE KONGRE VE SERGİ MERKEZİ Bayraklı-İzmir.

5. **Nusret KAYA**, Mücahit SÜTÇÜ, Mustafa CAN, Şerafettin DEMİÇ, Investigation of rheological properties of three different particles sized 50% silicon carbide (SiC) loaded polypropylene (PP) matrix based composites. The International Conference on Materials Science, Machine and Automotive Engineerings and Technology in Çeşme/İZMİR (IMSMATEC).
6. **Nusret KAYA**, Mücahit SÜTÇÜ, Ebubekir ATAN, Şerafettin DEMİÇ, Investigation of rheological properties of waste tungsten carbide (WC) particles loaded high density polyethylene (HDPE) matrix based composites. The International Conference on Materials Science, Machine and Automotive Engineerings and Technology in Çeşme/İZMİR (IMSMATEC).
7. **Nusret KAYA**, Orhan AKYÜZ, Hakan BİLGİLİ, Mustafa CAN, Şerafettin DEMİÇ. Investigation of Alumina/Graphene Mixtures Thermal and Electrical Properties into Polypropylene (PP) Matrix Based Composites. APMAS 2018

8. Projeler

1. TEYDEP 1501 Sanayi ve Tubitak iş birlikli proje, Tavukçuluk Sektöründe kullanılan Antibiyotiklerin yerine bölgedeki florada doğal yetişen kekik bitkisinin timin ve kavraktol gibi esansiyel yağ asitlerinin zeolitlere emdirilerek yem katkısı olarak kullanılması.300.000 TL
2. TEYDEP 1501 Sanayi ve Tubitak iş birlikli proje, “Avrupa Birliği yasalarına uygun Aromatik yağ yerine Nanoromatik Yağ kullanarak çeşitli ebatlarda ve yüksek kalitede Lastik üretimi” 1.000.000 TL
3. Ege Üniversitesi Mühendislik Fakültesi Biyomühendislik bölümünde yapılan 115M605 nolu TÜBİTAK projesi,"Mekanik germe altında merkezi sinir sistemi nöronlarının incelenmesi ve in vitro bir tramvatik beyin hasarı modeli." yardımcı uzman olarak çalıştı. Yardımcı Uzman olarak görev aldı.
4. Ahi Evran Üniversitesi Merkezi Araştırma Uygulama Laboratuvarı DPT projesi. 17.000.000 TL
5. 4005 Ahi Evran Üniversitesi Merkezi Araştırma Uygulama Laboratuvarı için altyapı projesi hazırladı ve Proje kapsamında merkeze Thermo Scientific NXR 6700 FTIR-RAMAN Enstrümantal analiz sistemi temini. 200.000 TL
6. ”Bağ çubuğu ve pirina atıklarının geri dönüştürülmüş PP ve HDPE kompozitlerinin üretilmesi ve karakterizasyonu” İzmir Kâtip Çelebi Üniversitesi Mühendislik Mimarlık Fakültesi, Makine Mühendisliği Bölümü 214M350 nolu TUBİTAK projesi. 60.000 TL
7. “Mineral Katkılı Termoplastik Kompozit Malzemelerin Üretilmesi ve Özelliklerinin İncelenmesi”, 2015-ÖDL-MÜMF-0002 nolu İKCU BAP Proje Yürütücüsü: Doç.Dr. Kutlay SEVER, Proje Başlama Tarihi: 28/07/2015, Proje Bütçesi: 16.213 TL
8. “Karbon Esaslı Dolgu Malzemeleri İle Termal İletken Polipropilen Kompozitlerin Üretimi ve Karakterizasyonu”, 2016-GAP-MÜMF-0030 nolu: Doç.Dr. Kutlay SEVER, Proje Başlama Tarihi: 17/08/2016, Proje Bütçesi: 39.985,48 TL

9. “Seramik Dolgulu Termal İletken Polimerlerik Kompozitlerin Üretimesi Ve Karakterizasyonu” 26.05.2016 tarihli İKCU BAP Proje Yürütücüsü: Nusret KAYA . Proje Bütçesi: 14850,3 TL
10. “D-A-D Type NIR Small Molecules For High Performance Organic Solar Cells” Proje Başlama Tarihi: 01/01/2017. Proje Yürütücüsü: Doç.Dr. Şerafetin DEMİÇ

9. İdari Görevler

Görev	Kurum	Süre
Müdür Yardımcılığı	Ahi Evran Üniversitesi Merkezi Araştırma Uygulama Laboratuvarı Müdürlüğü	2 Yıl